DISSERTATION

REACTIVE OXYGEN SPECIES REGULATE ACTIVITY-DEPENDENT TRANSPORT AND DELIVERY OF AMPA RECEPTORS TO SYNAPSES

Submitted by

Rachel Doser

Department of Biomedical Sciences

In partial fulfillment of the requirements

For the Degree of Doctor of Philosophy

Colorado State University

Fort Collins, Colorado

Spring 2022

Doctoral Committee:

Advisor: Frederic Hoerndli
Co-Advisor: Gregory Amberg

Jozsef Vigh
Santiago Di Pietro

Copyright by Rachel Doser 2022

All Rights Reserved

ABSTRACT

REACTIVE OXYGEN SPECIES REGULATE ACTIVITY-DEPENDENT TRANSPORT AND DELIVERY OF AMPA RECEPTORS TO SYNAPSES

In neurons, changes in the subcellular localization of the AMPA subtype of ionotropic glutamate receptors (AMPARs) is necessary for learning and memory. AMPARs are primarily translated in the cell body and transported through dendrites to their destinations by molecular motors. This means that their localization, and therefore synaptic function and plasticity, requires proper intracellular transport to the synapse. Our lab and others have shown that AMPAR transport is regulated by activity-dependent calcium signaling. Neuronal activity and intracellular transport are energy demanding requiring high rates of ATP production from which reactive oxygen species (ROS), a class of chemically reactive molecules, are a normal byproduct. For my dissertation work, I build upon this knowledge by demonstrating a physiological role for ROS in the regulation of AMPAR transport in the transparent genetic model *C. elegans*. In Chapter 2, we show that slight increases in ROS decreased transport and synaptic delivery of AMPARs by attenuating calcium influx. Diminished ROS levels also decreased AMPAR transport but via a calcium-independent mechanism. This prompted us to assess how ROS signaling is initiated *in vivo,* which was the aim of experiments in Chapter 3. The results from these experiments demonstrated that calcium buffering and ROS production at mitochondria are positively regulated by activity. So, the rest of Chapter 3 was devoted to experiments addressing how AMPAR transport dynamics are impacted by localized ROS signaling originating at mitochondria. In the neurite, we found that localized increases in ROS from mitochondria regulate the stopping of AMPAR

transport events by potentially altering local calcium influx. Further investigation on how local calcium influx, mitochondrial ROS production and AMPAR transport are interrelated *in vivo* necessitates optimization of optogenetic tools for high spatial and temporal control of cytoplasmic calcium levels. To this end, Chapter 4 overviews the optimization and characterization of a few optogenetic approaches for simultaneously manipulating and measuring neuronal activity *in vivo.* This work begins to detail how ROS signaling regulates synaptic function and plasticity which describes a novel mechanism in which metabolic rate indirectly regulates synaptic activity. Understanding this mechanism would provide insight into why altered glutamatergic synaptic transmission accompanies elevated calcium/ROS and mitochondrial dysfunction in neuronal aging and degeneration.

ACKNOWLEDGEMENTS

Many thanks must be given to those who have lifted me up and provided guidance over the last 15 years. First, I must acknowledge the support from my family despite their non-traditional ways of showing it. In particular, I must thank my father who raised me with grit and tenacity. He has been a constant reminder to prioritize what matters most to me in life. Also, to my boyfriend Bryce and his family, thank you for making Colorado my home away from home and for your endless encouragement. Bryce has continued to boost my ambitions and support me in every way especially during the last year in which big decisions were made regarding how my scientific interests guide the next step of our life.

Next, I wish to share gratitude for the unrelenting support from my undergraduate advisors, Drs. Lynne Oland and Leslie Tolbert. Since my last year at the University of Arizona, Dr. Oland has been there any time that I have needed guidance or insights. It was Dr. Tolbert who proved to me my own aptitude, instilled in me an appetite for discovery, and has continued to cheer me on ever since. I know the support I received from them is extremely rare and makes me grateful to have them to look up to. I only hope to be as encouraging of a mentor as either of them.

Lastly, thank you to my immediate support system at Colorado State University. Foremost, my advisor Dr. Fred Hoerndli who kept me busy with his ideas and excitement for neuroscience. It was his enthusiasm for research that supplemented my own drive and pushed me to be a scientist who thinks critically and objectively. There are many past and present members of the Hoerndli lab that have helped directly with my research over the last 5 years and help to develop my mentorship abilities. To name a few key players – thank you Dayton Pierce, Ashley Lipinski,

Ennis Deihl and Kaz Knight. Dr. Jozsef Vigh, a member of my doctoral committee, is responsible for getting me hooked on exploring the molecular and cellular processes that control neuronal excitation – his guidance over the last 5 years was instrumental to my confidence and precision as a scientist. I also must also acknowledge Dr. Mike Tamkun for allowing me to conduct many hours of imaging in his lab and for entertaining the biophysical and optical conundrums I was faced with during the latter part of my dissertation work. Thanks to Dr. Santiago Di Pietro, another member of my committee, for always being encouraging and to Dr. Greg Amberg, my co-advisor, for being so willing to help in any way needed.

All my successes (and failures) would not have been possible without each of you.

TABLE OF CONTENTS

Chapter 1 – Introduction

1.1 Overview of Glutamatergic Synapse Function and Plasticity

The majority of excitatory neurotransmission is carried out by glutamatergic signaling between synapses. These glutamatergic synapses allow for cognition and are highly plastic which gives rise to learning and memory. The importance of normal glutamatergic synapse function is made evident by the fact that many cognitive disorders that alter cognition, learning and memory are caused by altered glutamatergic transmission (Eltokhi et al., 2020). Therefore, we must understand how this type of synapse is normally maintained and strengthened in order to comprehensively address the abnormal glutamatergic synapse function that accompanies disorders of the nervous system.

1.1A Glutamatergic Synapse Content and Function

A glutamatergic synapse is one in which the presynaptic bouton is equipped with the molecular components that coordinate activity-dependent release of glutamate (Figure 1.1 A), an amino acid that is a metabolic precursor and the primary excitatory neurotransmitter in the central nervous system (Niciu et al., 2012). Once released into the synaptic cleft, glutamate binds to glutamate receptors (Figure 1.1 B) before being rapidly taken up via glutamate transporters positioned on the plasma membrane of neurons and surrounding support cells (i.e. astrocytes; Figure 1.1 C; Niciu et al., 2012). Glutamate receptors subtypes are divided into two major categories: metabotropic and ionotropic.

Metabotropic glutamate receptors (mGluRs) initiate intracellular signaling involving G-proteins, tetrameric proteins that come in a few flavors and act on well characterized signaling

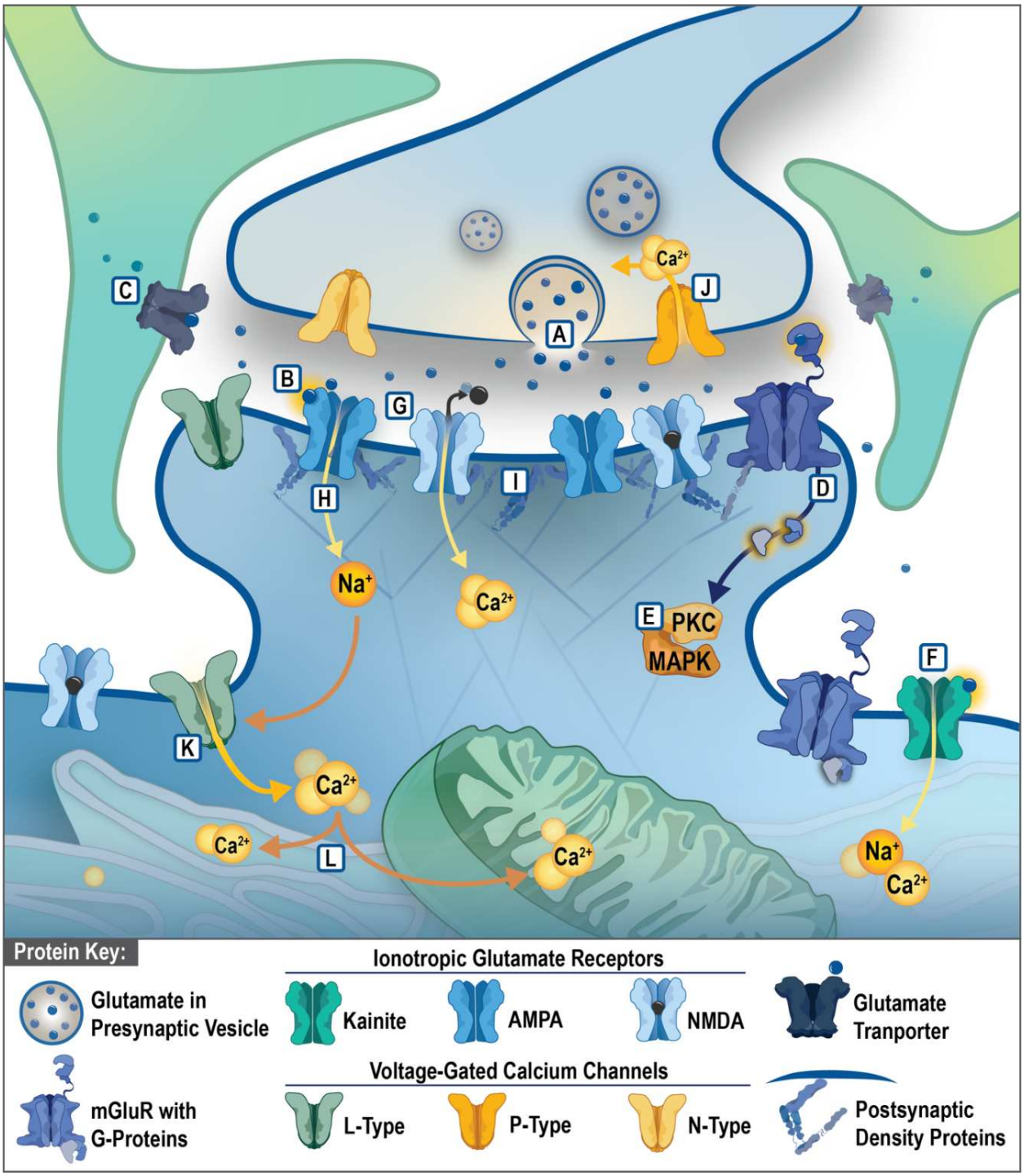

Figure 1.1 - Graphical representation of the functional components at glutamatergic synapses. Glutamate released from presynaptic vesicles (A) binds to glutamate receptors (B) before being taken up into neurons (blue cells) or astrocytes (green cells) via glutamate transporters (C). Glutamate-dependent activation of mGluRs (D) initiates intracellular signaling (E), such as those involving activation of protein kinase C (PKC) and mitogen-activated protein kinase (MAPK). The kainite (F) and NMDA subtype of iGluRs (G) are calcium permeable. Most of the AMPA subtype are calcium-impermeable, but fast depolarization from AMPARs (H) opens L-type voltage-gated calcium channels (K).

Figure 1.1 - Calcium channels found at presynaptic terminals (J), such as the P- and N-type, supply the calcium required for fission of glutamate-containing vesicles with the presynaptic membrane to achieve glutamate release. L) Calcium is readily buffered by the endoplasmic reticulum (aqua compartment) and mitochondria (green organelle) that are positioned at postsynaptic sites. Various proteins compose the postsynaptic density (I) and are important for structural organization of receptors at the postsynaptic membrane.

pathways (Figure 1.1 D). Currently, eight subtypes of mGluRs have been identified and their glutamate-dependent activation either increases or decrease neuronal excitability. For example, glutamate binding to group 1 mGluRs increases excitability by initiating calcium release from intracellular stores as well as activating kinases (Figure 1.1 E) that regulate mGluR expression and localization (Niciu et al., 2012; Wang and Zhuo, 2012). The different subtypes in addition to the many downstream targets of their signaling make mGluRs especially important for long-lasting changes to neuronal excitability.

Ionotropic glutamate receptors (iGluRs) have a more direct role in neuronal excitation because these receptors are equipped with a cation pore that is opened by glutamate binding. Opening of this pore allows for influx of cations, mainly sodium (Na^+) but sometimes calcium (Ca^{2+}) as well, which depolarizes the synaptic membrane and leads to the opening of voltage-dependent ion channels that propagate depolarization throughout the neuron. The three subtypes of iGluRs are named after their specific agonists and include kainite, N-methyl-d-aspartate (NMDA), and α-amino-3-hydroxy-5-methyl-4-isoxazolepropionic acid (AMPA). Kainite receptors are the least studied iGluR, but it has been more recently identified that they participate in both ionotropic and metabotropic signaling while localized to pre-, extra-, and postsynaptic sites (Figure 1.1 F; Nair et al., 2021). The NMDA subtype of iGluRs (NMDAR) are found at post- and extrasynaptic locations and have two distinguishing functional features: First, the opening of their cation pore requires both glutamate binding and postsynaptic depolarization. This is due to the presence of a magnesium ion (Mg^{2+}) in the pore opening that is extruded by repulsion to a positively charged

synaptic membrane. Second, their pore is highly permeable to Ca^{2+} specifically, which makes them especially important in the initiation of calcium signaling (Figure 1.1 G; Blanke and VanDongen, 2009).

The AMPA subtype of iGluRs (AMPAR) is concentrated at postsynaptic sites where they are responsible for fast, excitatory synaptic transmission. Glutamate binding to AMPARs initiates opening of their cation pore and depolarization (Figure 1.1 H; Niciu et al., 2012). The type of cations that can pass through AMPARs depend on the receptor's subunit composition. Those only composed of the GluA1, GluA3, or GluA4 subunits pass Ca^{2+} in addition to Na^{+}. If the GluA2 subunit is incorporated into the tetramer, then those receptors are Ca^{2+}-impermeable (Rao and Finkbeiner, 2007). The majority of AMPARs at glutamatergic synapses are heteromeric with GluA1/GluA2 or GluA2/GluA3 subunits. Fewer than 10% of these receptors are calcium-permeable GluA1 homomers meaning AMPAR activation causes depolarization predominantly through Na^{+} influx (Wenthold et al., 1996), but this depolarization allows for calcium influx through activated NMDARs and voltage-gated calcium channels (VGCCs; Figure 1.1 J and K; Kapur et al., 1998; Luebke et al., 1993).

Other components that contribute to the basic function of the glutamatergic synapse include proteins that compose the postsynaptic density (PSD; Figure 1.1 I; Ehlers, 1999). It is also important to note that dendritic mitochondria and endoplasmic reticulum (ER) are localized adjacent or within the excitatory synapse spines (Figure 1.1 L; Hollenbeck, 2005; Wu et al., 2017). In addition to supplying energy and synthesizing proteins, these subcellular compartments are important for Ca^{2+} buffering. Plasticity mechanisms modulate the function of all these components to cause synaptic strengthening and weakening.

1.1B Plasticity of the Glutamatergic Synapse

Synaptic plasticity is a change in strength of synapses in response to the activity pattern at that synapse or surrounding synapses. The strength of a connection as it pertains to synapses refers to how efficient electrical signals are transduced into chemical ones and vice versa. A change in synaptic strength can be achieved via presynaptic mechanisms that alter the amount of glutamate released in response to activity and/or modulation of a postsynaptic site's electrical response to glutamate release. The activity-dependent strengthening of a synapse is known as long-term potentiation (LTP) whereas weakening is known as long-term depression (LTD).

Induction of LTP can be achieved electrically (i.e. high-frequency stimulation (HFS); 100 Hz) or chemically (i.e. with glutamate receptors agonists; Fujii et al., 2004) and results in enhanced synaptic transmission which is measured at glutamatergic synapses by the excitatory postsynaptic potential (EPSP; Citri and Malenka, 2008). During the early phase of LTP, the EPSP increases dramatically. This is due to an increase in number of glutamate vesicles constituting the readily releasable pool (Vandael et al., 2020) allowing for more glutamate release. At the postsynaptic membrane, more glutamate receptors are present due to the lateral diffusion of AMPARs from extrasynaptic sites (Park, 2018; Penn et al., 2017). In the meantime, calcium-dependent signaling pathways that were activated during the LTP induction protocol have activated several key players that initiate exocytosis and contribute to stabilization of new AMPARs.

Specifically, rapid increases in postsynaptic calcium due to opening of VGCCs and especially NMDARs activates the calcium-dependent messenger protein Calmodulin (CaM). The main target for CaM as it pertains to LTP is calcium/CaM-dependent protein kinase II (CaMKII). Once activated by Ca^{2+}/CaM binding, CaMKII has many downstream effectors. For instance, activated CaMKII can bind NMDARs to prevent downregulation of channel function while also

allowing CaMKII to phosphorylate AMPARs in a way that increases the conductance of cations through their pore (Sumi and Harada, 2020). Phosphorylation of AMPARs and/or auxiliary proteins at synaptic endosomes by CaMKII or other kinases increases the rate of their exocytosis (Opazo and Choquet, 2011). Additionally, CaMKII phosphorylation of AMPAR auxiliary subunits increase their association with postsynaptic density proteins thus trapping new AMPARs at the postsynaptic membrane (Park, 2018; Penn et al., 2017). These mechanisms result in more AMPARs at a synapse therefore increasing the EPSP. However, for synaptic strengthening to be maintained long-term, additional consolidation steps are required involving the reorganization of the postsynaptic actin cytoskeleton and protein synthesis (Abraham and Williams, 2008; Baltaci et al., 2019; Citri and Malenka, 2008).

The study of synaptic weakening has been more challenging due to the stimulus for LTD being less clear-cut. In the hippocampus, LTD has been induced using low-frequency stimulation (1 Hz) which is thought to increase postsynaptic calcium modestly and less frequently than HFS. These lower calcium levels activate phosphatases with high calcium-affinities resulting in the inactivation of kinases involved in synaptic strengthening (Malenka and Bear, 2004). However, it has become clear that activation of CaMKII is also required for LTD. Low and persistent increases in calcium result in additional phosphorylation of CaMKII causes a decrease in synaptic AMPARs due to phosphorylation of a different site (Cook et al., 2021; Coultrap et al., 2014). Dephosphorylation of AMPARs by protein kinase A or calcineurin also contributes to LTD by decreasing their open channel probability (Malenka and Bear, 2004; Reyes-García and Escobar, 2021). These changes in AMPAR localization and function cause synaptic weakening due to less efficient depolarization of the postsynaptic membrane in response to glutamate release. Taken together, it is clear how local trafficking of AMPARs is important for Hebbian plasticity, but the

regulation of AMPAR localization is also central to the compensatory mechanisms regulating synaptic strength known as homeostatic plasticity.

1.2 Long-distance Transport of Ionotropic Glutamate Receptors

It is clear that long-distance transport of iGluRs is dependent on microtubule molecular motors, specifically kinesin (Kayadjanian et al., 2007; Kim and Lisman, 2001; Setou et al., 2000). Unfortunately, an understanding of this motor-dependent transport has advanced slowly in the years to follow due to the difficulty of visualizing iGluR transport events. In recent years, new *in vivo* techniques and temporal control of iGluR release from the endoplasmic reticulum (ER) have permitted experiments that have begun to detail how the long-distance transport of newly synthesized iGluRs, especially of the AMPA subtype (Bourke et al., 2021; Hangen et al., 2018; Hoerndli et al., 2015, 2013).

1.2A An Overview of Protein Transport

In most cell types, including neurons, the synthesis and assembly of membrane-bound proteins predominantly occurs in the somatic ER. New proteins are then passed to the Golgi apparatus for further modification and packaging into transport vesicles. The contents of a transport vesicle determine what neuronal compartment it is directed toward. Cargo adaptors and other scaffolding proteins are required for binding to specific molecular motors and access into the axon or dendrite (Rosenberg et al., 2014). For instance, the adaptor protein glutamate receptor interacting protein 1 (GRIP1) is vital for transport of AMPARs via kinesin-1 into dendrites (Setou et al., 2002) whereas the small GTPase Rab3 is important for axonal transport of synaptic vesicle precursors (Niwa et al., 2008). The dogmatic differentiation between axonal vs. dendritic transport of is that plus-end directed kinesin motors drive axonal transport and minus-end directed dyneins are responsible for dendritic transport. This dogma is an oversimplification since

kinesins have been shown to carry out anterograde transport of iGluRs and other cargos in dendrites (Kim and Lisman, 2001; Maeder et al., 2014; Setou et al., 2000; Wang and Xu, 2015). So, the neuronal compartment transport vesicles are destined for seems to be determined by cargo composition.

Another phase of long-distance transport occurs after proteins are tagged for degradation. These proteins remain in early endosomes that are transported via both dynein and kinesin during maturation into late endosomes which are also transported bidirectionally but are biased toward retrograde trafficking (Cai et al., 2010; Cheng et al., 2015; Loubéry et al., 2008). Since observations of late endosome/lysosome transport has been predominantly retrograde, it is thought that degradation occurs in the cell body. Although the majority of protein degradation does seem to occur in the cell body, there is evidence of proteasomal degradation in neuronal processes (Jin et al., 2018). Regardless, it is clear that coordinated long-distance transport is vital for the bulk of protein degradation in neurons (Tammineni et al., 2017; Wong and Holzbaur, 2014).

1.2B Transport of the NMDA subtype of Ionotropic Glutamate Receptors

Although there are reports of iGluR synthesis at postsynaptic sites (Ju et al., 2004), the majority are synthesized via the ER-Golgi system described above (Hanus et al., 2016). Then, their method of microtubule-based transport into dendrites is specific to the iGluR type. For instance, NMDARs rely on synaptic scaffolding proteins (MAGUKs) for their transport via the kinesin KIF17. The specific MAGUKs in these complexes is determined by NMDAR subunit composition (Horak et al., 2014), which is thought to impact their recruitment to and retention at synapses (Yin et al., 2012). Although an activity-dependent mechanism has not been defined for this transport, loss or functional modification of these key players lead to impaired LTP

induction and memory defects. This suggests that long-distance transport of NMDARs is regulated by synaptic activation (Yin et al., 2012).

Interestingly, the AMPA and NMDA receptor subtypes are not co-transported to synapses. Early evidence of this came from the observation of AMPAR transport and delivery being delayed an hour or more after NMDAR integration to a synapse (Washbourne et al., 2002). Additionally, NMDARs are subject alternative sorting in the somatic ER and often diverted to Golgi outposts within the dendrite from which they can be supplied to synapses (Jeyifous et al., 2009). So, it's becoming increasingly clear that transport of these iGluR subtypes is regulated independently of one another.

1.2C Transport of the AMPA subtype of Ionotropic Glutamate Receptors

After AMPARs are synthesized and packaged into transport vesicles (Figure 1.2 – Step 1), they are loaded onto molecular motors for export into the dendrite (Figure 1.2 – Step 2). The kinesin KIF5 carries out AMPAR transport with help from GRIP-1 which mediates the interaction between AMPARs and the motor. GRIP-1 is also important for directing vesicles to the dendrite (Setou et al., 2002). Recently, it was shown that redistribution of AMPARs from dendritic endosomes to postsynaptic sites during LTP depends on microtubule-based transport via KIF13A (Gutiérrez et al., 2021). There are also indications that KIF1A can associate with AMPARs via and interaction between GRIP-1 and liprin-α (Wyszynski et al., 2002); however, there is no direct proof that KIF1A carries out long-distance transport of AMPARs. A recent study in cultured vertebrate neurons showed that AMPAR transport is upregulated by activity-dependent calcium signaling which was partially mediated by phosphorylation of AMPARs (Hangen et al., 2018).

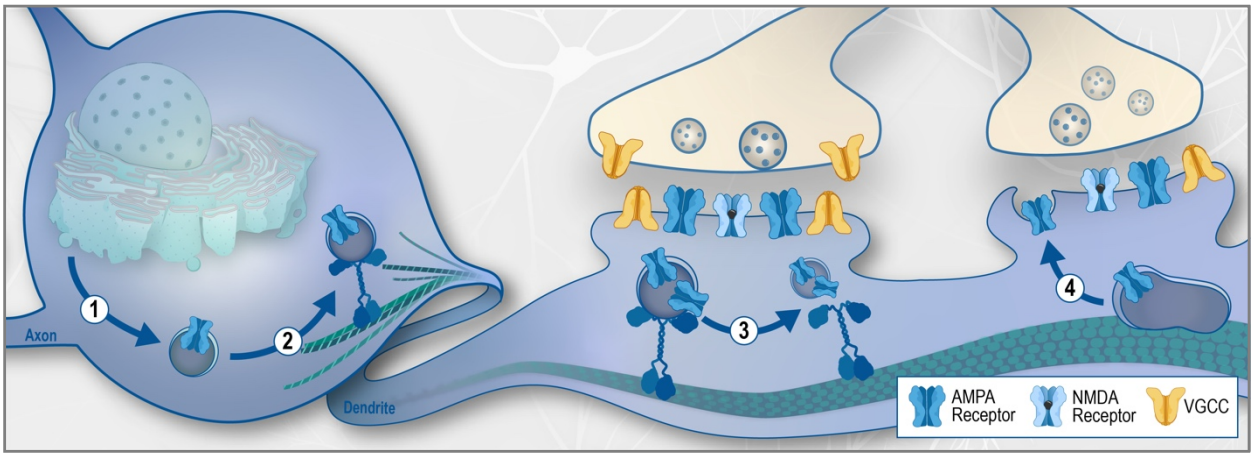

Figure 1.2 – The major steps involved in AMPAR translocation from the cell body to synapses.
① AMPARs are synthesized and packaged in vesicles in somatic Golgi. ② Vesicles containing AMPARs are loaded onto the molecular motor kinesin for transport into and through dendrites. ③ These vesicles are then targeted to specific synapses for delivery of their cargo. ④ AMPARs from transport vesicles or synaptic endosomes are then recruited to the synaptic membrane to contribute to the EPSP.

In vivo studies using in the nematode *Caenorhabditis elegans* (*C. elegans)* have supported and added to these findings by detailing the regulation of GLR-1 (GluA1 homologue) transport by VGCCs and CaMKII activity. Specifically, calcium influx through EGL-19 (L-type VGCC) upregulates the amount of GLR-1 transport. This is due to the initiation of a calcium signaling pathway involving activation of UNC-43, the *C. elegans* homologue of CaMKII, which initiates the loading of GLR-1-containing vesicles onto UNC-116 (KIF5 homologue; Hoerndli et al., 2015). The proper function and plasticity of glutamatergic synapses requires KIF5-mediated export of AMPARs from the cell body (Hoerndli et al., 2015; Zhao et al., 2020). Consistent with recent observations in vertebrates (Gutiérrez et al., 2021), GLR-1 receptor transport through dendrites is also carried out by KIF13 in *C. elegans* (Monteiro et al., 2012). This KIF13-mediated transport is regulated by cyclin-dependent kinase-5 (Monteiro et al., 2012) which has been implicated in homeostatic and activity-dependent synaptic plasticity (Guan et al., 2011).

Once AMPARs are transported into the dendrite, fine regulation of their targeting to dendritic endosomes or postsynaptic sites (Figure 1.2 – Step 3) is required for integration of new receptors at the synaptic membrane (Figure 1.2 – Step 4) and therefore strengthening and maintenance of a synapse. The signals within the dendrite that regulate cargo delivery remains unclear. However, some proteins important for AMPAR transport via kinesins, such as liprin-α and CaM, have been implicated in the capturing of KIF1A and unloading of other types of cargo at postsynaptic sites (Stucchi et al., 2018). An indication that there is activity-dependent regulation of AMPAR delivery comes from observations that glutamate uncaging and high dendritic Ca^{2+} slow and stop vesicular transport of AMPARs (Hangen et al., 2018). Future work dedicated to unraveling the regulation of cargo delivery will be necessary for a complete understanding of how long-distance transport of iGluRs and other proteins contribute to synaptic plasticity and maintenance.

1.2D Metabolic Regulation of Long-distance Transport

The motor-dependent transport of iGluRs relies on the continuous supply of energy in the form of adenosine triphosphate (ATP). This is because ATP hydrolysis by kinesin and other molecular motors drive conformational changes that physically move motors along cytoskeletal filaments. The activity-dependent regulation of this process by Ca^{2+} is also dependent upon ATP since Ca^{2+} removal is carried out by the plasma membrane Ca^{2+}-ATPase (PMCA) that moves Ca^{2+} against its ionic gradient at the expense of ATP. Additional intracellular Ca^{2+} buffering is predominantly carried out by the sarcoendoplasmic reticulum Ca^{2+}-ATPase (SERCA; Nikoletopoulou and Tavernarakis, 2012). Interestingly, production of ATP via mitochondrial oxidative phosphorylation (OXPHOS) creates reactive oxygen species (ROS) as a byproduct (Halliwell, 1992). ROS have been mostly studied for their ability to induce oxidative stress,

however, it is becoming increasingly clear that ROS act as physiological signaling molecules in many cellular processes including those underlying learning and memory (Kishida and Klann, 2006; Massaad and Klann, 2011).

1.3 Reactive Oxygen Species, Calcium Signaling and Energy Production

ROS are a class of chemically reactive molecules that include free radicals derived from oxygen such as superoxide (O_2^-), hydrogen peroxide (H_2O_2), and hydroxyl radicals ($^{\cdot}OH$) (Bolisetty and Jaimes, 2013). They were regarded as harmful, pathophysiological signaling molecules due to cytotoxic effects of elevated ROS levels. It is becoming increasingly clear that ROS have signaling roles in neurons under physiological conditions.

1.3A ROS Production and Breakdown

The majority of a cell's ATP is produced by mitochondrial OXPHOS which involves the shuttling of electrons between proteins that compose the electron transport chain (ETC). Some of these electron carriers can reduce the available oxygen (O_2) within mitochondria. Specifically, there are two primary electron carriers and conditions under which electrons are donated to O_2 to create O_2^-: First, Complex I of the ETC reduces O_2 when NADH levels are high and if coenzyme Q is unavailable for reduction. Reduction of O_2 by Complex I is upregulated by ROS levels which partially explains why mitochondrial dysfunction is accompanied by elevated ROS. Second, if coenzyme Q is reduced but ATP synthesis is low, then the resultant high proton motive force will drive electrons back to Complex I often leading to reduction of O_2 or NAD^+ (Angelova and Abramov, 2018; Murphy, 2009). Physiological rates of mitochondrial ROS production have been measured to account for 0.25% to 11% of the oxygen consumed by mitochondria (Zorov et al., 2014). Outside of the mitochondria, plasma membrane-associated NADPH oxidases produce

O_2^- and are regulated by ligands involved in inflammation, calcium signaling and pathogen defense (Tauffenberger and Magistretti, 2021). Less-significant cytoplasmic sources of ROS include xanthine and amino acid oxidases (Bolisetty and Jaimes, 2013).

The breakdown of ROS is necessary for maintaining physiological levels of ROS. The majority of O_2^- produced by OXPHOS or by other processes undergoes dismutation by superoxide dismutases (SOD) into H_2O_2 (Tauffenberger and Magistretti, 2021). In the mitochondria, H_2O_2 is broken down into H_2O and O_2 by glutathione peroxidases and peroxiredoxins. Mitochondria-derived H_2O_2 readily escapes into the cytoplasm where catalases are responsible for their breakdown (Murphy, 2009; Tauffenberger and Magistretti, 2021). ROS can also be reduced non-enzymatically by glutathione as well as metal-binding proteins (i.e. myoglobin, and transferrin) and other natural compounds (i.e. vitamin C and E) (Bouayed and Bohn, 2010; Tauffenberger and Magistretti, 2021). Accumulating evidence supports that ROS act as a second messenger in many cellular processes. So, maintaining ROS within the physiological range (10-100nM) is necessary for normal reduction-oxidation (redox) signaling and prevention of oxidative stress (Sies and Jones, 2020; Tauffenberger and Magistretti, 2021).

1.3B Redox Regulation of Calcium Influx

The majority of what is known about ROS signaling in neurons pertains to its involvement in calcium homeostasis. Redox regulation occurs at extracellular and intracellular Ca^{2+} sources as well as at pumps that remove cytoplasmic Ca^{2+}. Regulation of Ca^{2+} influx via plasma membrane Ca^{2+} channels by oxidation differs depending on channel subtype and cell type (Table 1.1). Oxidation of ryanodine and inositol 1,4,5-trisphosphate (IP_3) receptors at the ER membrane consistently stimulate the release of Ca^{2+} from intracellular stores. Removal of cytoplasmic Ca^{2+}

by PMCAs is downregulated by oxidation; however, the oxidation site can be occluded by CaM binding suggesting that prior initiation of Ca^{2+} signaling may prevent redox modification of PMCAs. Similarly, Ca^{2+} uptake into the ER by SERCAs is inhibited by oxidation (Hidalgo and Arias-Cavieres, 2016; Hidalgo and Donoso, 2008). These examples of redox regulation demonstrate how cytoplasmic Ca^{2+} influx and efflux are regulated in various ways by ROS signaling. Interestingly, the reciprocal regulation of ROS signaling by calcium also occurs in neurons (Görlach et al., 2015).

Table 1.1 - Observations of functional changes due to plasma membrane Ca^{2+} channel oxidation.

Channel Type	Cell Type	Functional Change Due to Oxidation
L-type VGCC	Ventricular Myocytes	⇳ Ca^{2+} currents
	Smooth Muscle	⇧ Ca^{2+} currents
	Cortical Neurons	⇩ Ca^{2+} currents
	HEK293 Cells	⇳ Ca^{2+} currents
T-type VGCC	Sensory and Thalamic Neurons	⇩ Ca^{2+} currents
P/Q-Type VGCC	*Xenopus* oocytes	⇧ Ca^{2+} currents
TRP Channel	Dorsal Root Ganglion Neurons, Endothelial Cells, HEK293 Cells	Channel activation

⇳: Increases and decreases have been observed (Hidalgo and Donoso, 2008; Hool and Corry, 2007; Pires and Earley, 2017; Shirotani et al., 2001; Todorovic and Jevtovic-Todorovic, 2014)

1.3C Calcium Regulation of Oxidative Phosphorylation and ROS Production

Calcium uptake into mitochondria involves passage of Ca^{2+} through the outer mitochondrial membrane (OMM) by voltage-dependent anion channels (VDACs), which are large, voltage-gated pores that can pass Ca^{2+} and ATP in addition to anions (Sander et al., 2021). Then, increasing Ca^{2+} opens the pore of mitochondrial calcium uniporters (MCU) at the inner membrane for Ca^{2+} uptake into the matrix (De Stefani et al., 2015). This calcium uptake can be upregulated by ROS due to oxidation of MCU increasing rate of Ca^{2+} uptake (Dong et al., 2017). Once in the matrix, high Ca^{2+} upregulates ATP production via direct and indirect mechanisms.

Ca^{2+} positively regulates three key players of the tricarboxylic acid cycle, which produces electron donors for the ETC and therefore OXPHOS (De Stefani et al., 2015). The production of electron donors by the malate-aspartate shuttle is also upregulated by Ca^{2+} (Szibor et al., 2020). There is some evidence for direct regulation of ATP synthase, the key protein in OXPHOS, by Ca^{2+}. However, further research is needed to understand if this occurs under physiological conditions (Territo et al., 2000; Wacquier et al., 2019). Lastly, it has been observed that Ca^{2+} concentrations in the nanomolar range increase the rate of OXPHOS, but supraphysiological Ca^{2+} levels downregulate the rate of mitochondrial ATP production (Fink et al., 2017). This observation supports positive regulation of OXPHOS by physiological Ca^{2+}, which results in an unavoidable increase in ROS production. Resultant ROS signaling reciprocally regulates calcium influx (section 1.3B) as well as the function of other proteins important for synaptic maintenance and plasticity.

1.3D Redox Regulation of Synaptic Proteins

ROS act as a second messenger by participating in reversible and non-reversible redox modification of synaptic protein. This involves the oxidation of accessible amino acids containing a thiol group (cysteine and methionine). The oxidation of thiol groups modifies protein function by altering structure or interactions with other molecules. There are several proteins involved in the maintenance and plasticity of glutamatergic synapses that are subject to redox modifications (Tauffenberger and Magistretti, 2021). Oxidation of CaM decreases its activation of CaMKII (Robison et al., 2007; Snijder et al., 2011). Additionally, CaMKII has multiple sites that can be targeted for oxidation depending on the kinase's conformation. Following binding of Ca^{2+}/CaM, a conformational change exposes sites in CaMKII's regulatory domain whose oxidation results in autonomous activity of the kinase (Erickson et al., 2008; Zhang et al., 2021).

Together, this suggests that the timing of ROS signaling in relation to calcium influx can either inhibit or prolong calcium signaling via CaM/CaMKII. It has been shown that oxidized CaM results in NMDA receptor hypofunction (Bodhinathan et al., 2010; Foster et al., 2017), and although targets of CaMKII are well characterized, the downstream effects of CaMKII autonomy due to oxidation remain unclear (Bayer and Schulman, 2019).

Other oxidizable proteins involved in synaptic function and plasticity include NMDARs, PKC, and calcineurin. There are four cysteine residues on NMDARs that when oxidized, reduce channel function (Hidalgo and Donoso, 2008). Oxidation of PKC results in constitutive activation of the kinase and LTP-induced activation of PKC is inhibited by antioxidants suggesting that this redox modification is necessary for LTP (Knapp and Klann, 2002a). Lastly, inactivation of the calcium-dependent phosphatase calcineurin occurs due to oxidation-induced proteolytic cleavage (Oswald et al., 2018). The diverse effects of oxidation on synaptic protein function coupled with the reciprocal regulation of ROS and Ca^{2+} levels suggest an integrated role for Ca^{2+} and ROS signaling in synaptic function and plasticity.

1.4 Reactive Oxygen Species and Calcium Signaling in Synaptic Function

An interplay between Ca^{2+} and ROS levels and their downstream signaling proposes that this relationship is involved in maintenance and plasticity of glutamatergic synapses. With this theory still in its infancy, there is little direct evidence that a Ca^{2+}-ROS interplay regulates glutamatergic synapse function. However, there are examples of how abnormal Ca^{2+} or ROS signaling independently result in plasticity defects of these synapses. Early studies suggest that induction of synaptic plasticity requires ROS signaling. Increases in ROS scavengers (exogenously applied or overexpressed) and inhibition of ROS production both prevent induction of LTP as

well as cause impaired performance on learning and memory tasks. (Kishida et al., 2006; Klann, 1998). Similar impairments in LTP and LTD induction as well as memory result from loss of ROS scavengers or exogenous application of ROS (Kamsler and Segal, 2003; Knapp and Klann, 2002b). Together, these studies suggest that the role of ROS in LTP is determined by the type of ROS, where it is produced and the relative concentration of ROS (Massaad and Klann, 2011).

There is some evidence for convergence of ROS signaling with Ca^{2+}-dependent regulation of synaptic plasticity. For instance, Ca^{2+}/CaM-dependent activation of CaMKII was shown to be abnormal in the absence of the peroxiredoxins responsible for H_2O_2 breakdown (Kim et al., 2011). Activation of PKC by oxidation can free up CaM through the phosphorylation of neurogranin which decreases its sequestration of CaM (Massaad and Klann, 2011; Ordyan et al., 2020). Additionally, a Ca^{2+}-dependent increase in mitochondrial ROS production was found to prolong the activation of CREB, a transcription factor that has been heavily implicated in the maintenance of LTP (Hongpaisan et al., 2003). These examples of redox-mediated changes in Ca^{2+} signaling support that mechanisms underlying synaptic plasticity are co-regulated by ROS and Ca^{2+}. Future research dedicated to studying how this interplay is normally involved in synaptic function under basal conditions as well as during LTP/LTD induction is required for our understanding of why synaptic function and plasticity is perturbed in conditions of high ROS and Ca^{2+}. This understanding would provide insight into why cognition, learning and memory is altered in aged and diseased brains where Ca^{2+} and ROS are elevated.

1.5 Thesis Work: Regulation of AMPA Receptor Transport by Reactive Oxygen Species

1.5A Premise and Initial Hypothesis

Activity-dependent changes in the availability of AMPARs at a synapse is crucial for the maintenance and plasticity of a synapse. If synapse activity is high but there are insufficient AMPARs present in synaptic endosomes to allow for LTP mechanisms, then that synapse will not undergo strengthening. Therefore, activity-dependent regulation AMPAR transport is pertinent for plasticity. As mentioned, this long-distance transport relies on a continuous ATP supply and Ca^{2+} signaling, which are linked by ROS signaling. This suggests a potential role for ROS signaling in AMPAR transport and delivery to synapses. Specifically, ROS-mediated changes in Ca^{2+} influx were hypothesized to in turn alter AMPAR transport. Since oxidation had been shown to up- and downregulate Ca^{2+} influx depending on the cellular context (Table 1.1), it was difficult to predict if AMPAR transport would be positively or negatively regulated by ROS signaling. Regardless, I hypothesized that ROS signaling regulates AMPAR transport and synaptic delivery. To test this hypothesis, I used genetic and pharmacological manipulations to alter ROS and Ca^{2+} signaling in combination with various *in vivo* imaging techniques in *C. elegans*.

The hypothesis-driven questions addressed in this dissertation include how increased and decreased ROS levels impact AMPAR transport and delivery to synapses (Chapter 2), how ROS signaling is initiated in *C. elegans* glutamatergic neurons as well as how local ROS signaling regulates Ca^{2+} influx and AMPAR delivery at synapses (Chapter 3). Together, these results suggest that physiological ROS signaling regulates the synaptic content of AMPARs by modulating Ca^{2+}-dependent transport and delivery of AMPARs to synapses.

1.5B Studying Glutamate Receptor Transport and ROS Signaling in C. elegans

The simple nervous system and complete synaptic connectome in *C. elegans* make it a great model for studying fundamental mechanisms of neuronal function (Sengupta and Samuel, 2009). There is conservation of key neuronal proteins including the L-type VGCC (EGL-19), GluA1 (GLR-1) and CaMKII (UNC-43) (Hart et al., 1995; Jospin et al., 2002; Rongo and Kaplan, 1999). The genetical malleability of *C. elegans* has allowed for manipulation of genes whose products were hypothesized to regulate GLR-1 transport. This combined with the nematode's transparent cuticle allow for the visualization of fluorescently-tagged GLR-1 in real time *in vivo*. We specifically analyze GLR-1 transport in the AVA neurons, a set of glutamatergic, unipolar interneurons with a long neurite that spans the entire length of the ventral nerve chord (Maricq et al., 1995). The AVA neurons are essential for the expression of long-term memory in *C. elegans* (Rose et al., 2003; Stetak et al., 2009). Key players in the regulation of GLR-1 transport in *C. elegans* AVA neurons are consistent with the regulation of GluA1 transport in vertebrate neurons (Hangen et al., 2018; Hoerndli et al., 2015), which supports the relevance of using this approach for studying AMPAR transport.

C. elegans have also been vital for our understanding of physiological ROS signaling. ROS signaling is involved in *C. elegans* reproduction, cuticle biogenesis, cuticle molting and epidermal wound healing (Miranda-Vizuete and Veal, 2017). Like in vertebrate neurons, changes in physiological ROS levels have also been shown to modulate the activation of *C. elegans* neurons (Li et al., 2016). Components involved in ROS homeostasis, such as NAPHD oxidase, SOD and catalases, are also functionally conserved (Chávez et al., 2009; Suzuki et al., 1996). These components provide targets for manipulating ROS levels which can be used in combination with GLR-1 transport analysis to address the proposed hypothesis.

Chapter 2 – Reactive Oxygen Species Signaling Regulates the Long-Distance Transport and Delivery of Glutamate Receptors

2.1 Introduction

To begin to understand if ROS signaling has a role in the regulation of GLR-1 transport, we used both genetic and pharmacological methods for increasing ROS levels. We specifically modulated H_2O_2 levels since it has a slightly longer half-life than other ROS subtypes and is present within the cytoplasm making it the most likely species to participate in intracellular signaling pathways (Halliwell, 1992). In *C. elegans* with a loss-of function (lf) mutation in a peroxisomal catalase (*ctl-2)*, we observed a decrease in total GLR-1 transport out of the cell body and decreased GLR-1 delivery to synapses (Chapter 2.2). The effect on transport and delivery was nearly identical when wildtype worms were acutely treated with low concentrations of H_2O_2 (Chapter 2.2). These molecular changes appear to alter locomotion and cause defects in olfactory associative memory (Chapter 2.3). These data suggest that ROS are acting as a necessary regulator of GLR-1 localization. If this were true, then diminishing ROS would also perturb GLR-1 transport. Thus, we assessed this possibility by decreasing ROS using a genetic and pharmacological approach. Both methods of diminishing ROS led to decreased GLR-1 transport (Chapter 2.4). Taken together, the data presented in this chapter demonstrate how ROS act as a necessary regulator of GLR-1 transport to synapses.

2.2 Reactive Oxygen Species Modulate Activity-Dependent AMPA Receptor Transport in *C. elegans*

The following material was published online September 23, 2020, in *The Journal of Neuroscience* (Doser et al., 2020).

2.2A Summary

The AMPA subtype of synaptic glutamate receptors (AMPARs) play an essential role in cognition. Their function, numbers and change at synapses during synaptic plasticity is tightly regulated by neuronal activity. Although we know that long-distance transport of AMPARs is essential for this regulation, we do not understand the associated regulatory mechanisms of it. Neuronal transmission is a metabolically demanding process in which ATP consumption and production are tightly coupled and regulated. Aerobic ATP synthesis unavoidably produces reactive oxygen species (ROS), such as hydrogen peroxide, which are known modulators of calcium signaling. Although a role for calcium signaling in AMPAR transport has been described, there is little understanding of the mechanisms involved and no known link to physiological ROS signaling. Here, using real-time in vivo imaging of AMPAR transport in the intact C. elegans nervous system, we demonstrate that long-distance synaptic AMPAR transport is bidirectionally regulated by calcium influx and activation of calcium/calmodulin-dependent protein kinase II. Quantification of in vivo calcium dynamics revealed that modest, physiological increases in ROS decrease calcium transients in C. elegans glutamatergic neurons. By combining genetic and pharmacological manipulation of ROS levels and calcium influx, we reveal a mechanism in which physiological increases in ROS cause a decrease in synaptic AMPAR transport and delivery by modulating activity-dependent calcium signaling. Taken together, our results identify a novel

role for oxidant signaling in the regulation of synaptic AMPAR transport and delivery, which in turn could be critical for coupling the metabolic demands of neuronal activity with excitatory neurotransmission.

2.2B Significance and Impact

Synaptic AMPARs are critical for excitatory synaptic transmission. The disruption of their synaptic localization and numbers is associated with numerous psychiatric, neurological, and neurodegenerative conditions. However, very little is known about the regulatory mechanisms controlling transport and delivery of AMPAR to synapses. Here, we describe a novel physiological signaling mechanism in which ROS, such as hydrogen peroxide, modulate AMPAR transport by modifying activity-dependent calcium signaling. Our findings provide the first evidence in support of a mechanistic link between physiological ROS signaling, AMPAR transport, localization, and excitatory transmission. This is of fundamental and clinical significance since dysregulation of intracellular calcium and ROS signaling is implicated in aging and the pathogenesis of several neurodegenerative disorders including Alzheimer's and Parkinson's disease.

2.2C Introduction

The alpha-amino-3-hydroxy-5-methyl-4-isoxazole-propionic acid (AMPA) subtype of glutamate receptors (AMPARs) are essential for fast excitatory synaptic transmission (Ashby et al., 2008). The number of AMPARs at the synaptic surface is a key determinant of synaptic efficacy and is the result of a dynamic equilibrium between the number of receptors in intracellular pools and at the synaptic surface (Groc et al., 2009; Henley and Wilkinson, 2013; Rosendale et

al., 2017). Although a few AMPARs can be synthesized locally (Hanus et al., 2016), the vast majority of AMPARs are synthesized in the neuronal soma, often far away from synapses, and are trafficked in a complex multistep process to dendrites and synapses (Brechet et al., 2017; Hanus et al., 2016; Henley and Wilkinson, 2016). Intracellular transport by molecular motors (Esteves da Silva et al., 2015; Hangen et al., 2018; Hoerndli et al., 2013; Kim and Lisman, 2001; Setou et al., 2002), exo- and endocytosis (Ehlers, 2000; Yudowski et al., 2007) as well as surface diffusion dynamics (Choquet and Triller, 2013) are all important steps of this complex trafficking. Intracellular AMPAR transport between different cellular pools of AMPARs is the least understood of these steps but is essential for synaptic transmission and plasticity (Hoerndli et al., 2013; Kim and Lisman, 2001; Setou et al., 2002). In addition, several studies have now shown that transcription of Kinesin-1 motors (Puthanveettil et al., 2008) and the number of AMPARs transported increase with neuronal activity (Hangen et al., 2018; Hoerndli et al., 2015). Furthermore, AMPAR exocytosis (Yudowski et al., 2007) and stopping during transport in dendrites also increases with activity (Hangen et al., 2018) suggesting that vesicle stops correlate with AMPARs delivery (Hoerndli et al., 2013). The correlation between stopping of vesicular cargo and delivery has also been observed for other postsynaptic cargoes (Bommel et al., 2019; Guillaud et al., 2008; Ichinose et al., 2015; Stucchi et al., 2018), but the regulation of stops and delivery of AMPARs is so far unknown.

Neuronal activity is associated with increased energy demands that is largely fulfilled by mitochondrial ATP production (Hall et al., 2012), which concurrently produces reactive oxygen species (ROS; Halliwell, 1992). The main ROS subtypes are hydrogen peroxide (H2O2), the superoxide anion (O2-) and the hydroxyl radical (HO-) (Halliwell, 1992). Previous studies have shown that ROS can affect calcium signaling mediated by N-methyl-D-aspartate (NMDA)

glutamate receptors, voltage-gated calcium channels (VGCCs) and calcium release from the endoplasmic reticulum (ER) (Akaishi et al., 2004; Amberg et al., 2010; Hidalgo and Arias-Cavieres, 2016; Todorovic and Jevtovic-Todorovic, 2014). Interestingly, the effect of ROS varies widely depending on dosage, cell type and model system used (Hidalgo and Arias-Cavieres, 2016; Wilson et al., 2018). This is illustrated by the fact that long-term potentiation (LTP) is disrupted by elevated ROS (Bliss and Collingridge, 1993; Kamsler and Segal, 2003; Klann, 1998) as well as depletion of ROS (Kishida and Klann, 2006). Thus, the literature supports a link between ROS signaling and changes in neuronal excitability. However, whether this is due to ROS modulation of calcium signaling remains uncertain. In particular, there is a lack of direct evidence for the roles of physiological ROS on neuronal calcium signaling *in vivo*.

The transparent model *C. elegans* is well-suited to study the effects of ROS on calcium signaling in neurons *in vivo* where circuits remain intact. More specifically, calcium and ROS sensors have been successfully used *in vivo* in *C. elegans* to study conserved signaling pathways (Braeckman et al., 2016; Luo et al., 2014; Sengupta and Samuel, 2009). In addition, *C. elegans* have been instrumental in uncovering translationally conserved calcium and ROS signaling mechanisms regulating neuronal activity, organismal aging and neurodegeneration (Alvarez et al., 2020; Back et al., 2012; Griffin et al., 2019; Petriv and Rachubinski, 2004; Tardiff et al., 2013; Treusch et al., 2011; Zullo et al., 2019).

In this study, we start to address the possible link between ROS production and regulation of AMPAR transport using C. elegans. Single neuron expression of SEP::mCherry::GLR-1 (the *C. elegans* homologue of the AMPAR subunit GluA1 tagged at the N-terminus with SEP, a pH-sensitive form of GFP, and mCherry) and the calcium sensor GCAMP6f enabled us to quantify and characterize GLR-1 transport as well as changes in cytoplasmic calcium *in vivo*, in real

time. Together with genetic and pharmacological manipulation of VGCC activity and ROS levels, our results show that AMPAR transport is directly regulated by activity-dependent calcium signaling. We also find that physiological increases in ROS levels decreases calcium and, as a result, AMPAR transport, delivery and exocytosis. We further show that the targets of increased ROS are specific and involve L-type VGCC-dependent calcium signaling upstream of calcium/calmodulin-dependent protein kinase II (CaMKII) activation. Altogether, our results suggest a mechanism by which physiological ROS signaling acts as a negative feedback mechanism regulating excitatory glutamatergic transmission by decreasing activity-dependent calcium influx and subsequent AMPAR transport.

2.2D Results

C. elegans is a useful model for studying long-distance AMPAR transport dynamics *in vivo*. Here we use a dual tagged AMPAR subunit, SEP::mCherry::GLR-1 in the *glr-1(ky176)* genetic background, expressed in a single pair of glutamatergic neurons (AVA) to analyze how transport, delivery and exocytosis of GLR-1 are modulated by cytoplasmic calcium and reactive oxygen species (ROS). AVA are long, ventrally running unipolar interneurons with cell bodies in the head of the animal that express AMPA and NMDA subtypes of glutamate receptors (Maricq et al., 1995). To reveal dim GLR-1 transport events, we used a photobleaching approach combined with continuous imaging of the mCherry signal to visualize GLR-1 transport in the proximal region of AVA (see Figure 2.1 A). Both anterograde (Figure 2.1 A, blue arrowheads) and retrograde (Figure 2.1 A, fuchsia arrowheads) transport events can be visualized as single particles advancing in opposite directions at different time points (Figure 2.1 A, timepoint images 1-3). The trajectories of these transport events can be visualized and analyzed in a kymograph

representing their position on x-axis and time on the y-axis (Figure 2.1 A, bottom right). The total amount of GLR-1 transport as well as velocities and stopping of transport events can be quantified using these kymographs. In control animals, the number of transport events as well as the average anterograde velocity obtained in our hands (Figure 2.1 C and F) are similar to what we reported previously and reported for vertebrate AMPAR transport in hippocampal neurons (Hangen et al., 2018; Hoerndli et al., 2015; Ju et al., 2004).

Activity-dependent calcium signaling regulates AMPAR transport

Recently, we and others have shown that long distance AMPAR transport is regulated dynamically by neuronal activity. Although studies have shown that CaMKII activation is required for activity-dependent AMPAR transport, the exact signaling pathways leading to CaMKII activation are still unclear (Hangen et al., 2018; Hayashi et al., 2000; Hoerndli et al., 2015). In *C. elegans* neurons, the majority of neuronal depolarization is achieved by VGCCs, specifically by L-type VGCC (L-VGCC), while voltage-gated sodium channels are absent (Serrano-Saiz et al., 2013). *C. elegans* animals expressing VGCCs with reduced calcium conductance have altered synaptic distribution (Rongo C and Kaplan J, 1999) and diminished transport of AMPARs (Hoerndli et al., 2015). A necessary next step in understanding the regulation of long-distance transport of AMPARs to and from synapses is to determine if this process is directly regulated by increased cytoplasmic calcium leading to CaMKII activation. If this is the case, then we would expect transport characteristics, such as export from the soma as well as transport velocities and pausing, to correlate with activity-dependent changes in cellular calcium levels.

To test this hypothesis, we took a genetic approach using strains with a reduced- or gain-of-function mutation in *egl-19*, the sole L-VGCC gene in *C. elegans*, leading respectively to a

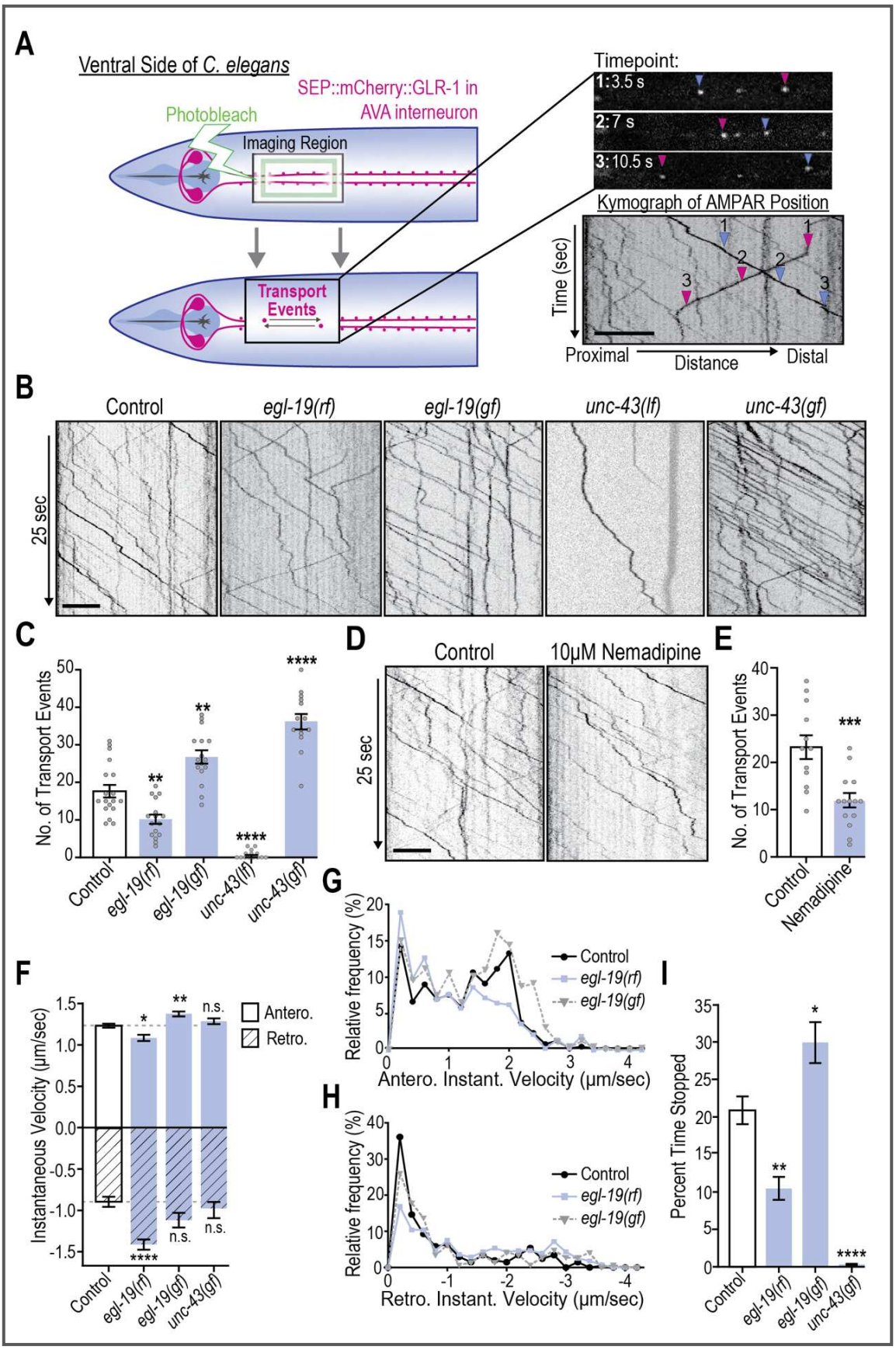
A
Ventral Side of C. elegans
SEP::mCherry::GLR-1 in AVA interneuron
Photobleach
Imaging Region
Transport Events
Timepoint:
1:3.5 s
2:7 s
3:10.5 s
Kymograph of AMPAR Position
Time (sec)
Proximal
Distance
Distal
B
Control
egl-19(rf)
egl-19(gf)
unc-43(lf)
unc-43(gf)
25 sec
C
No. of Transport Events
D
Control
10μM Nemadipine
25 sec
E
No. of Transport Events
Control
Nemadipine
F
Instantaneous Velocity (μm/sec)
Antero.
Retro.
n.s.
G
Relative frequency (%)
Antero. Instant. Velocity (μm/sec)
H
Relative frequency (%)
Retro. Instant. Velocity (μm/sec)
I
Percent Time Stopped

Figure 2.1 - Activity-dependent calcium signaling regulates GLR-1 transport. A) Left, Diagram illustrating the location and procedure for *in vivo* imaging of mCherry::SEP::GLR-1 in AVA. Top right, representative images at three timepoints showing positions of AMPAR-containing vesicles as they progress away from the cell body (blue arrowhead) and toward the cell body (fuchsia arrowhead). Bottom right, a kymograph displaying the position (x-axis) of AMPAR-containing vesicles over time (y-axis). Arrowheads indicate position of vesicles in kymograph that correspond to representative images at timepoints 1-3. Scale bar = 5 μm. All animals are expressing SEP::mCherry::GLR-1 in the *glr-1(ky176)* background. For all transport experiments, animals with no additional mutations in this background are referred to as "controls". B) 25 seconds of representative kymographs from controls, *egl-19* reduced-function (rf), *egl-19* gain-of-function (gf), *unc-43* loss-of-function (lf) and *unc-43* gain-of-function (gf) mutants. Scale bar = 5 μm. C) Total GLR-1 transport (anterograde and retrograde events) quantified from kymographs representative of a 50 second image stream (n>14 worms for each group; **: p=0.036, ****: p<0.00001 compared to controls). D) 25 seconds of representative kymographs of DMSO (control) and 10 μM nemadipine treated worms. Scale bar = 5 μm. E) Total GLR-1 transport from DMSO controls (n=12) and nemadipine treated groups (n=14, ***: p=0.005 compared to DMSO control). F-I) Stop and velocity analysis of more than 60 transport events from controls, *egl-19(rf)*, *egl-19(gf)* and *unc-43(gf)* mutants. F) Instantaneous velocity of AMPAR vesicles traveling in either an anterograde (solid) or retrograde fashion (diagonal lines; n>60 transport events; n.s.=not significant, *: p=0.012, **: p=0.003, ****: p<0.0001 compared to controls). G and H) Distribution of instantaneous velocities (binned every 0.2 μm/sec) for anterograde (G) and retrograde (H) transport for controls, *egl-19(rf)* and *egl-19(gf)* mutants. I) The percent of time GLR-1-containing vesicles spent stopped in each genotype as quantified from the same transport events in part A (*: p=0.043, **: p=0.001, ****: p<0.0001 compared to controls). Error bars for all bar graphs represent standard error of the mean (SEM).

decrease or increase in calcium influx (Liu et al., 2018). In the *egl-19* reduced-function (rf) mutant, GLR-1 transport out of the cell body was significantly decreased (10.2 ± 1.2, mean ± SEM, transport events per kymograph, n=16, p=0.0036, Figure 2.1 B and C) compared to controls (17.9 ± 1.7 events, n=19). Conversely, in the *egl-19* gain-of-function (gf) mutant, GLR-1 transport was upregulated (26.7 ± 1.7 events, n=17, p=0.0037, Figure 2.1 B and C). To ensure that these changes in transport are in fact due to altered calcium influx, we acutely treated animals containing SEP::mCherry::GLR-1 in the *glr-1(ky176)* background with the L-type-specific VGCC blocker, nemadipine (Kwok et al., 2006). A 30-minute pre-treatment with 10 μM nemadipine caused a decrease in total transport (12.0 ± 1.5 events, n=14, compared to 23.4 ± 2.5 events in untreated controls, n=12, p=0.0005, Figure 2.1 D and E) similar to *egl-19(rf)* (10.2 ± 1.2, Figure 2.1 C). Both nemadipine treatment and *egl-19(rf)* showed a similar reduction in calcium in AVA as measured by GCAMP6f (data not shown). These results indicate that not only is

calcium through VGCCs required (Hoerndli et al., 2015), but also that neuronal calcium directly and bidirectionally regulates AMPAR transport to and from the cell body.

To better understand how AMPAR transport dynamics are impacted by calcium, we quantified the velocity and stop frequency of individual GLR-1-containing vesicles in the *egl-19* mutants. We found that the increased calcium in *egl-19(gf)* mutants results in a slightly faster anterograde instantaneous velocity (1.37 ± 0.03 μm/sec, n=87 events, p=0.003) compared to control animals (1.23 ± 0.02 μm/sec, n=90, Figure 2.1 F). The distribution frequency of the anterograde velocities in each group revealed that the increase in *egl-19(gf)* is due to more vesicles traveling at higher speeds (1.6-2.0 μm/sec, Figure 2.1 G). Retrograde transport velocities, however, were not significantly changed in the *egl-19(gf)* mutants (Figure 2.1 F and H). In addition, we observed a significant increase in the percent time spent stopped for vesicles moving in either direction in *egl-19(gf)* (29.9% ± 2.7) compared to controls (20.9% ± 1.8, p=0.043, n>95, Figure 2.1 I). Decreased calcium in *egl-19(rf)* mutants decreases the instantaneous velocity of anterograde GLR-1 transport (1.08 ± 1.1 μm/sec, n=50, p=0.0037), but surprisingly had the opposite effect on instantaneous velocity of retrograde transport (1.4 ± 0.06 μm/sec, n=59, compared to 0.9 ± 0.06 μm/sec in controls, n=44, p<0.0001, Figure 2.1 F). The percent time vesicles moving in either direction spent stopped was also drastically decreased in *egl-19(rf)* mutants (paused 10.5% ± 1.5 of the time, p=0.0011, n=79, Figure 2.1 I).

Cytoplasmic calcium increases from L-VGCC and other sources are known to activate CaMKII (Bayer and Schulman, 2019), which in turn has been shown to be required for normal AMPAR transport (Hangen et al., 2018; Hoerndli et al., 2015). We sought to determine if and to what degree CaMKII activation regulates AMPAR transport. For these experiments, we used strains harboring genetic loss- and gain-of-function mutations of UNC-43, the sole *C. elegans*

ortholog of CaMKII. The *unc-43* loss-of-function (lf) mutation leads to a complete loss of UNC-43 (Reiner et al., 1999), whereas the gain-of-function (gf) allele causes partial calcium-independent, constitutive activation of UNC-43 (Umemura, 2005). Animals with *unc-43(lf)* showed a drastic decrease in GLR-1 transport (0.78 ± 0.30, n=14, p<0.0001) whereas animals with *unc-43(gf)* showed a dramatic increase in GLR-1 transport (36.3 ± 2.04 events, n=14, p<0.0001, Figure 2.1 B and C) compared to controls. Interestingly, in *unc-43(gf)* mutants, instantaneous transport velocity was unchanged (Figure 2.1 F), but the percentage of time all transport vesicles spent stopped was drastically decreased to nearly 0% (vesicles stopped 0.06% ± 0.49 of the time, n=58, compared to 20.9% ± 1.8 in controls, n=95, p<0.0001, Figure 2.1 I). We were unable to quantify velocities and stop frequency of GLR-1 transport in *unc-43(lf)* due to the low numbers of transport events per kymograph (less than one per kymograph on average).

Collectively, these data demonstrate that calcium influx and calcium signaling by CaMKII directly regulate GLR-1 transport, with differential regulation of the dynamics (velocity and stops) of anterograde and retrograde transport events. These findings advance our understanding of AMPAR transport by delineating a mechanism in which neuronal activity up- and downregulates the quantity and dynamics of AMPAR transport.

Increased ROS levels within physiological range modulate activity-dependent changes in cytoplasmic calcium

A growing field of evidence shows that calcium-dependent signaling is modified or co-regulated by ROS (Görlach et al., 2015). Additionally, several studies have shown that neural excitability and synaptic plasticity are modified by ROS signaling (Kishida and Klann, 2006; Yermolaieva et al., 2000). More recently, a few studies have shown that function of VGCCs, including the L-type, are altered by increases in ROS above physiological concentrations (Dang et

al., 2018; Todorovic and Jevtovic-Todorovic, 2014). However, we have a poor understanding of if and how physiological ROS signaling impacts activity-dependent fluctuations in neuronal calcium levels. Given this gap in knowledge and the growing interest in how calcium and ROS signaling act to regulate neuronal excitation, we tested whether slight perturbations of ROS produce observable changes in cytoplasmic calcium levels and the resultant signaling. First, using cell-specific expression of the genetically encoded, fluorescent calcium indicator GCaMP6f (Akerboom et al., 2013), we were able to visualize calcium transients *in vivo* in the soma of AVA (Figure 2.2 A and B). Using this technique, we observe temporal dynamics (i.e. transient frequency and duration) of calcium transients similar to previous reports (Gordus et al., 2015; Larsch et al., 2013).

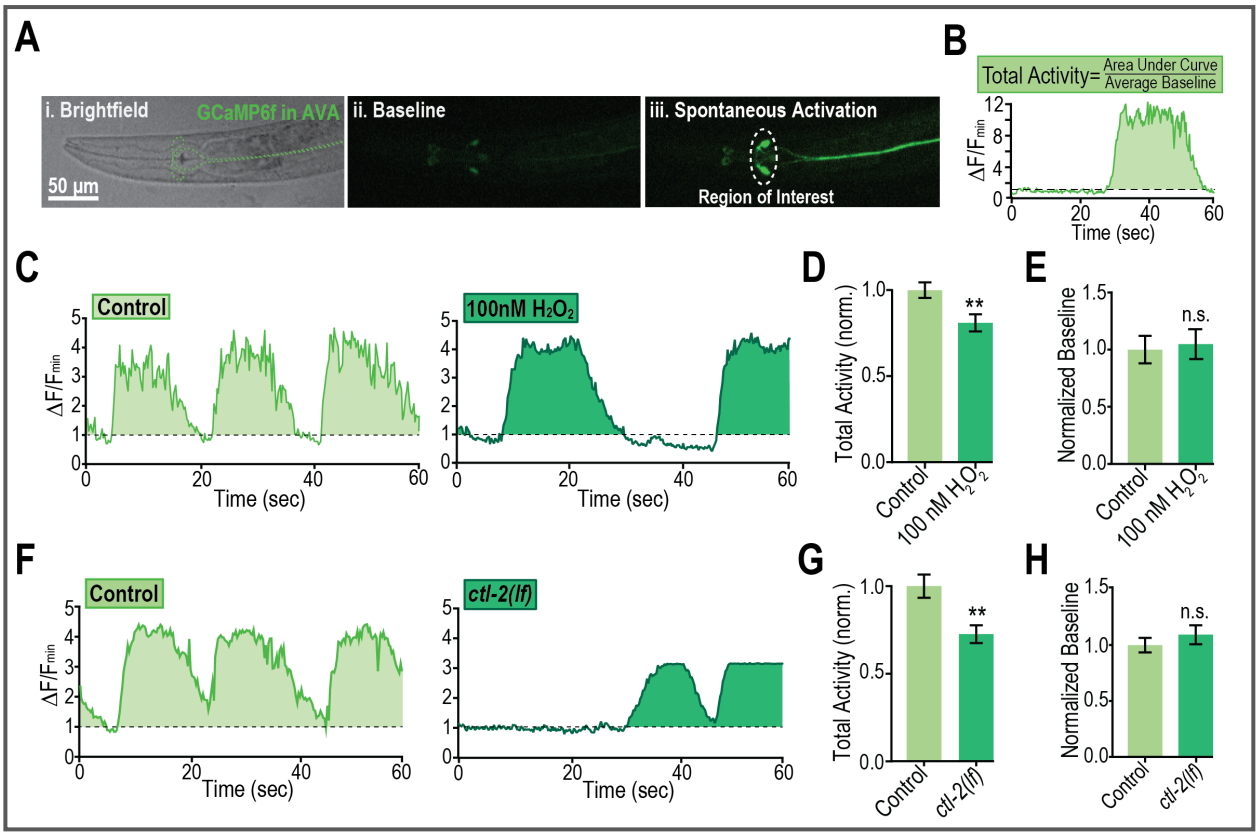

Figure 2.2 - Physiological increase in ROS leads to decreased activity-dependent fluctuations in somatic calcium. A) Brightfield and fluorescent confocal images of the ventral side of a *C. elegans* expressing GCaMP6f in the AVA interneuron. Scale bar = 50 µm. B) GCaMP6f $\Delta F/F_{min}$ over time. Grey dashed line represents baseline threshold (30% of minimum fluorescence value).

Figure 2.2 – B) Fluorescence values above that threshold are summed (area under the curve for all peaks) and normalized to the average baseline value (F_{min}) to calculate total activity during the 60 second recording. For all GCaMP experiments, all groups express GCaMP6f in AVA and are referred to as "control" if no additional H_2O_2 treatment or mutation was added. C) Representative traces of somatic GCaMP6f fluorescence in AVA interneurons for 60 seconds normalized to baseline fluorescence ($\Delta F/F_{min}$) from control (n=56) and 100 nM H_2O_2 treated (n=58) animals. Dashed line = F_{min}. D) Total activity of GCaMP normalized to untreated controls (**: p=0.006). E) Average fluorescence baseline of controls and H_2O_2 treated animals normalized to control group (n≥50, n.s. = not significant). F) Representative traces of somatic GCaMP6f fluorescence in AVA interneurons for 60 seconds, normalized to baseline fluorescence in control (n=50) and catalase mutants (*ctl-2(lf)*, n=51). Dashed line = F_{min}. G) Total activity normalized to controls (**: p=0.001). H) Average fluorescence baseline of controls and catalase mutants normalized to controls (n≥50, n.s. = not significant).

To determine if cytoplasmic calcium is impacted by hydrogen peroxide (H_2O_2), the most stable and common form of endogenous ROS in cells (Bienert et al., 2006), we subjected wild-type worms expressing GCaMP6f in the AVA to a 5-minute pretreatment of 100 nM H_2O_2 prior to imaging. With this technique, we determined that acute treatment with a H_2O_2 concentration within the physiological range (10-100 nM; Sies, 2017) decreased the total GCaMP activity to 80.9% ± 0.07 of that of untreated controls (n>55 for each group, p=0.006, Figure 2.2 C and D).

Furthermore, we saw no effect of H_2O_2 treatment on baseline fluorescence (Figure 2.2 E), indicating that the modest increase in ROS due to this treatment does not detectably change the fluorescence properties of GCaMP itself or basal calcium levels. We conclude that an acute increase in H_2O_2 decreases the total amount of cytoplasmic calcium over the recording time (60 seconds) without drastically modifying the amplitude of the changes in cytoplasmic calcium in the cell body of AVA. We sought additional evidence by using a genetic strategy to increase intracellular H_2O_2. To this end, we obtained a strain harboring a loss-of-function mutation in the gene encoding the primary *C. elegans* catalase (*ctl-2*), which decomposes approximately 80% of all intracellular H_2O_2 to water, including in neuronal tissue (Petriv and Rachubinski, 2004). In these catalase mutants, total GCaMP activity is significantly decreased (27.4% ± 0.08 lower, p=0.001; Figure 2.2 F and G). Again, the baseline of GCaMP fluorescence in *ctl-2(lf)* was not different than in control animals (Figure 2.2 H). These results support that both acute and chronic

increases in H_2O_2 within the physiological range attenuate activity-dependent increases in cytoplasmic calcium in *C. elegans* neurons. Based on the identified regulatory role of calcium on GLR-1 transport, we then hypothesized that these same modest increases in ROS may affect GLR-1 transport and delivery to synapses.

Physiological ROS signaling regulates AMPAR transport and delivery to synapses

To test if ROS levels impact GLR-1 transport, we quantified GLR-1 transport as previously described following a 5-minute pretreatment with 10, 50 or 100 nM H_2O_2 in which animals swam freely before imaging in the same H_2O_2-containing solution. We found that worms treated with H_2O_2 had significantly fewer AMPAR transport events ranging from 14.65 ± 1.59 events at 10 nM H_2O_2 to 11.35 ± 1.14 at 100 nM H_2O_2 (compared to 23.0 ± 1.09 events in untreated animals, n=22, $p<0.0001$, Figure 2.3 A and 3B). Given, that all treatments affected GLR-1 transport to a similar degree, we used 50 nM of H_2O_2 in all following experiments. In addition, quantification of GLR-1 transport in *ctl-2(lf)* mutants revealed a significant decrease in GLR-1 transport events (12.3 ± 1.10 events per kymograph, n=28, $p=0.0012$, compared to 19.0 ± 1.71 events in controls, n=20, Figure 2.3 C and D). The H_2O_2 treatment also led to significantly decreased anterograde transport velocities (1.31 ± 0.02 μm/sec, n=107 events, $p<0.0001$) compared to untreated controls (1.52 ± 0.03 μm/sec, n= 90 events, Figure 2.3 E and F). The *ctl-2(lf)* mutation caused a 17% decrease in anterograde transport velocity (1.10 ± 0.02 μm/sec, n=107 events, $p<0.0001$) compared to controls (1.33 ± 0.02 μm/sec, n=59, Figure 2.3 G and H). Neither H_2O_2 treatment nor *ctl-2(lf)* altered retrograde transport velocity (data not shown), so remaining velocity analyses were focused on that of anterograde transport. In addition, the percent of time GLR-1 containing vesicles spent paused was decreased by these modest elevations in ROS levels ($p<0.0001$, Figure 2.3 I and J). Thus, both acute and chronic increase of H_2O_2 lead to decreased

transport of GLR-1 containing vesicles to and from the cell body, as would be predicted by our observations of decreased somatic calcium in response to modest ROS elevations. Furthermore,

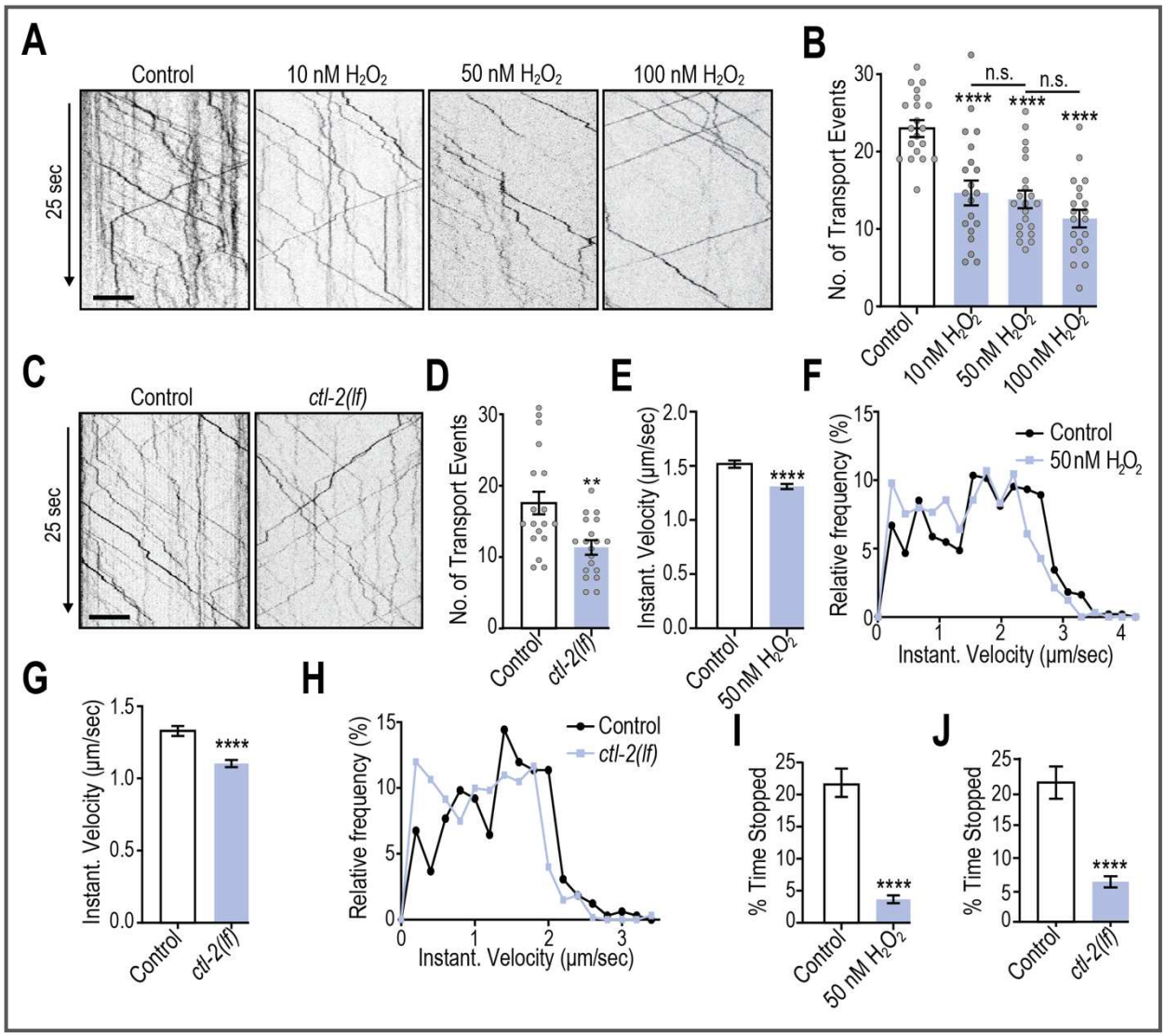

Figure 2.3 - Physiological increase in ROS levels cause decreased GLR-1 transport and alters transport dynamics. For all transport experiments, each group is expressing SEP::mCherry::GLR-1 in the *glr-1(ky176)* background and groups not subject to H_2O_2 treatment or additional mutations are referred to as "controls". A) Representative kymographs from controls, 10, 50 and 100 nM H_2O_2 treated worms. Scale bar = 5 µm. B) Quantification of total transport events from 50 second recordings from control (n=22), 10 (n=20), 50 (n=21), and 100 nM H_2O_2 treated (n=22) worms (****: p<0.0001, n.s.=not significant). C) Representative kymographs from controls and *ctl-2(lf)* mutants. D) Quantification of total transport events in controls (n=21) and *ctl-2(lf)* (n=28, **: p=0.0012). E and G) Instantaneous velocity analysis of anterograde transport events in (E) control and 50 nM H_2O_2 treated worms (n>90 events; ****: p<0.0001 compared to controls) or (G) controls and *ctl-2(lf)* mutants (n>50 events; ****: p<0.0001 compared to controls). F and H) Frequency distribution of the anterograde instantaneous velocities (binned every 0.2 µm/sec) in F) controls and 50 nM H_2O_2 treated worms or H) controls and *ctl-2(lf)* mutants. I and J) Percent of time GLR-1 vesicles spent stopped in each group (****: p<0.0001 compared to controls).

these slight increases in ROS were sufficient enough to alter the normal characteristics of vesicle transport including transport velocity as well as the frequency and/or duration of stops along the neuronal process.

Altogether, these changes in GLR-1 transport could impact GLR-1 delivery and exocytosis at synapses. To test this hypothesis, we turned to fluorescence recovery after photobleaching (FRAP) using GLR-1 tagged with mCherry and SEP (a pH-sensitive for of GFP) at the N-terminus (Figure 2.4 A) as previously described (Hoerndli et al., 2013; Kennedy et al., 2010). We monitored recovery of mCherry signal from the dual tagged GLR-1 after bleaching to quantify new delivery of GLR-1 to synaptic sites in the proximal region of the AVA processes. SEP fluorescence, on the other hand, is quenched while in acidic endosomes and therefore protected from photobleaching (Hoerndli et al., 2015; Kennedy et al., 2010), meaning its signal is revealed once released to the membrane providing a measure of exocytosis of GLR-1-containing receptors to synapses (Figure 2.4 A). Worms were again pretreated for 5 minutes with 50 nM H_2O_2 then immediately mounted for imaging without any change in solution. During treatment, the rate of GLR-1 delivery was significantly decreased (as determined by the nonlinear fit of the percentage of fluorescence recovery throughout the 16 minutes following photobleaching, n=10, p=0.0011) in comparison to untreated controls (n=10, Figure 2.4 B and C). Similar to the acute H_2O_2 treatment, *ctl-2(lf)* also led to a significant reduction in the rate of synaptic GLR-1 delivery (n=10, p<0.0001, Figure 2.4 B and C). This decrease in delivery could in part be due to the decreased time in which transported vesicles are stopped when ROS is elevated (Figure 2.3 I and J), which likely perturbs the ability to be delivered to synaptic sites. Together, these results show that even a modest, acute elevation of ROS can lead to decreased GLR-1 delivery at synapses.

The efficacy of excitatory neurotransmission is determined in part by the number of AMPARs at the surface of synapses (Henley and Wilkinson, 2016; Huganir and Nicoll, 2013) and although ROS elevation decreased GLR-1 delivery to synapses, it may not affect exocytosis rates or the number of receptors at the synaptic membrane. To determine if this is the case, we quantified the SEP signal following GLR-1 photobleaching in both acute and genetic conditions of ROS elevation. Interestingly, the exocytosis rate of GLR-1 seemed to be unaffected by acute H_2O_2 treatment whereas *ctl-2(lf)* significantly decreased GLR-1 exocytosis rates (n=10 for all groups, $p<0.0001$, Figure 2.4 D and E). This difference in SEP recovery suggests that acute and chronic ROS elevation differentially affect GLR-1 exocytosis at synapses. Chronic ROS elevation could lead to sustained decreases in GLR-1 delivery resulting in a time-dependent depletion of the synaptic reserves required for the GLR-1 exocytosis. If true, then a marked decrease in SEP::mCherry::GLR-1 signal at steady state in *ctl-2(lf)* mutants would be expected. Surprisingly, measurements of SEP::mCherry::GLR-1 fluorescence along the neuronal process before FRAP in *ctl-2(lf)* and controls did not show a significant change in mCherry or SEP signal (data not shown). We postulate that the overexpression of GLR-1 necessary to follow single vesicle dynamics might mask changes in steady state levels of synaptic AMPARs.

To quantify the effect of physiological elevation of ROS levels in *ctl-2(lf)* mutants on global glutamatergic circuit function and circumvent potential overexpression issues of the SEP::mCherry::GLR-1 in AVA, we turned to behavioral analysis. The spontaneous reversal of *C. elegans* animals has been shown to reflect the function and number of synaptic GLR-1 receptors (Burbea et al., 2002; Monteiro et al., 2012; Park et al., 2009; Zheng et al., 1999). In addition, AVA activation has been shown to be essential for spontaneous reversals (Ben Arous et al., 2010; Gray et al., 2005). Thus, we obtained reversal data for *ctl-2(lf)* and found that *ctl-2(lf)*

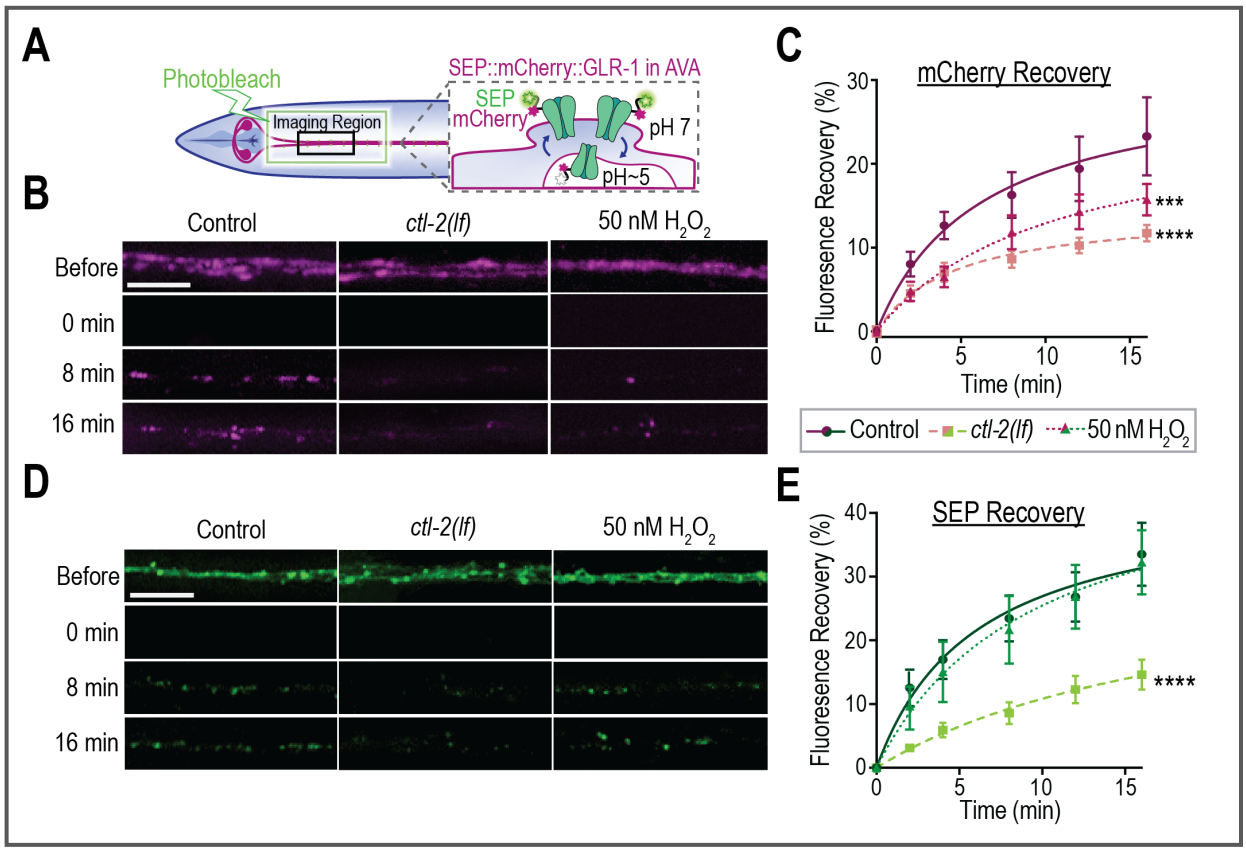

Figure 2.4 - Physiological increase in ROS cause decreased GLR-1 delivery and exocytosis to synapses
A) Illustration of imaging location of fluorescence recovery after photobleaching (FRAP) in the AVA interneurons expressing GLR-1 tagged with SEP, a pH-sensitive GFP, and mCherry. All experimental groups express this dual tagged GLR-1 in the AVA in the *glr-1(ky176)* background. Groups that were not subject to H_2O_2 treatment or additional mutations are referred to as "control". B) Representative maximum projections of the mCherry fluorescence in the AVA interneurons before, immediately after (0 min), 8 and 16 minutes after photobleaching of the imaging region. Scale bar = 5 µm. C) Percent recovery of mCherry fluorescence after photobleaching over time in control, untreated *ctl-2(lf)*, and 50 nM H_2O_2 treated worms (n=10 for each group, **: p=0.001, ***: p<0.0001 compared to controls). D) Representative maximum projections of the SEP fluorescence in the AVA interneurons before, immediately after, 8 and 16 minutes after photobleaching of the imaging region. Scale bar = 5 µm. E) Percent recovery of SEP fluorescence compared to before photobleaching from the same worms as in Figure 2.4 C (***: p<0.0001 compared to controls).

mutants exhibited fewer spontaneous reversals (1.37 ± 0.19 reversals per minute, p<0.0001, n=38) compared to controls (3.78 ± 0.26, n=37, data not shown). This behavioral change supports our calcium imaging data in which the total spontaneous activity of AVA is decreased in *ctl-2(lf)*. Altogether, our results clearly show that modest ROS elevation is sufficient to modify synaptic GLR-1 transport, delivery and, with chronic elevations, exocytosis to synapses ultimately affecting glutamatergic circuit function.

Increased ROS modulate GLR-1 transport at or directly downstream of L-type VGCC

Our results indicate that modest increases in ROS (within the physiological range for neurons; Sies, 2017) decrease the activity-dependent fluctuations in cytoplasmic calcium in the AVA interneurons of *C. elegans* (Figure 2.2). This results in decreased GLR-1 transport into and out of the cell body as well as decreased anterograde transport velocity and time vesicles spent stopped along the neurite (Figure 2.3). Together, these changes in transport likely contribute to decreased delivery and, in the case of prolonged elevations in ROS, exocytosis of GLR-1 at synapses (Figure 2.4). To add clarity, we investigated mechanisms by which excess ROS decreases cytoplasmic calcium, CaMKII activation, and therefore GLR-1 transport.

Our data presented above suggest a regulatory signaling pathway (Figure 2.5 A), in which depolarization of AVA via glutamate receptor activation leads to calcium influx through VGCCs to activate CaMKII. This model led us hypothesize that elevated ROS could be affecting calcium signaling needed for CaMKII activation. We used a genetic epistasis strategy to test whether this is a linear pathway in which ROS function upstream of CaMKII activation to modulate GLR-1 transport. We made double mutants with *unc-43(lf)* and *ctl-2(lf)* as well as *unc-43(gf)* and *ctl-2(lf)*. If ROS are acting upstream of CaMKII activation, then one would predict that *unc-43(gf/lf); ctl-2(lf)* double mutants would be similar to the single *unc-43* mutations alone as the modest decrease in calcium due to *ctl-2(lf)* would not affect the activation of calcium-independent CaMKII in the *unc-43(gf)* mutants.

To test this, we analyzed mCherry::GLR-1 transport and again observed that *ctl-2(lf)* alone decreases GLR-1 transport, but interestingly, the addition of the *ctl-2(lf)* to *unc-43(lf or gf)* mutations does not change the amount of transport compared to *unc-43* mutations alone (Figure 2.5 B and C). Analysis of anterograde transport velocity and stopping in the *unc-43(gf)* mutants

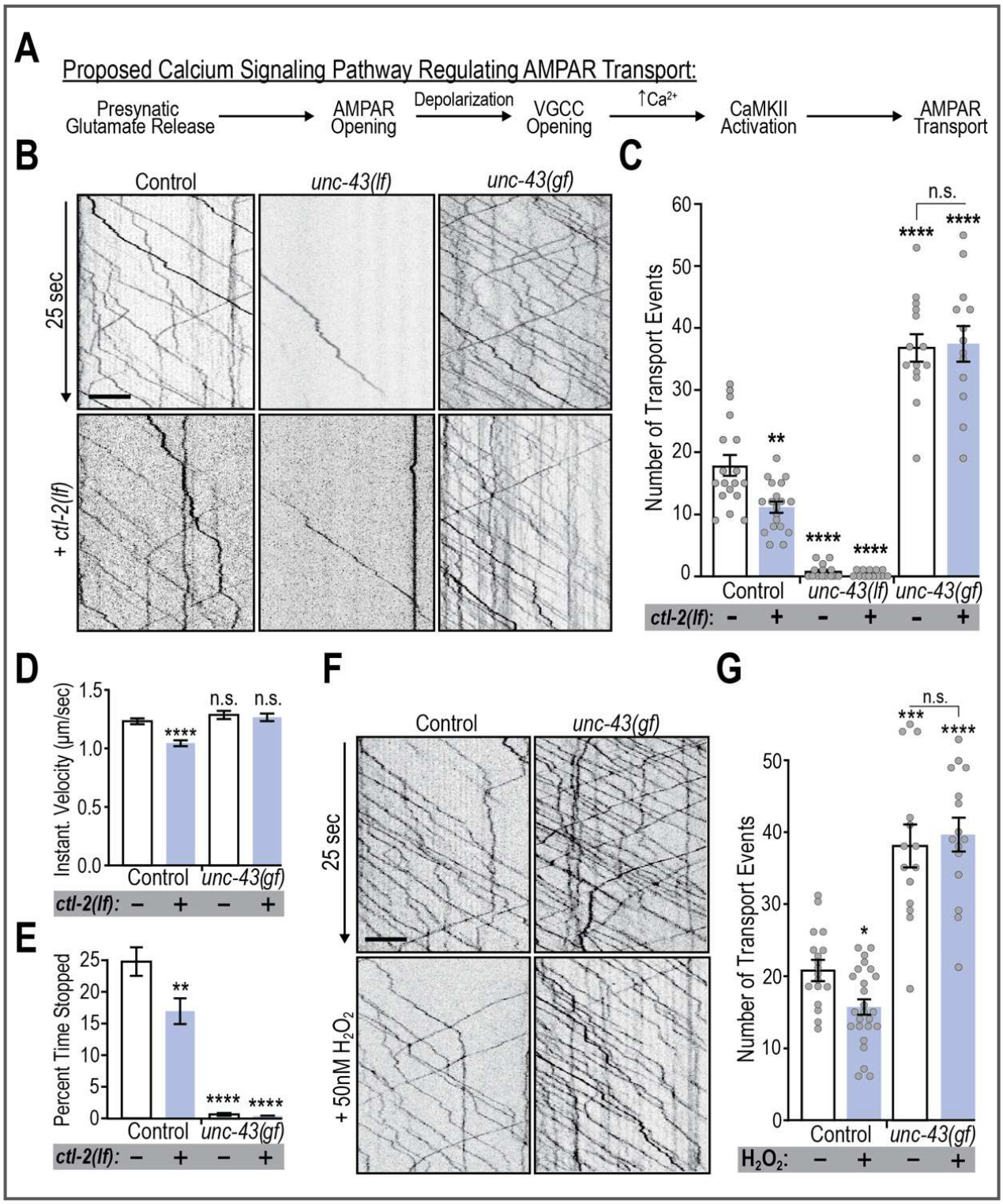

Figure 2.5 - Increased ROS acts on GLR-1 transport upstream of CaMKII activation. A) Previously proposed model of an activity-dependent calcium signaling pathway regulating AMPAR transport (Hoerndli et al., 2015). All experimental groups express SEP::mCherry::GLR-1 in the *glr-1(ky176)* background.

Figure 2.5 - B) 25 seconds of representative kymographs from each experimental group. Scale bar = 5 μm. C) Quantification of transport events from full-length kymographs (50 s) in control, *unc-43(lf)*, and *unc-43(gf)* without (-, white bars) and with (+, blue bars) the *ctl-2(lf)* mutation (n≥13; n.s.=not significant, **: p=0.0012, ****: p<0.0001 compared to controls lacking the *ctl-2(lf)* mutation). D) Instantaneous velocity of anterograde transport for the same animals from part B and C (n>60 events, ****: p<0.0001 compared to controls lacking the *ctl-2(lf)* mutation). E) Percent of time GLR-1 vesicles spent stopped in these same genotypes (n>60 events, **: p=0.009, ****: p<0.0001 compared to controls lacking the *ctl-2(lf)* mutation). F) 25 seconds of representative kymographs from each experimental group. Scale bar = 5 μm. G) Quantification of transport events in control or *unc-43(gf)* with (+, blue bars) or without (-, white bars) 50 nM H_2O_2 treatment (n≥14; *: p=0.025, ***: p=0.0002, ****: p<0.0001 compared to untreated control).

mirror these results in that the velocity and stopping is the same in the *unc-43(gf); ctl-2(lf)* as in the *unc-43(gf)* single mutant (Figure 2.5 D and E). It is interesting to note that the addition of the *ctl-2(lf)* mutation to *unc-43(gf)* did not affect transport velocity when compared with *unc-43(gf),* which indicates that modest ROS elevation likely does not lead to global perturbations of cellular processes which would indirectly affect molecular motor-dependent activity. To determine whether this is unique to *ctl-2(lf),* we also treated *unc-43(gf)* animals with 50 nM H_2O_2 prior to imaging transport. Similar to *ctl-2(lf)*, acute treatment with H_2O_2 had no effect on the *unc-43(gf)* mediated increase in GLR-1 transport (Figure 2.5 F and G). Together, these data indicate that ROS signaling regulates GLR-1 transport upstream of CaMKII activation.

To pinpoint potential targets of ROS upstream of CaMKII activation, we next investigated L-VGCCs, which we have shown to play an important role in regulating GLR-1 transport events and delivery (Figure 2.1). To determine if L-VGCCs or downstream calcium signaling is a target of ROS modulation, we used a genetic epistasis approach. We made double mutants with *ctl-2(lf)* and either *egl-19(rf)* or *egl-19(gf),* then analyzed GLR-1 transport. These analyses reveal that the amount of GLR-1 transport in *egl-19(rf); ctl-2(lf)* is not significantly different from *egl-19(rf)* (Figure 2.6 A and B). However, *egl-19(gf); ctl-2(lf)* mutants have significantly decreased GLR-1 transport events in comparison to *egl-19(gf)* alone (13.9 ± 1.17 vs 26.7 ±1.76

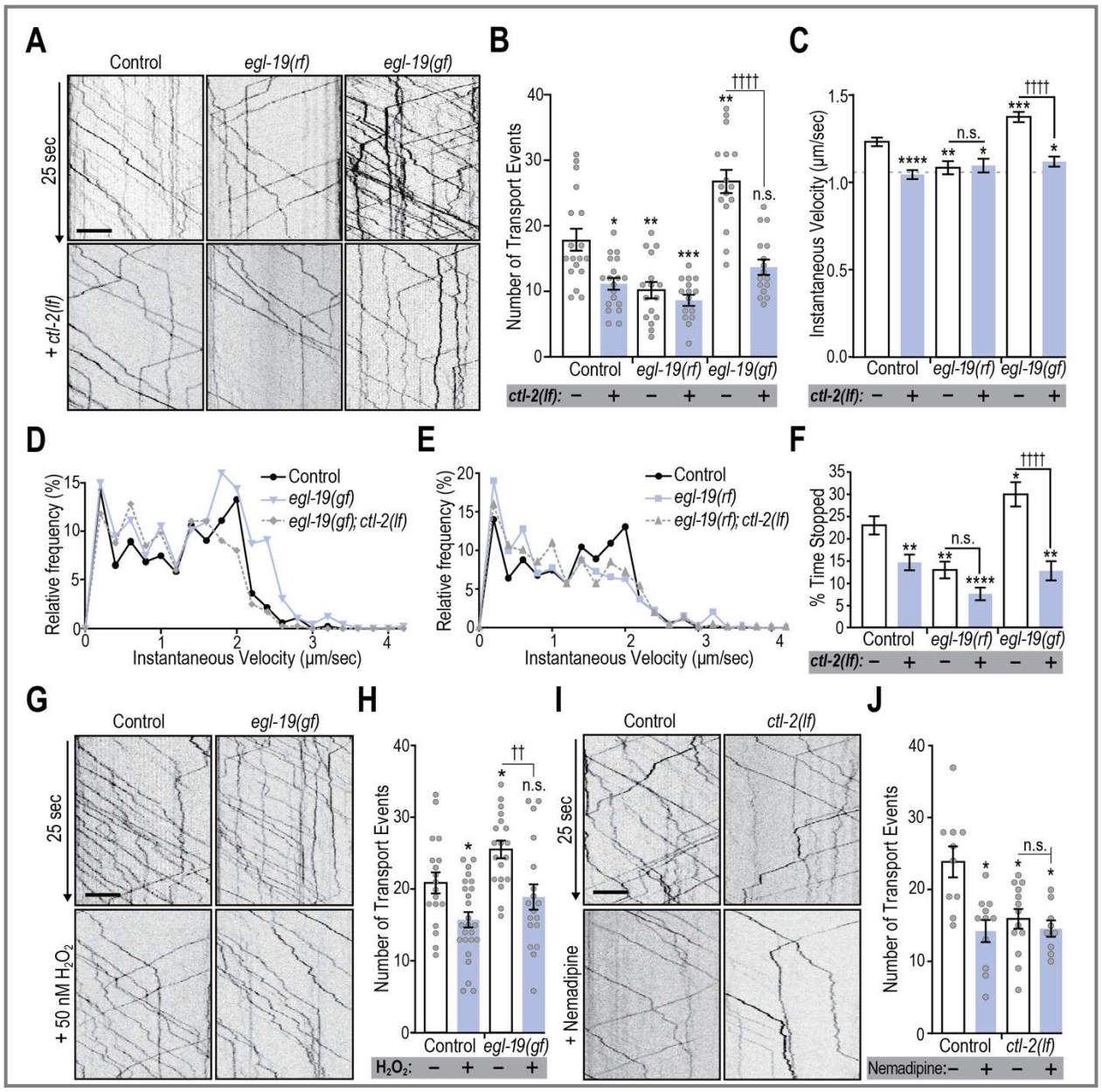

Figure 2.6 - ROS decrease GLR-1 transport numbers and alter transport dynamics by acting on or downstream of L-VGCC. All experimental groups express SEP::mCherry::GLR-1 in the *glr-1(ky176)* background. A, G and I) 25 seconds from representative kymographs from each experimental group. Scale bar = 5 µm. B) Quantification of transport events from controls, *egl-19(rf)*, or *egl-19(gf)* without (-, white bars) or with (+, blue bars) the *ctl-2(lf)* mutation (n≥15; n.s.=not significant, *: p=0.012,**: p=0.007, ***: p=0.0005, compared to controls lacking the *ctl-2(lf)* mutation; ††††: p<0.0001 compared to *egl-19(gf)* alone). C) Instantaneous velocity of anterograde transport events in each group (n≥44 events, n.s.=not significant, *: p<0.05, **: p=0.0035, ***: p=0.0005, ****: p<0.0001 compared to controls lacking the *ctl-2(lf)* mutation; ††††: p<0.0001 compared to *egl-19(gf)* alone). D and E) Frequency distribution of instantaneous velocity (binned every 0.2 µm/sec) of anterograde transport events for *egl-19(gf)* single and double mutants (D) as well as *egl-19(rf)* single and double mutants (E) in comparison to controls lacking *ctl-2(lf)*. F) Percent of time each GLR-1 vesicles spent stopped for each group (n≥44 events, *: p=0.044, **: p≤0.009, ****: p<0.0001 compared to controls lacking *ctl-2(lf)*; ††††: p<0.0001 compared to *egl-19(gf)* alone).

Figure 2.6 - H) Quantification of transport events from controls and *egl-19(gf)* without (-, white bars) or with (+, blue bars) 50 nM H_2O_2 treatment (n≥18; *: p≤0.038 compared to untreated controls; ††: p=0.007 compared to untreated *egl-19(gf)*). J) Quantification of transport events in controls and *ctl-2(lf)* with (+, blue bars) and without (-, white bars) 10 μM nemadipine treatment (n>10; *: p<0.05 compared to untreated controls).

respectively, n=16, p<0.0001, Figure 2.6 A and B). In fact, the double mutant was not significantly different than *ctl-2(lf)* alone (11.2 ± 0.91 events, n=19, p=0.42, Figure 2.6 A and B). Quantification of the anterograde velocity and stopping of transport events in these strains further support the idea that ROS affect calcium signaling at or just downstream of L-VGCCs. In the *egl-19(gf)* mutant, instantaneous velocity of anterograde transport is increased compared to controls (1.37 ± 0.03 vs 1.23 ± 0.02 μm/sec, n>40 events, p=0.0005, Figure 2.6 C and D). When combined with *ctl-2(lf)*, anterograde transport velocity is decreased to around that of the *ctl-2(lf)* mutation alone (1.12 ± 0.03, n=43, vs 1.04 ± 0.02, n=82, p=0.66, Figure 2.6 C and D). The percent of time GLR-1 vesicles spent stopped along the neuronal process was increased in the *egl-19(gf)* mutants (stopped 29.9% ± 2.72 of time, n=96) compared to controls (20.8% ± 1.86, n=95, p=0.044; Figure 2.6 F). When combined with *ctl-2(lf),* stopping was drastically decreased compared to *egl-19(gf)* alone (11.65% ± 1.94, n=44, p<0.0001) and controls (20.88% ± 1.86, n=89, p=0.015, Figure 2.6 F). These data suggest that elevated ROS change transport velocity and stopping throughout the neurite via decreased calcium. If true, then we hypothesized that transport velocity and stopping should be decreased in the *egl-19(rf)* mutant.

Similar to our quantification of GLR-1 transport numbers, the transport velocity of *egl-19(rf)*, is decreased compared to controls (1.08 ± 0.04 μm/sec, n=86, p=0.0001) and is unaffected by the addition of the *ctl-2(lf)* mutation (Figure 2.6 C and E). The percentage of time vesicles were stopped was also decreased in *egl-19(rf)* mutants (14.93% ± 2.15, n=79, p=0.001; Figure 2.6 F). However, in contrast to our velocity results, we observed a slight, but not significant decrease in stopping with the addition of *ctl-2(lf)* (8.7% ± 1.60, n=67, p=0.43, Figure 2.6 F). These

data indicate that the *ctl-2(lf)* mutation is acting in the same pathway as *egl-19* to regulate GLR-1 transport. To ensure that these results are due to elevated ROS levels and not developmental effects of *ctl-2(lf),* we also treated *egl-19(gf)* animals with 50 nM H_2O_2. As previously observed, H_2O_2 treatment of control animals reduced the amount of GLR-1 transport and reduced *egl-19(gf)* transport to the same level as H_2O_2 alone (26.11 ± 1.15 vs 18.9 ± 1.76 events, n>18, Figure 2.6 G and H). To eliminate the possibility of these results being caused by developmental changes in the *egl-19(gf/rf)* mutants, we also analyzed GLR-1 transport in control and *ctl-2(lf)* mutants following treatment with the L-VGCC blocker, nemadipine. As we previously showed, a 10 μM nemadipine treatment significantly reduced the total amount of GLR-1 transport (14.36 ± 1.53 events, n=11, compared to controls 24.00 ± 2.15 events, n=10; p=0.008; Figure 2.6 I and 6J). However, nemadipine treatment did not further reduce transport in *ctl-2(lf)* mutants (14.56 ± 1.13 events, n=9, in nemadipine-treated animals compared to 15.92 ± 1.38 events, n=13, in untreated controls; Figure 2.6 I and 6J). Altogether, these observations suggest that ROS elevation is affecting L-VGCC/EGL-19 dependent calcium signaling.

To obtain additional insight into how ROS modulate GLR-1 transport and delivery, we combined FRAP of SEP::mCherry::GLR-1 and our genetic epistasis strategy (Figure 2.7). We quantified synaptic delivery of GLR-1 using FRAP of mCherry signal (Figure 2.7 A and B) and synaptic exocytosis using FRAP of SEP signal (Figure 2.7 C and D) in single *egl-19(rf)* or *egl-19(gf)* mutants and when doubled with *ctl-2(lf)*. Similar to our GLR-1 transport results, quantification of mCherry and SEP FRAP showed that the rate of GLR-1 delivery and exocytosis is decreased in *egl-19(rf)* mutants and addition of *ctl-2(lf)* causes no change in those rates (n=10, Figure 2.7). Alternatively, the FRAP of mCherry in *egl-19(gf); ctl-2(lf)* is reduced compared to *egl-19(gf),* but not identical to *ctl-2(lf)* (Figure 2.7 B) as is the case with the FRAP of SEP in these

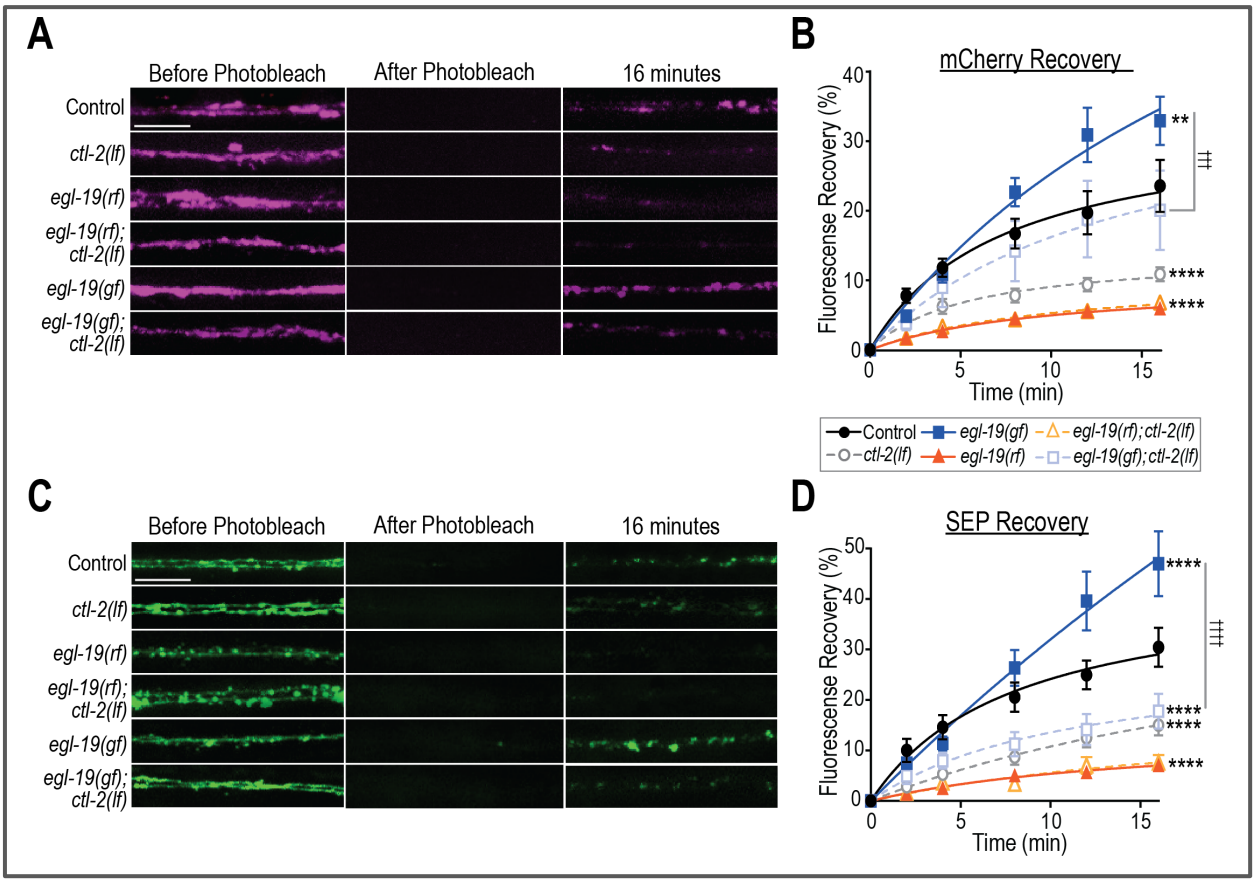

Figure 2.7- ROS decrease GLR-1 synaptic delivery and exocytosis by acting on or downstream of L-VGCC.
All experimental groups express mCherry::SEP:: GLR-1 in the AVA in the *glr-1(ky176)* background. Groups without additional mutations are referred to as "control". A) Representative maximum projections of the mCherry fluorescence in the AVA interneurons before, immediately after and 16 minutes after photobleaching of the imaging region from each experimental group. Scale bar = 5 µm. B) Recovery of mCherry fluorescence following photobleaching in control, *egl-19(rf)* and *egl-19(gf)* with (dashed curves) and without (solid curves) *ctl-2(lf)* (n≥8; **: p=0.003, ****: p<0.0001 compared to controls; †††: p=0.0001 compared to *egl-19(gf)* single mutant). C) Representative maximum projections of the SEP fluorescence in the same groups. Scale bar = 5 µm. D) SEP fluorescence recovery in the same experimental groups (****: p<0.0001 compared to controls; ††††: p<0.0001 compared to *egl-19(gf)*).

genotypes (Figure 2.7 D). These results suggest that ROS not only modulate GLR-1 transport, but also delivery and exocytosis by affecting the signaling cascade initiated by calcium influx through L-VGCC/EGL-19.

Our data provide a better understanding of the mechanism by which activity-dependent calcium signaling regulates AMPAR transport to ultimately affect synaptic delivery and

exocytosis of AMPARs. We go on to show that L-VGCCs play a central role in regulating cytoplasmic calcium dynamics and that this process is modified by ROS. This leads to our suggested model (Figure 2.8) in which physiological elevations of ROS can modulate synaptic GLR-1 transport at the soma and in the dendritic process by modifying calcium signaling originating to a large extent from L-VGCCs.

2.2E Conclusion and Discussion

Activity-dependent calcium signaling is required for AMPAR transport in vertebrate and *C. elegans* glutamatergic neurons (Hangen et al., 2018; Hoerndli et al., 2015). Here we show that in *C. elegans*, calcium influx mediated by L-VGCC/EGL-19 is not only required, but that the magnitude of calcium influx directly corresponds to changes in AMPAR transport to and from the cell body as well as AMPAR transport dynamics within neuronal processes. Furthermore, we

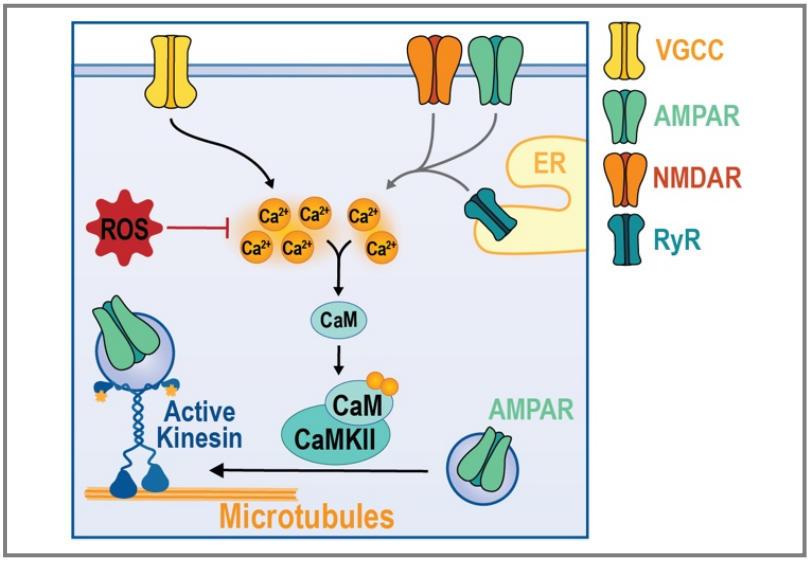

Figure 2.8 - Proposed ROS signaling effect on GLR-1 transport.
Model showing that increases in ROS inhibit the activity-dependent changes in cytoplasmic calcium which occurs mostly due to calcium influx through L-VGCC (yellow channel, VGCC), but also AMPAR (green channel) and NMDARs (orange channel). Intracellular release of calcium, such as from the ER via ryanodine receptors (blue channel, RyR), can also contribute to cytoplasmic elevations in calcium. Therefore, decreased cytoplasmic calcium limits calmodulin (CaM) binding and activation of CaMKII reducing the number of AMPAR transport and delivery to synapses.

show that physiological increases in ROS decrease somatic calcium signaling (Figure 2.2) causing a subsequent decrease in somatic AMPAR export and synaptic delivery (Figure 2.3). This study reveals a physiological interplay between ROS and calcium signaling that directly affects AMPAR transport and delivery (Figure 2.8). It also prompts fundamental questions regarding how AMPAR transport is regulated by activity in a spatially specific manner, such as how do somatic vs local dendritic calcium signaling pathways regulate AMPAR transport and what are their effects on synaptic function and plasticity?

Long-distance AMPAR transport is one of the least characterized components of the multistep trafficking of AMPAR from the cell body to the periphery (Henley and Wilkinson, 2016). It is clear that transport requires molecular motors, including kinesin-1 (Hoerndli et al., 2013; Kim and Lisman, 2001; Setou et al., 2002), and is regulated by neuronal activity and CaMKII (Esteves da Silva et al., 2015; Hangen et al., 2018; Hoerndli et al., 2015). However, we do not understand the roles of other key players required for activity-dependent regulation and at which steps (i.e. cargo loading, transport, delivery and removal) they act. Consistent with previous reports (Hoerndli et al., 2015), we show decreased somatic export of AMPARs in mutants with reduced L-VGCC function or after treatment with the L-VGCC blocker, nemadipine (Figure 2.1 and 6). On the contrary, increased calcium influx in gain-of-function L-VGCC mutants leads to more AMPAR transport demonstrating that activity-dependent calcium influx through L-VGCCs bidirectionally regulates AMPAR transport out of the cell body (Figure 2.1).

Once motors and cargoes have entered the dendrites, they are subject to the conditions of those compartments. For instance, GLR-1 transport in the AVA neurite is bidirectional and heterogenous, displaying increased stopping probabilities at synaptic localizations of GLR-1 (Hoerndli et al., 2013). Several studies suggest that stopping of transport vesicles correlate with

delivery of AMPARs to synapses (Hangen et al., 2018; Hoerndli et al., 2013), but it is unclear how that is regulated and if vesicular stops affect synaptic delivery. Here, we demonstrate that manipulations of calcium influx through L-VGCC modify AMPAR transport dynamics, such as stops and velocity profiles (Figure 2.1), and lead to changes in synaptic delivery (Figure 2.7). We show that decreased calcium influx through L-VGCCs decreases anterograde velocity and stopping of AMPAR-containing vesicles within the neurite. Conversely, increasing calcium influx through L-VGCC led to increased anterograde velocities and stops (Figure 2.1). Decreased velocity and stopping corresponds to less GLR-1 delivery and insertion to synapses whereas higher velocities and stops correspond to higher delivery and insertion (Figure 2.1 and 7), which is consistent with previous findings (Hangen et al., 2018; Hoerndli et al., 2013) and demonstrates that regulation of AMPAR transport dynamics in dendrites is a key factor in controlling AMPAR delivery and synaptic function. Interestingly, there is a drastic decrease in stop frequency in *unc-43*(gf) mutants suggesting that stop frequency of GLR-1 transport could be mediated by calcium-dependent changes in CaMKII activity. Taken together, these results provide evidence for a model in which calcium signaling controlled by L-VGCCs and CaMKII regulate AMPAR transport into and out of the cell body as well as in the dendritic process in an activity-dependent manner.

The AVA interneurons have long, relatively flat processes in the ventral cord that enable high-resolution, time-lapse imaging and cell specific expression using the AVA-specific promoters rig-3 and flp-18. Although powerful, this analysis is limited to AVA interneurons which leaves open the possibility that other glutamatergic neurons, such as those with specific compartmentalized calcium signaling (Hendricks et al., 2012), might have different ROS sensitivity thresholds or regulatory mechanisms. However, our results using this approach concur with

studies using vertebrate neurons in which long-term increases in dendritic calcium increased the amount of AMPAR transport and delivery (Hangen et al., 2018). Nevertheless, our data is a new, *in vivo* demonstration of activity-dependent calcium signaling bidirectionally regulating AMPAR transport throughout the neuron, determining transport vesicle numbers, dynamics and delivery at synapses at short and long timescales.

Importantly, gain- or loss-of-function CaMKII mutants have a much stronger effect on GLR-1 somatic export than L-VGCC mutations alone. This could be due to the mutations in L-VGCCs not being a complete loss- or gain-of-function. However, it could also suggest that additional signaling pathways converge onto CaMKII to regulate GLR-1 somatic export. These signaling pathways could involve other calcium sources (i.e. NMDAR and ryanodine receptors) or other signaling cascades such as those involving protein kinase A/C or mitogen-activated protein kinase (Boehm et al., 2006; Eales et al., 2014; Ren et al., 2013; Tang and Yasuda, 2017; Zheng and Keifer, 2008). Although these signaling pathways change synaptic AMPAR trafficking, their roles in somatic export and/or long-distance transport dynamics are yet unknown.

Compartmentalized calcium signaling

Calcium signaling originating from the plasma membrane, endoplasmic reticulum, Golgi or mitochondria at neuronal cell bodies, dendrites and axons differentially regulate a variety of neuronal functions (reviewed in Brini et al., 2014). Calcium influx in the dendritic shaft and dendritic spines comes from various ion channels including AMPAR, NMDAR and voltage-sensitive calcium channels localized to the membrane, endoplasmic reticulum and mitochondria (Catterall, 2011; Higley and Sabatini, 2012). Calcium imaging in cell culture has shown calcium to remain within the spine following single spine activation (Nimchinsky et al., 2002; Sabatini et al., 2001). Interestingly, vertebrate and invertebrate neurons have compartmentalized calcium

transients that are important for neuronal function and computation (Ali and Kwan, 2019; Donato et al., 2019; Higley and Sabatini, 2012). However, it is unclear how compartmentalization of calcium regulates downstream processes such as trafficking of synaptic proteins.

Compartmentalized calcium signaling is conserved in *C. elegans* interneurons (Donato et al., 2019; Hendricks et al., 2012). Our data shows that AMPAR transport in the long process of AVA is affected by altered calcium influx due to mutations in L-VGCC and ROS levels. Some of these effects are likely to be local in scope. However, we have no knowledge regarding distribution of VGCCs, including EGL-19, or about compartmentalization of calcium signaling in the AVA. It is unclear how synaptic inputs and calcium signaling are integrated at dendritic and cellular levels to tailor AMPAR distribution. Our study provides a platform to start understanding *in vivo* calcium and ROS signaling mechanisms regulating AMPAR distribution ultimately affecting synaptic strength and behavior of animals.

Reactive Oxygen Species

Neuronal excitation and synaptic plasticity have high energy demands and correlate with physiological fluctuations in ROS levels (Bindokas et al., 1996). Pathophysiological ROS elevation is observed in aging and neurodegenerative conditions such as Parkinson's, Huntington's and Alzheimer's (Stefanatos and Sanz, 2018). Intriguingly, some amount of ROS, in particular superoxide (O_2^-), is required for LTP induction and memory formation (Thiels et al., 2000). This suggests that ROS are required for LTP formation, supporting a necessary signaling role in excitatory neuronal function, perhaps specifically in AMPAR trafficking. However, there is currently no direct mechanistic link between ROS signaling and regulation of AMPAR trafficking. Our results show that physiological ROS elevation decreases AMPAR transport, delivery and exocytosis (Figure 2.3) through a mechanism involving decreased calcium influx (Figure 2.2).

Consistent with our results, hypoxic conditions triggering increases in ROS production leads to decreased GLR-1 trafficking in *C. elegans* (Park and Rongo, 2016).

Although there have been quite a few studies of the regulation of L-VGCC function by physiological ROS in several cell types (Chaplin and Amberg, 2012; Cserne Szappanos et al., 2017; Todorovic and Jevtovic-Todorovic, 2014) there have been extremely few in neurons (Hidalgo and Arias-Cavieres, 2016; Massaad and Klann, 2011; Wilson et al., 2018) and none *in vivo*. Our study is the first to show how small increases in ROS affect whole cell activity-dependent calcium signaling and direct downstream targets such as synaptic AMPAR transport and delivery. We show that genetically and pharmacologically induced increases in ROS within the range of physiological signaling levels (~50 nM; Sies, 2017) leads to decreased calcium signaling in the cell bodies of *C. elegans* AVA neurons (Figure 2.2). This contrasts with what has been found in vertebrate arterial smooth muscle and gonadotropes (Chaplin and Amberg, 2012; Dang et al., 2018), but is consistent with reports of mitochondrial ROS elevation inhibiting L-VGCCs in cardiomyocytes (Scragg et al., 2008). Discrepancies in the concentration of ROS treatment between these studies and the one presented here could explain the opposing results. Several cellular processes have been shown to be impacted differently by ROS levels within vs outside of the physiological range (Wilson and González-Billault, 2015; Beckhauser et al., 2016). It is possible that ROS regulation of calcium sources follows suit in that moderate increases in ROS cause decreased calcium influx but greater increases in ROS cause increased calcium influx.

Taken together, our results identify a novel role for ROS signaling in the regulation of AMPAR transport and synaptic delivery, providing a link between the metabolic demands of neuronal activity and excitatory neurotransmission. Future studies are required to test our proposed model and understand its biological significance. Importantly, follow-up studies will first

be aimed at determining the source and targets of activity-induced ROS signaling. The ability to answer these questions will rely on the development of high affinity, genetically encoded ROS sensors enabling *in vivo* subcellular imaging of these dynamics. It is interesting to note that dysregulation of calcium signaling and ROS homeostasis is associated with aging and neurodegeneration (Barja, 2013; Grimm and Eckert, 2017; Kim and Jin, 2015; Stefanatos and Sanz, 2018). In this context, several *C. elegans* models of Alzheimer's diseases have provided key *in vivo* evidence to demonstrate the causal role of calcium dysregulation in neuronal (Griffin et al., 2019) and muscular degeneration (Sarasija et al., 2018; Sarasija and Norman, 2015). Furthermore, it has been shown that neurodegenerative models in *C. elegans* are translationally relevant for vertebrate studies (Tardiff et al., 2013; Treusch et al., 2011). Thus, once a fundamental understanding of how ROS signaling normally regulates excitatory neuronal function has been obtained in our model, future studies will determine how ROS and excitatory neurotransmission change in aging and neurodegeneration.

2.2F Materials and Methods

Strains

C. elegans strains were maintained on nematode growth media (NGM) and fed with the *E. coli* strain OP50 at 20°C (Brenner, 2003). All animals used in experiments were hermaphrodites and the strains used in these experiments contained alleles listed in Table 2.1 below.

Table 2.1 - List of genetic alleles used, the corresponding gene, the effect of the mutation and reported functional changes along with original references characterizing the allele.

Gene	Allele	Mutation	Functional Change	References
glr-1	*ky176*	Premature stop	Truncated, unfunctional receptor	(Maricq et al., 1995)
egl-19	*n582* (rf)	Missense mutation in S4 domain	No calcium spikes	(Liu et al., 2018; Trent et al., 1983)
	n2368 (gf)	Missense mutation in IS6	Delayed inactivation, prolonged calcium spikes	(Laine et al., 2014; Lee, 1997)
unc-43	*n498n1186* (lf)	Premature stop	Protein null	(Park and Horvitz, 1986; Reiner et al., 1999; Umemura et al., 2005)
	n498sd (gf)	Missense mutation in the active site	Partial calcium-independent, constitutive activation	
ctl-2	*ok1137* (lf)	~1kb deletion	Protein null	(Spiró et al., 2012)
lin-15	*n765ts*	Frameshift mutation	Protein null	(Kim and Horvitz, 1990)

Transgenic Strains

To visualize GLR-1, we used the integrated array *akIs201* containing Prig-3::SEP::mCherry::*glr-1* (Hoerndli et al., 2015) to express dual-tagged GLR-1 in the AVA glutamatergic interneurons. Transgenic strains were created by microinjection of *lin-15(n765ts)* worms with plasmids containing *lin-15(+)* to allow for phenotypic rescue of transgenic strains. The GCaMP6f-containing plasmid (Prig-3::GCaMP6f::*unc-54*) was a gift from Attila Stetak and was used to create the strain *csfEx62* [Prig-3::GCaMP6f::*unc-54*].

Confocal Microscopy

Imaging was carried out on a spinning disc confocal microscope (Olympus IX83) equipped with 488 nm and 561 nm excitation lasers (Andor ILE Laser Combiner). Images were captured using an Andor iXon Ultra EMCCD camera through either a 10x/0.40 or a 100x/1.40

oil objective (Olympus). Devices were controlled remotely for image acquisition using MetaMorph 7.10.1 (Molecular Devices).

Transport Imaging and Analysis

All transport imaging was conducted on strains containing *akIs201* in the *glr-1* null background (*ky176*). One-day-old adults from these strains were mounted on a 10% agarose pad with 1.6 μL of a mixture containing equal measures of polystyrene beads (Polybead CAT No. 00876-15, Polysciences Inc.) and 30 mM muscimol (CAT No. 195336, MP Biomedicals). The worm was positioned to place the AVA interneurons in close proximity to the coverslip through which the AVA neurites would be imaged. Once the neurons were located using the 100x objective and a 561 nm excitation laser, a proximal section of the neurites was photobleached using a 3 W, 488 nm Coherent solid-state laser (Genesis MX MTM) set to 0.5 W output and a 1 s pulse time. The photobleaching laser was targeted to a defined portion of AVA using a Mosaic II digital mirror device (Andor Mosaic 3) controlled through MetaMorph. Immediately following photobleaching, a 500-frame image stream was collected in a single z-plane with the 561 nm excitation laser and a 100 ms exposure time. Kymographs were generated using the Kymograph tool in MetaMorph with a 20 pixel line width as previously reported (Hoerndli et al., 2013). Transport quantification was done blinded to the genotype and condition by manually counting all transport events from resultant kymographs. Transport stops and velocities on the other hand were analyzed unblinded by manually tracing ~10 transport events per kymograph using the ImageJ plugin KymoAnalyzer (Neumann et al., 2017). Individual traces were selected for inclusion in this analysis if the fluorescence and image focus allowed for the event to be readily traced throughout the entirety of the kymograph (500 ms). At least 10 kymographs per experimental group were used for the stop and velocity analyses.

FRAP

Strains containing *akIs201* were mounted for imaging as described above. First, an appropriate proximal region of AVA localized and memorized using MetaMorph's stage position memory function. Second, an image stack was acquired using the 561 nm then the 488 nm excitation laser (500 ms exposure) around the AVA process (20 images were taken every 0.25 μm starting 2.5 μm below to 2.5 μm above the process, which required ~30 seconds total imaging time). Third, ~80 μm long sections of AVA proximal and distal to the imaging region were photobleached using the same photobleaching settings as previously described. The imaging region was photobleached and immediately after, two image stacks (with 561 nm then 488 nm excitation) were acquired for the 0-minute time point. This was repeated at 2, 4, 8 and 16 minutes following the photobleaching of the imaging region. Finally, image stacks from all time points were converted to maximum projections using MetaMorph's stack arithmetic function. The average fluorescence in the imaging region at each time point was analyzed using the region measurement tool in ImageJ 1.51s (Java 1.8). The background fluorescence (i.e. outside of the AVA) from each maximum projection was then subtracted from the average fluorescence of the imaging region. The resulting fluorescence from the maximum projections immediately following photobleaching (0 minutes) was subtracted from the fluorescence values of all subsequent time points. These values were then divided by the average fluorescence of the neurite before photobleaching to determine the percent of signal recovery for each channel within the imaging region.

In Vivo *Calcium Imaging*

All strains used for calcium imaging experiments contained the extrachromosomal array *csfEx62* expressing GCAMP6f in the AVA interneurons in the *lin-15(n765ts)* genetic

background. Eight to ten one-day-old adult animals with the array were selected and placed on a 10% agar pad with 2 μL of standard M9 buffer (common *C. elegans* culturing buffer; Stiernagle, 2006). *C. elegans* were thus constrained but not immobilized similar to when placed in a microfluidics chamber (Chronis et al., 2007). Animals were imaged using the 10x objective on the spinning disc confocal. A 60-second image stream consisting of 240 images with a 250 ms exposure time was acquired using the 488 nm excitation laser. During imaging, animals spontaneously attempt reversals, which is correlated with activation of the AVA thus increasing cytoplasmic calcium (Ben Arous et al., 2010) and resulting in changes in GCaMP6f fluorescence in our strains. We report the total activity or total cytoplasmic calcium during each 60-second stream (Figure 2.2 A and B). This was calculated using the following approach. For each frame, the maximum fluorescence ($F_{(t)}$) was quantified using MetaMorph's region measurement tool by manually defining the region of the image stream containing the AVA cell bodies. Attempts at reversals exhibited large calcium transients whereas attempts at forward movement or absence of movement was correlated with only small variations considered as basal fluctuations. The baseline (F_{min}) was defined as the average GCAMP6f signal when worms are immobile or during forward movement as this was previously shown not to activate AVA (Ben Arous et al., 2010). GCAMP6f signal during this time was observed to be within 30% of the overall minimum value of GCAMP6f. Maximum fluorescence values for each frame was imported into a customized Excel document containing modules created with Excel's visual basic editor. One module calculates the average baseline (F_{min}) by averaging all values within 30% of lowest value. This value was used to determine the ΔF ($F_{(t)} - F_{min}$) for each frame normalized to the average baseline ($\Delta F/F_{min}$; Larsch et al., 2013). Total activity was defined as the sum of all $F_{(t)}$ values greater than

F_{min} (green area below the curve of all peaks of the 60 s recording, Figure 2.2 B) normalized to the average baseline (average of the values below dotted line of the 60 s recording, Figure 2.2 B).

Spontaneous Reversal Quantification

The spontaneous reversal rate (reversal/min) was quantified using the semi-automated tracking system of the WormLab System (MBF Bioscience). Briefly, for each trial, five to eight one-day-old adult worms were selected off plates with bacterial food and transferred on food free plates twice with a rest of ~2 minutes after each transfer. Spontaneous locomotion was then recorded for 1 minute on the second plate and the video analyzed blinded to genotype. After detection of all animals and tracks by the semi-automatic tracking system, all tracks were manually verified and corrected if necessary, still blind to genotype. N2, wild-type animal locomotion and reversal rates were consistent with previously reported values: 3.78 ± 0.26 reversal/minute compared to reported ~ 4 ± 0.2 (Monteiro et al., 2012).

Hydrogen Peroxide and Nemadipine Treatments

Worms were acutely treated with H_2O_2 by placing the worm in 1.6 µL of solution containing the appropriate concentration of H_2O_2 with either 30 mM Muscimol and polystyrene beads (for transport imaging) or M9 buffer (for calcium imaging). Approximately 5 minutes following the beginning of the treatment, image streams were acquired. Physiological intracellular concentrations of H_2O_2 range from 10-100 nM in vertebrate neurons (Sies, 2017), so 10, 50 and 100 nM were used for our experiments.

A 0.5 mM stock of nemadipine (VWR, cat. no. 89151-228) was dissolved in 0.1% DMSO and the concentration was adjusted to 10 µM (a concentration reported to decrease calcium influx in exposed neurons *in vivo* by ~70%; Larsch et al., 2013) with M9 buffer and OP50 liquid culture immediately before a 30-minute treatment. During the treatments, one-day-old adult control

worms were placed into 1.5 mL Eppendorf tubes containing either control media or the pharmacological agent and placed on a rocker for oxygenation. The worms were then pipetted onto fresh NGM/OP50 plates immediately before being moved to an agar pad for imaging.

Image Presentation and Data Analysis

All images were acquired under non-saturating conditions. Quantification of GLR-1 transport FRAP and calcium imaging is described in the appropriate sections above. Representative images shown were chosen and processed following analysis only to the extent necessary to appreciate the corresponding quantifications. Image processing (RGB colors, cropping, adjustment of brightness and contrast) was performed in Photoshop (21.1.1). For FRAP images, the mCherry signal of SEP::mCherry::GLR-1 is shown in magenta for colorblind vision. This was achieved in Photoshop by duplicating the 561 nm information to create the red and blue channels of the RGB image which was then merged to create the magenta image as published previously (Hoerndli et al., 2013). All images in each panel were identically processed.

Experimental Design and Statistical Analysis

All experiments were performed using one day old adult hermaphrodite *C. elegans* animals as determined by a single row of eggs and by picking as precisely identifiable L4 stage larva 24 hours before imaging and behavior experiments. Each dataset contained at least three experimental replicates with 4-5 replicates needed for datasets containing more genotypes or conditions (Figures 5, 6, and 7). The total number of animals analyzed is indicated in the figure legends for each figure. All mutant strains were back-crossed at least 2x with N2 wild-type animals. All imaging reagents such as SEP::mCherry::GLR-1 and GCAMP6f were crossed into strains carrying genetic mutations in the exact same way, verifying the presence of the knock-out

glr-1 allele *ky176* and genetic mutations using PCR genotyping on at least 2 generations. Primer sequences are available on request.

For statistical analysis, all datasets were screened for outliers using a Thompson Tau test. For datasets including only two experimental groups, statistical significance was tested using a two-tailed student's t-test. For datasets comparing more than two experimental groups, a one-way Brown-Forsythe ANOVA with a Dunnett's correction for multiple comparisons was used. FRAP differences between groups was determined using an extra sum-of-squares F-test of the nonlinear hyperbolic regression fit to the data. All statistical analyses were performed using Prism 8 software. Statistical details, numbers of ROIs and animals analyzed, and p-values are indicated in detail in each results section. Data are presented as mean ± SEM unless otherwise stated.

Code/Software

Code for custom Excel modules used for analysis of calcium imaging is available online at: https://github.com/racheldoser/GCaMP_Analysis_Excel_VBA.git.

2.3 Elevated ROS Signaling Causes Abnormal Neuronal Activation and Impaired Learning in *C. elegans*

Changes in transport and synaptic targeting of GLR-1 alter neuronal excitation and synaptic plasticity in *C. elegans* (Hadziselimovic et al., 2014; Hoerndli et al., 2015; Stetak et al., 2009). The abnormal GLR-1 transport and delivery due to elevated ROS led us to hypothesize that catalase mutants would have altered neuronal activation and plasticity. We can assess this possibility behaviorally since the AVA is an interneuron that integrates sensory information to determine *C. elegans* locomotion. Additionally, glutamatergic plasticity within the AVA-circuit

is required for olfactory associative memory (Ben Arous et al., 2010; Gray et al., 2005; Morrison and Kooy, 2001; Stetak et al., 2009). So, we can assay spontaneous locomotion and associative memory assays as a proxy for activation and plasticity of the AVA neuron.

2.3A Chronic elevations in ROS decrease the frequency of C. elegans *reversals*

The synaptic content of GLR-1 in the AVA determines the frequency of spontaneous reversals of *C. elegans* (Ben Arous et al., 2010; Gray et al., 2005; Park et al., 2009; Zheng et al., 1999). Thus, quantification of spontaneous reversals (see Chapter 2.2F) is a measure of the glutamatergic transmission in which the AVA neuron is central (Figure 2.9 A). Loss of GLR-1 significantly reduces the number of spontaneous reversals (Figure 2.9 B) which demonstrates that glutamatergic synapse function is necessary for wildtype locomotor behavior. Interestingly, reversal frequency was significantly decreased in two of the three catalases expressed in *C. elegans* (Figure 2.9 B). Specifically, strains with loss-of-function mutations in *ctl-1,* a cytoplasmic catalase, had reduced reversal frequency compared to wildtype. Similarly, loss of the peroxisomal

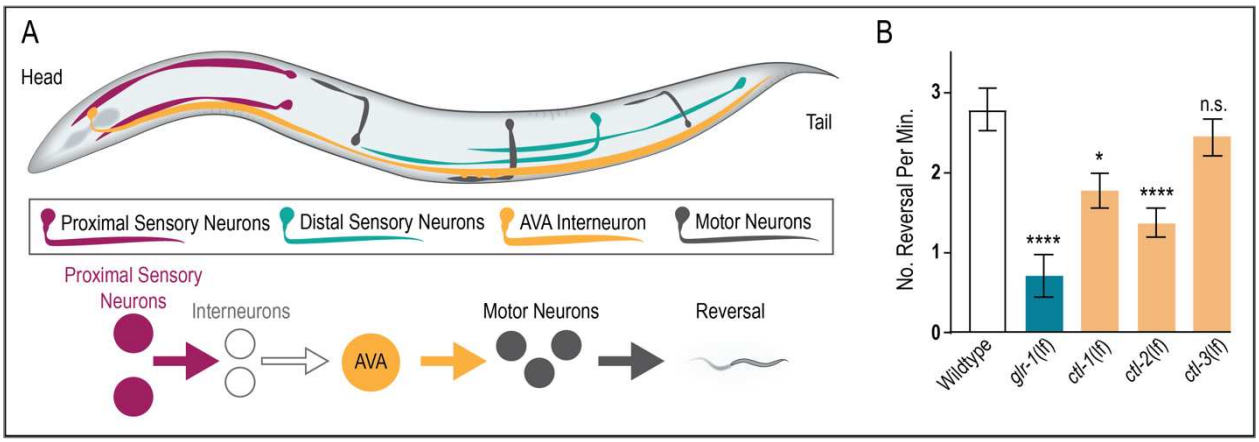

Figure 2.9 - Spontaneous reversal frequency is decreased in catalase mutants. A) Top. Illustration of anatomical location of major sensory and motor neurons in relation to AVA interneuron. Bottom. Schematic of how input from proximal sensory neurons leads to activation of AVA which then outputs to motor neurons that initiate backward movement. B) Number of spontaneous reversals per minute in wildtype (N_2, n = 36), glr-1loss-of-function (lf) mutants (*ky176*, n = 14), *ctl-1*(lf) (*ok1242*, n = 30), *ctl-2*(lf) (*ok1137,* n = 38), and *ctl-3*(lf) (*ok2042*, n = 34). *: $p < 0.05$, ****: $p < 0.0005$, n.s. = not significant. One-way ANOVA with Dunnett's correction.

catalase encoded by the *ctl-2* gene resulted in decreased reversals. The loss-of-function mutants for *ctl-3* had reversal frequencies that were comparable to wildtype.

2.3B Chronic elevations in ROS prevent olfactory associative learning in C. elegans

Redistribution of GLR-1 at AVA synapses is required for olfactory associative memory (Hadziselimovic et al., 2014; Stetak et al., 2009), so diminished transport and delivery was hypothesized to impair the learning and memory expression in catalase mutants. The *ctl-2*(lf) strain was subjected to an olfactory associative memory assay since we and others have observed that loss of *ctl-2* has a more pronounced effect on behavior and survival than other catalase mutants (Petriv and Rachubinski, 2004). Interestingly, *ctl-2*(lf) mutants showed impaired learning in the chemotaxis assay immediately after olfactory conditioning (Figure 2.10). This learning impairment made it difficult to assess memory expression at later timepoints.

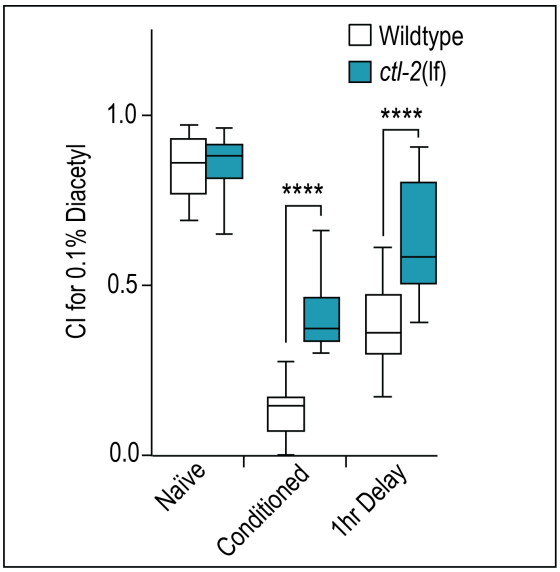

Figure 2.10 - Catalase mutants have impaired olfactory associative learning. Wildtype and ctl-2(lf) mutants were tested over 5 trials for preference of 0.1% Diacetyl (DA) immediately (Conditioned) or 1 hr (1hr Delay) after being conditioned with DA and starving. ****: $p<0.0005$. Two-way ANOVA. Whiskers rep. min-max.

2.3C New Materials and Methods

Olfactory Associative Memory Assay

C. elegans strains were synchronized via an egg preparation that involves lysing gravid adults with bleach, plating eggs onto a 10 cm NGM plate (no OP50) overnight before transferring hatched L1s with M9 onto a fresh 10 cm NGM/OP50 plate. For olfactory conditioning, day-one-old adults are washed with M9 before being placed onto chemotaxis plates (5 mM KH_2PO_4/K_2HPO_4 [pH 6.0], 1 mM $CaCl_2$, 1 mM $MgSO_4$, 2% agar) with or without a piece of Whatman paper containing 0.1% Diacetyl. Plates are sealed with parafilm and left at room temperature for 1 hour. Immediately after, a chemotaxis assay is performed in which worms are washed from conditioning plates with M9 onto the middle of CTX testing plates that contain a droplet of 0.1% Diacetyl (diluted in ethanol) or ethanol on opposite sides of the plate. Sodium azide (1M) is added to the regions of these droplets just before worms are transferred to testing plates. After 1 hour, worms in each region are counted, and a chemotaxis index (CI) is calculated. CI = (No. on 0.1% Diacetyl - No. on ethanol) / Total (Bargmann et al., 1993). Short-term memory was assessed by transferring worms via an M9 wash to an NGM/OP50 plate for 1 hour prior to running the chemotaxis assay. These assays were carried out in the lab of Dr. Attila Stetak at the University of Zürich, Switzerland.

2.4 Decreased Reactive Oxygen Species Signaling Alters Glutamate Receptor Transport to Synapses in *C. elegans* AVA Neurons

The following material was published online on March 17ty, 2022 in *microPublication Biology* (Doser et al., 2022)

2.4A Summary

Reactive oxygen species (ROS) are chemically reactive molecules normally produced during cellular respiration. High ROS levels negatively impact forms of synaptic plasticity that rely on changes in the number of ionotropic glutamate receptors (iGluRs) at synapses. More recently, we have shown that physiological increases in ROS reduce iGluRs transport to synapses by acting on activity-dependent calcium signaling. Here, we show that decreasing mitochondria-derived ROS decrease iGluR transport albeit in a calcium-independent manner. These data demonstrate differential regulatory mechanisms by elevated or diminished ROS levels which further support a physiological signaling role for ROS in regulating iGluR transport to synapses.

2.4B Description

In the brain, signal transmission between neurons mainly occurs at electrochemical junctions or synapses where release of presynaptic neurotransmitters activates postsynaptic receptors. In most nervous systems, the primary excitatory neurotransmitter is glutamate. When released by presynaptic neurons, it activates glutamate receptors containing cation channels and causes excitation through membrane depolarization. The AMPA subtype (AMPAR) of glutamate receptors is especially central to excitatory transmission (Ashby et al., 2008). The amplitude of a postsynaptic response to glutamate release depends on the number of postsynaptic AMPARs, and changes in synaptic content of AMPARs is the basis for the synaptic plasticity that underlies learning and memory (Groc and Choquet, 2020). Most AMPARs are synthesized in the cell body and must undergo long-distance transport to these sites. This transport is a multistep process involving loading of AMPAR-containing vesicles onto molecular motors (Esteves da Silva et al., 2015; Hangen et al., 2018; Hoerndli et al., 2013; Kim and Lisman, 2001; Setou et al., 2002), delivery of these vesicles (Heisler et al., 2014; Setou et al., 2002), and exocytosis of AMPARs to

the synaptic membrane (Yudowski et al., 2007). Regulation of receptor endocytosis (Ehlers, 1999) and surface diffusion (Choquet and Triller, 2013) further contribute to controlling the synaptic content of AMPARs.

Regulation of motor-dependent transport and delivery are the least understood steps, but we now know they are regulated by activity-dependent calcium signaling (Hangen et al., 2018; Hoerndli et al., 2015). Additionally, we have recently shown in *C. elegans* that the calcium influx that upregulates AMPAR transport and delivery is attenuated by increased reactive oxygen species (ROS; Doser et al., 2020), a class of reactive molecules that are normal byproducts of oxidative phosphorylation (Halliwell, 1992). These findings begin to explain observations of synaptic plasticity defects (i.e. less induction) in elevated ROS conditions (Bliss and Collingridge, 1993; Kamsler and Segal, 2003; Klann, 1998). Interestingly, ROS depletion leads to similar defects in synaptic plasticity (Gahtan et al., 1998; Kishida and Klann, 2006), suggesting that ROS concentrations must be within a specific physiological range for normal synaptic plasticity. So, we asked if ROS are required for AMPAR transport by depleting ROS via pharmacological and genetic methods in *C. elegans* then analyzing transport of the AMPAR subunit GLR-1 (Doser et al., 2020).

In *C. elegans*, the AVA glutamatergic interneurons are ideal for these studies because they are unipolar with a single neurite that spans the length of the entire ventral nerve chord (Maricq et al., 1995). Additionally, cell-specific promoters for the AVA neuron allow for molecular replacement of native GLR-1 with a fluorescent-tagged GLR-1 in these neurons alone (Figure 2.11 A). This has enabled visualization of the transport of individual vesicles containing GLR-1 as they are exported from the AVA cell body through the long AVA neurite (Doser et al., 2020; Hoerndli et al., 2015). Using these methods, we have shown decreased GLR-1 transport

when ROS levels were elevated within the physiological range (Doser et al., 2020). Since we were able to pinpoint that elevated ROS downregulates GLR-1 transport by attenuating activity-dependent calcium influx, we hypothesized that ROS act as regulatory molecule in this process.

If this hypothesis is correct, then reducing ROS would alter the amount of GLR-1 transport. To test this, we overexpressed the neuronal catalase encoded by the *ctl-2* gene in AVA (Figure 2.11 A, top), which would presumably lead to decreased ROS levels only in these neurons. To image GLR-1 transport, we photobleached a proximal portion of the AVA neurite to uncover the dim fluorescence of GLR-1-containing vesicles (Figure 2.11 B). Then, we continuously imaged GLR-1::mCherry for 50s at a single confocal plane within a section of the AVA neurite. Transport events within this image stream are represented in kymographs as black traces with position on the x-axis and time on the y-axis (Figure 2.11 B, C and E). Quantification of the number of GLR-1 transport events from kymographs revealed that *C. elegans* with AVA-specific overexpression of CTL-2 had decreased transport compared to the control strain (Figure 2.11 D). It is important to note that this difference in transport between strains is unlikely due to discrepancies in their GLR-1::mCherry expression since the average fluorescence of GLR-1::mCherry in the AVA neurite is nearly the same in each (*csfEx63*: 470.4 ± 66.1 and *csfEx65*: 465.6 ± 68.2; mean ± SEM; $p = 0.95$, two-tailed Student's t-test). These results suggest that chronic CTL-2 overexpression decreased ROS levels which in turn led to a reduction in GLR-1 transport. A major source of ROS is mitochondrial oxidative phosphorylation (Halliwell, 1992), so we hypothesized that CTL-2 overexpression decreased the effect of mitochondrial-derived ROS signaling.

To test this hypothesis and rule out developmental effects of CTL-2 overexpression, we treated *C. elegans* with mitoTEMPO, a mitochondrial-targeted antioxidant (Murphy and Smith, 2007), to acutely diminish ROS signaling. Following a 2-hour mitoTEMPO treatment, we found

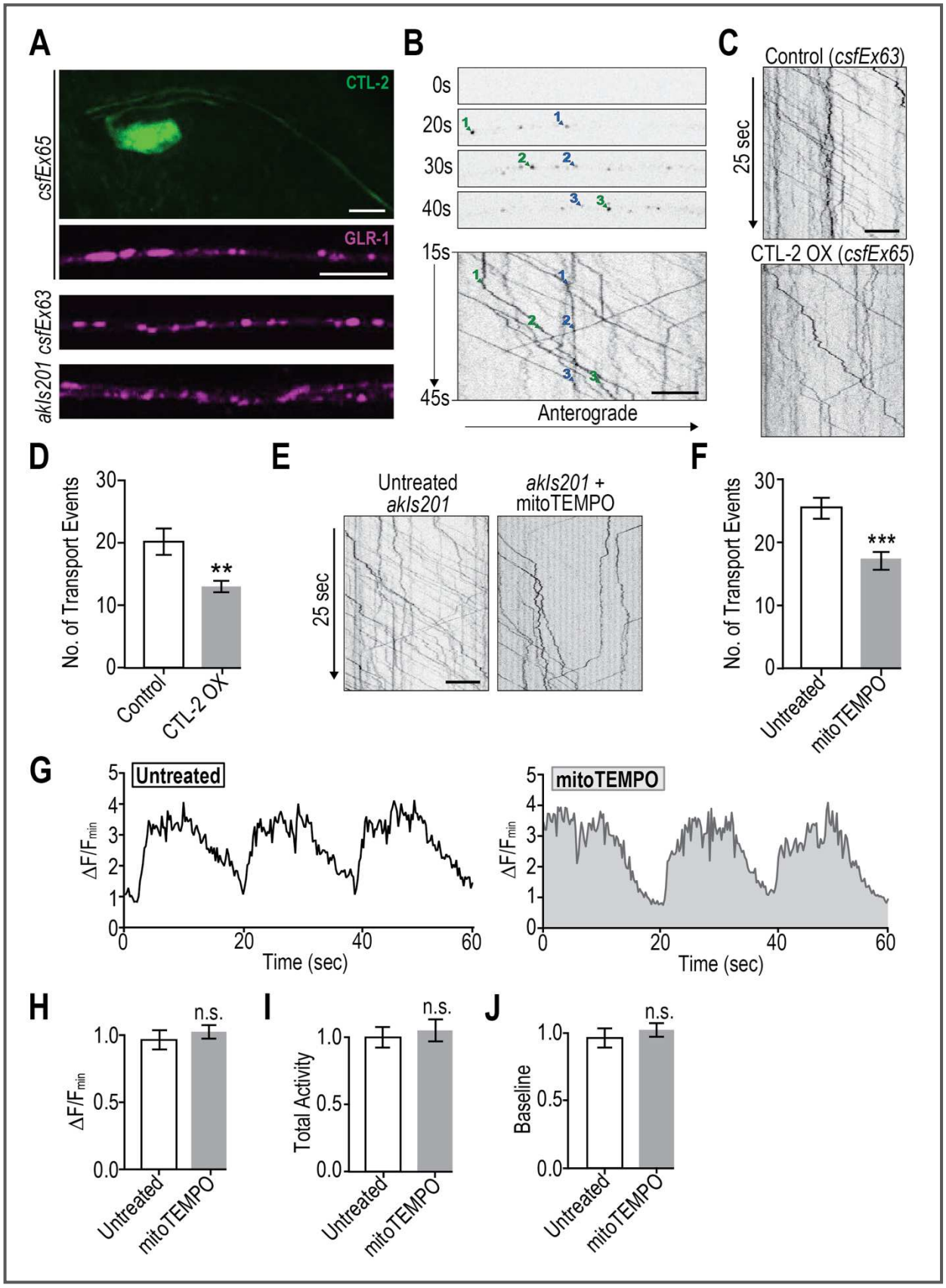
A
CTL-2
csfEx65
GLR-1
csfEx63
akIs201
B
0s
20s
30s
40s
15s
45s
Anterograde
C
Control (csfEx63)
25 sec
CTL-2 OX (csfEx65)
D
No. of Transport Events
30
20
10
0
**
Control
CTL-2 OX
E
Untreated
akIs201
akIs201 +
mitoTEMPO
25 sec
F
No. of Transport Events
30
20
10
0
***
Untreated
mitoTEMPO
G
Untreated
mitoTEMPO
ΔF/Fmin
5
4
3
2
1
0
0
20
40
60
Time (sec)
H
ΔF/Fmin
1.0
0.5
0.0
n.s.
Untreated
mitoTEMPO
I
Total Activity
1.0
0.5
0.0
n.s.
Untreated
mitoTEMPO
J
Baseline
1.0
0.5
0.0
n.s.
Untreated
mitoTEMPO

Figure 2.11 - Diminished ROS levels decrease AMPAR transport out of the cell body via a calcium independent mechanism. A) Representative images showing expression of contents of transgenic arrays used. Scale bar = 5 μm. B) GLR-1::mCherry transport. Top: Single time points from 50 s of continuous imaging (100 ms/frame). Two GLR-1-containing vesicles (blue and green numbers) are pointed out for three timepoints. Bottom: Kymograph derived from 30 s of a 50 s image stream depicting position (x-axis) of GLR-1 transport vesicles over time (y-axis). Scale bar = 5 μm. C and E) Representative kymographs depicting GLR-1 transport vesicles (black lines) as they are transported through the length of the neurite (x-axis) over time (y- axis). Scale bar = 5 μm. D) Quantification of transport events in control (*lin-15(n765ts)* X; *glr-1(ky176)* III; *csfEx63*, n=15) and worms overexpressing catalase (CTL-2(OX)) in the AVA (*lin-15(n765ts)* X; *glr-1(ky176)* III; *csfEx65*, n=11, **:p=0024, two-tailed Student's t-test). F) Quantification of transport events from untreated (n=18) and mitoTEMPO treated (n=20) worms (*glr-1(ky176)* III; *akIs201*, ***:p=0.0008, two-tailed Student's t-test). G) Representative traces of changes in GCaMP6f fluorescence in the AVA cell body over 60 s *in vivo* normalized to baseline fluorescence ($\Delta F/F_{min}$) from untreated (n=35) and mitoTEMPO treated (n=35) worms (*lin-15(n765ts) X; csfEx62*). H) Average $\Delta F/F_{min}$ normalized to untreated controls. I) Total activity (sum of fluorescence values above baseline divided by baseline) normalized to untreated controls. J) Average baseline of these groups normalized to untreated controls.

that GLR-1 transport was decreased compared to untreated controls (Figure 2.11 E and F). The similar decrease in transport due to CTL-2 overexpression and acute mitoTEMPO treatment suggests two things: First, diminished ROS signaling has a direct effect on the regulation of GLR-1 transport. Second, since mitochondria-targeted antioxidants reduced transport to the same extent as overexpression of a cytoplasmic catalase, it is likely that mitochondrial respiration is a major contributor to ROS signaling involved in regulation of GLR-1 transport.

Since we previously determined that elevated ROS regulates GLR-1 transport by attenuating calcium influx (Doser et al., 2020), we next asked whether diminished ROS levels also attenuate calcium influx. To address this question, we subjected a *C. elegans* strain expressing the calcium indicator GCaMP6f in AVA neurons to a 2-hour mitoTEMPO treatment. Quantification of GCaMP fluorescence over a 60 s imaging session (Figure 2.11 G) did not reveal any changes in the amplitude of GCaMP peaks (Figure 2.11 H), total activity (summation of GCaMP fluorescence above baseline, Figure 2.11 I), or baseline GCaMP fluorescence (Figure 2.11 J) between untreated and mitoTEMPO treated worms.

Altogether, these results demonstrate that diminished ROS levels decrease the amount of GLR-1 transport out of the cell body via a mechanism that seems to be independent of activity-dependent calcium influx based on *in vivo* calcium imaging with GCaMP6f. However, since calcium imaging is not as sensitive as other measures of calcium influx, it remains possible that calcium channel activation, conductance, or inactivation is altered by diminished ROS signaling. The addition of these results to our previous findings (Doser et al., 2020) suggest that ROS are a necessary regulator of long-distance AMPAR transport. Since this transport is crucial for supplying receptors in a way that allows for synaptic plasticity, these studies begin to explain why synaptic plasticity defects are observed in conditions of non-physiological ROS.

2.4C Materials and Methods

Cloning

The catalase gene (*ctl-2)* was cloned from *C. elegans* cDNA using the forward primer 5'-GGGGACAAGTTTGTACAAAAAAGCAGGCTATGCCAAACGATCCATCGGA-3' and reverse primer 5'-GGGGACCACTTTGTACAAGAAAGCTGGGTCGATATGAGAGCGA GCCTGTTTC-3'designed on ApE (v.2.0.60). Using the gateway recombination cloning technique (Invitrogen), the *ctl-2* gene was positioned behind P*flp-18*, an AVA specific promoter, and followed by an eGFP 3'UTR (from pGH112, Erik Jorgensen) in the destination vector pCFJ150 (Erik Jorgensen, Addgene - Plasmid #19329).

Transgenic Strains

Transgenic strains were created by microinjection of *lin-15(n765ts)* worms as previously described (Doser et al., 2020). The above plasmids were used to create the following extrachromosomal arrays: *csfEx65 [Pflp-18::ctl-2::eGFP + Prig-3::glr-1::mCherry], csfEx63 [Prig-*

3::glr-1::mCherry] and *csfEx62 [Pflp-18::GCaMP6f + lin-15p::lin-15]*. The *csfEx65* and *csfEx63* transgenic strains have a loss-of-function mutation in *glr-1* (allele: *ky176*) in addition to *lin-15(n765ts)*.

MitoTempo Treatment

A stock of 1M mitoTEMPO (Sigma) was dissolved in deionized water and diluted to 0.5mM with M9 and OP50 liquid culture immediately before the 2-hour treatment as previously described (Xu and Chisholm, 2014). 20-40 one-day-old adult control worms were individually picked off NGM/OP50 plates and placed into a 1.5 mL Eppendorf tube containing either control media (M9/OP50) or 0.5mM mitoTEMPO in M9/OP50. The tubes were placed on a rocker to allow for oxygenation during the duration of the treatment. The worms were then pipetted out of the tubes onto fresh NGM/OP50 plates immediately before being moved to an agar pad for imaging as described above.

Imaging and Analysis

Confocal microscopy was carried out using a spinning disc confocal microscope (Olympus IX83) as previously described (Doser et al., 2020).

In vivo *Glutamate Receptor Imaging and Analysis*

In vivo imaging of glutamate receptors was conducted on strains containing either extrachromosomal *Prig-3*::*glr-1*::*mCherry* (*csfEx65* and *csfEx63*) or *Prig-3::SEP::mCherry::glr-1* (*akIs201*; Hoerndli et al., 2015) in a *glr-1* null background (*glr-1(ky176)*). All imaging experiments were done using one-day-old adults as described in more detail in Doser et al., 2020.

In Vivo *Calcium Imaging*

Calcium imaging experiments were conducted on strains containing the extrachromosomal array *csfEx62* in the *lin-15(n765ts)* genetic background. Eight to ten one-day-old adult

animals were placed on a 10% agar pad with 2uL of M9 buffer. They were imaged individually at 10x for 60 seconds (image stream was acquired using the 488nm excitation laser with a 250ms exposure time for 240 frames). The fluorescence was measured and analyzed as previously described (Doser et al., 2020).

Code Availability

Custom Excel modules used to analyze *in vivo* calcium imaging can be found at https://github.com/racheldoser/GCaMP_Analysis_Excel_VBA.git.

Statistical Analysis

All datasets were screened for potential outliers using a Thompson Tau test. Cleaned datasets were then tested for statistical significance using a two-tailed Student's T-test.

Reagents

Table 2.2 - *C. elegans* strains, transgenic arrays and pharmacological agents.		
Strain	**Genotype**	**Source**
FJH 15	*glr-1(ky176)* III; *akIs201*	Hoerndli Lab, Colorado State University
FJH 289	*lin-15(n765ts)* X; *glr-1(ky176)* III; *csfEx65*	Hoerndli Lab, Colorado State University
FJH 188	*lin-15(n765ts)* X; *glr-1(ky176)* III; *csfEx63*	Hoerndli Lab, Colorado State University
FJH 186	*lin-15(n765ts)* X*; csfEx62*	Hoerndli Lab, Colorado State University
Integrated arrays	**Contents**	**Source**
akIs201	*Prig-3::SEP::mCherry::glr-1*	Hoerndli Lab, Colorado State University
Extrachromosomal arrays	**Contents**	**Source**
csfEx62	*Prig-3::GCaMP6f + Plin-15::lin-15 + Pegl-20::nls::DsRed*	Hoerndli Lab, Colorado State University
csfEx63	*Prig-3::glr-1::mCherry + Plin-15::lin-15*	Hoerndli Lab, Colorado State University
csfEx65	*Pflp-18::ctl-2::eGFPlet858 + Prig-3::glr-1::mCherry + Plin-15::lin-15*	Hoerndli Lab, Colorado State University
Plasmid name	**Gene/insert**	**Source**
pRD21	*Pflp-18::ctl-2::eGFPlet-858*	Hoerndli Lab, Colorado State University
pAS1	*Prig-3::GCaMP6f::unc-54*	Stetak Lab, University of Basel
pDM1556	*Prig3::glr-1::mCherry*	Maricq Lab, University of Utah
pJM23	*Plin-15::lin-15*	Maricq Lab, University of Utah
pCT61	*Pegl-20*::*nls*::DsRed	Maricq Lab, University of Utah
Pharmacological agent	**Effect**	**Source**
MitoTEMPO	An antioxidant that accumulates in mitochondria due to conjugation to a lipophilic cation.	Sigma-Aldrich

2.5 Conclusion and Discussion

To conclude this chapter, there is a tightly regulated physiological range in which ROS levels must be maintained for normal GLR-1 transport, delivery and exocytosis to synapses

(Chapter 2.2 and 2.4). Increased ROS levels impact GLR-1 localization by attenuating somatic calcium influx which is required for CaMKII activation and loading of GLR-1-containing vesicles onto molecular motors for transport (Hoerndli et al., 2015). Consistent with the diminished calcium influx into the AVA soma in the presence of elevated ROS, loss of cytoplasmic and peroxisomal catalases decrease the spontaneous reversals of *C. elegans*, a behavior controlled by AVA activity (Chapter 2.3A). The decreased amount of transport observed in strains lacking the primary peroxisomal catalase (*ctl-2*) appears to be insufficient for the redistribution of receptors necessary for memory acquisition. This is indicated by the failure of *ctl-2*(lf) mutants to learn the negative association of an odor (Chapter 2.3B). In the case of diminished ROS, GLR-1 transport is also decreased but occurs via a calcium-independent mechanism (Chapter 2.4). Altogether, these finding support a role for ROS as a physiological signaling molecule in the regulation of GLR-1 localization in a way that is important for normal neuronal activity and plasticity.

To add to the detailed discussion of Chapter 2.2, the comparison of total GLR-1 transport in experimental groups with increased and decreased ROS is interesting because it reveals that transport is decreased to a similar extent in each group regardless of if ROS levels were altered via genetic or pharmacological methods. It can be assumed that our genetic and pharmacological methods changed ROS levels to different extents; however, in each instance, total GLR-1 transport was decreased by 30-40% (Figure 2.3 and 2.11). Additionally, increasing concentrations of exogenous H_2O_2 did not proportionally effect GLR-1 transport (Figure 2.3). Instead, GLR-1 transport during treatment with the lowest H_2O_2 concentration was no different than a 10-fold higher concentration. This suggests that ROS signaling outside of a tightly regulated physiological range impacts only a subset of transport, such as activity-dependent transport, and perhaps has no control over the basal flux of GLR-1-containing vesicles.

The behavioral data with *ctl-2*(lf) suggest that elevated ROS levels cause abnormal neuronal function. This observation is consistent with what has been seen in other model systems in which elevated ROS prevents induction of LTP at glutamatergic synapses and the expression of hippocampal-dependent memory (Kamsler and Segal, 2003; Kumar et al., 2018; Oswald et al., 2018). This indicates that the involvement of ROS in excitatory synapse function is conserved although targets of ROS signaling may differ between species. Despite altered *C. elegans* locomotion and olfactory associative learning in *ctl-2(*lf), there are no detectable differences in the average fluorescence intensity of synaptic GLR-1::mCherry::SEP between *ctl-2*(lf) and the controls (data not shown) meaning synaptic content of GLR-1 is changed very little if at all. Mechanisms the regulate local GLR-1 trafficking, such as endocytosis, could compensate for the decreased GLR-1 transport, delivery and exocytosis observed in the *ctl-2*(lf) mutants. In order to understand if this is the case, future experiments will include a detailed analysis of how synaptic delivery, exocytosis and endocytosis of GLR-1 is regulated by synaptic activation and local ROS signaling.

Chapter 3 – Local, Activity-dependent Reactive Oxygen Species Signaling Regulates Glutamate Receptor Dynamics in Dendrites

3.1 Summary

Our findings in Chapter 2 suggest that ROS and calcium influx regulate the AMPAR transport in neurites to control receptor delivery to individual synapses. In this chapter, we show that mitochondria may be acting to integrate calcium influx and ROS signaling within neuronal processes. The results presented in Chapter 3.3 indicate that upon activity-dependent elevations in cytoplasmic calcium, mitochondria take up calcium (Figure 3.2). Identical activation of the AVA also led to increased mitochondrial ROS production (Figure 3.3), which is likely a result of upregulation of OXPHOS by calcium. This data supports a role for mitochondria as a signal transducer that converts calcium uptake into ROS signaling. This led us to ask: how does localized calcium and mitochondrial ROS signaling alter GLR-1 delivery to individual synapses? In Chapter 3.4, we begin to address this two-part question. First, we provide more direct evidence that calcium levels are correlated with stopping of GLR-1 transport, which is thought to be indicative of receptor delivery events. Simultaneous calcium and GLR-1 transport imaging allowed us to quantify cytoplasmic calcium concentration in relation to the velocity and stopping of GLR-1 transport in a spatially and temporally specific manner (Figure 3.4). This approach revealed that when GLR-1 transport events were within regions of high calcium, they traveled at slower velocities or were stopped within that region of the neurite (Figure 3.4).

Next, we assessed how local increases in mitochondrial ROS production alter these GLR-1 transport dynamics. We found that cell-wide and local increases in ROS production at mitochondria altered the dynamics of GLR-1 transport (Figure 3.5 and 3.6). We hypothesized that

this postsynaptic ROS signaling acts on GLR-1 transport by altering calcium influx. So, we measured calcium transients in the AVA neurite following optical stimulation of mitochondrial ROS production. We saw a slight increase in calcium influx in regions of the neurite where ROS production was optically stimulated (Figure 2.7), which may explain the effect of ROS production on GLR-1 transport to synapses since calcium signaling is a key determinant of the quantity and dynamics of this transport. Altogether, these data suggest a model in which activity regulates ROS production via calcium buffering by mitochondria that in turn modulates calcium influx and calcium-dependent GLR-1 transport.

3.2 Introduction

The first step in understanding the regulation of GLR-1 transport and targeting to synapses by local ROS signaling is determining when and from where ROS signaling originates. The abundance of antioxidant enzymes and other reducing agents likely prevent cell-wide diffusion of ROS signals. Instead, it is more probable that ROS act locally within cellular microdomains, such as within individual synapses (Halliwell, 1992; Sies, 2017). Another thing to consider is that ROS production is unlikely static within dendrites, since this would make their newly uncovered role as a signaling molecule uninformative especially for mechanisms underlying synaptic plasticity. The first indication that ROS production may occur within dendrites in close proximity to synapses came from co-expression of GLR-1::mCherry and the fluorescent ROS indicator, roGFP that was localized to the outer mitochondrial membrane (mito-roGFP) facing the cytoplasm. Mitochondria were observed throughout the AVA neurite positioned at or just adjacent to GLR-1 clusters (Figure 3.1), which are presumed to be postsynaptic sites.

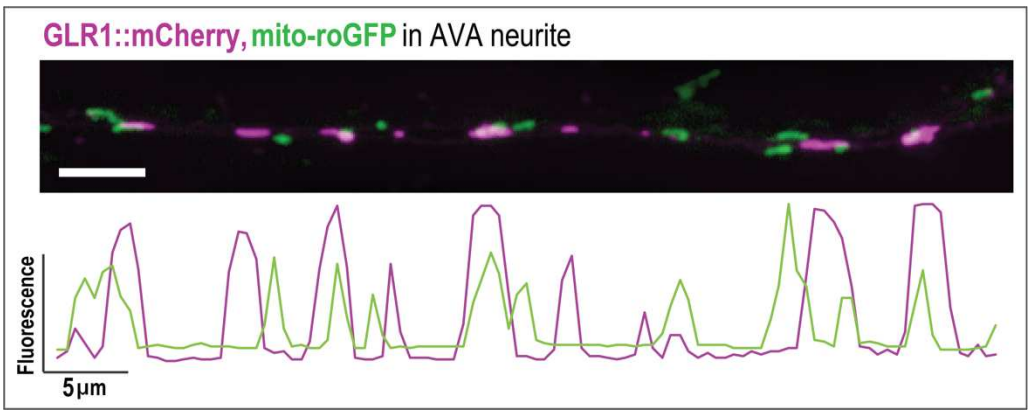

Figure 3.1 - Mitochondria are positioned near glutamatergic synapses in *C. elegans* AVA neurons. Cell-specific expression of GLR-1::mCherry and mito-roGFP in AVA neuron shown in a two-channel overlay of maximum projections from Z-stacks of confocal images.. (*csfEx67*: [*Prig-3::GLR-1::mCherry* + *Pflp-18::TOMM20::roGFP*]). Scale bar = 5 µm.

Mitochondrial ROS production is an unavoidable byproduct of OXPHOS, so factors that upregulate OXPHOS rates in turn increase ROS. As previously mentioned, OXPHOS is upregulated by calcium uptake into the mitochondria which occurs during high levels of cytoplasmic Ca^{2+} that accompany neuronal activation (Ashrafi et al., 2020; Nicholls, 2009). This led us to assess if in the AVA neurite, neuronal activation leads to increased mitochondrial calcium uptake and ROS production which has not been assessed *in vivo* or in *C. elegans* neurons to our knowledge. Then, to understand the relevance of activity-dependent ROS production from mitochondria, we conducted additional experiments to determine if and how ROS signaling originating at mitochondria impacts GLR-1 transport.

3.3 Mitochondrial Calcium Uptake and ROS Production is Activity-Dependent in *C. elegans* Neurons

To manipulate neuronal activity *in vivo* while imaging mitochondrial calcium dynamics, we first created strains that expressed the red-shifted Channelrhodopsin, ChRimson (Schild and Glauser, 2015), in the AVA neurons in addition to the cytoplasmic calcium indicator GCaMP6f.

We optimized a light stimulation and imaging protocol for reliable, whole-cell activation of ChRimson (Figure 3.8). The light-sensitivity of Channelrhodopsins in *C. elegans* requires supplement with all-Trans Retinal. Without Retinal, even the highest light dosage did not elicit an increase in GCaMP fluorescence (Figure 3.8 B) indicating that the calcium influx measured with GCaMP is indeed due to light-induced opening of ChRimson. This optimization experiment proved that whole-cell activation with ChRimson was feasible while imaging GCaMP and that a light dosage of 40 μW/mm^2 was most reliable in eliciting calcium transients. So, this intensity was used for whole-cell activation of ChRimson in all experiments (Figure 3.8).

To measure calcium level within the mitochondrial matrix, we co-expressed ChRimson and mitoGCaMP, a modified GCaMP localized to the mitochondrial matrix. Light-induced activation of AVA resulted in increased mitoGCaMP fluorescence (Figure 3.2 A and B). Further analysis the mitoGCaMP fluorescence of individual mitochondria showed that mitoGCaMP peaks were highly variable (Figure 3.2 C). This is partially illustrated by the population summary of maximum mitoGCaMP fluorescence (F_{max}) that shows maximums anywhere between 10-60% above minimum fluorescence values (Figure 3.2 D). Additionally, the latency to F_{max} following light stimulation ranged from 0 to nearly 5 seconds (Figure 3.2 E). It is also interesting to note that F_{max} values had no correlation with the latency to F_{max} for individual mitochondria (data not shown). These findings propose that dendritic mitochondria have variations in the rate and degree of calcium uptake.

As previously mentioned, increased OXPHOS rates due to mitochondrial calcium uptake would also increase ROS production. Unfortunately, tools that temporally control mitochondrial calcium uptake have not been well characterized (Kichuk et al., 2021). However, since we had observed mitochondrial calcium uptake as a result of ChRimson activation, we instead

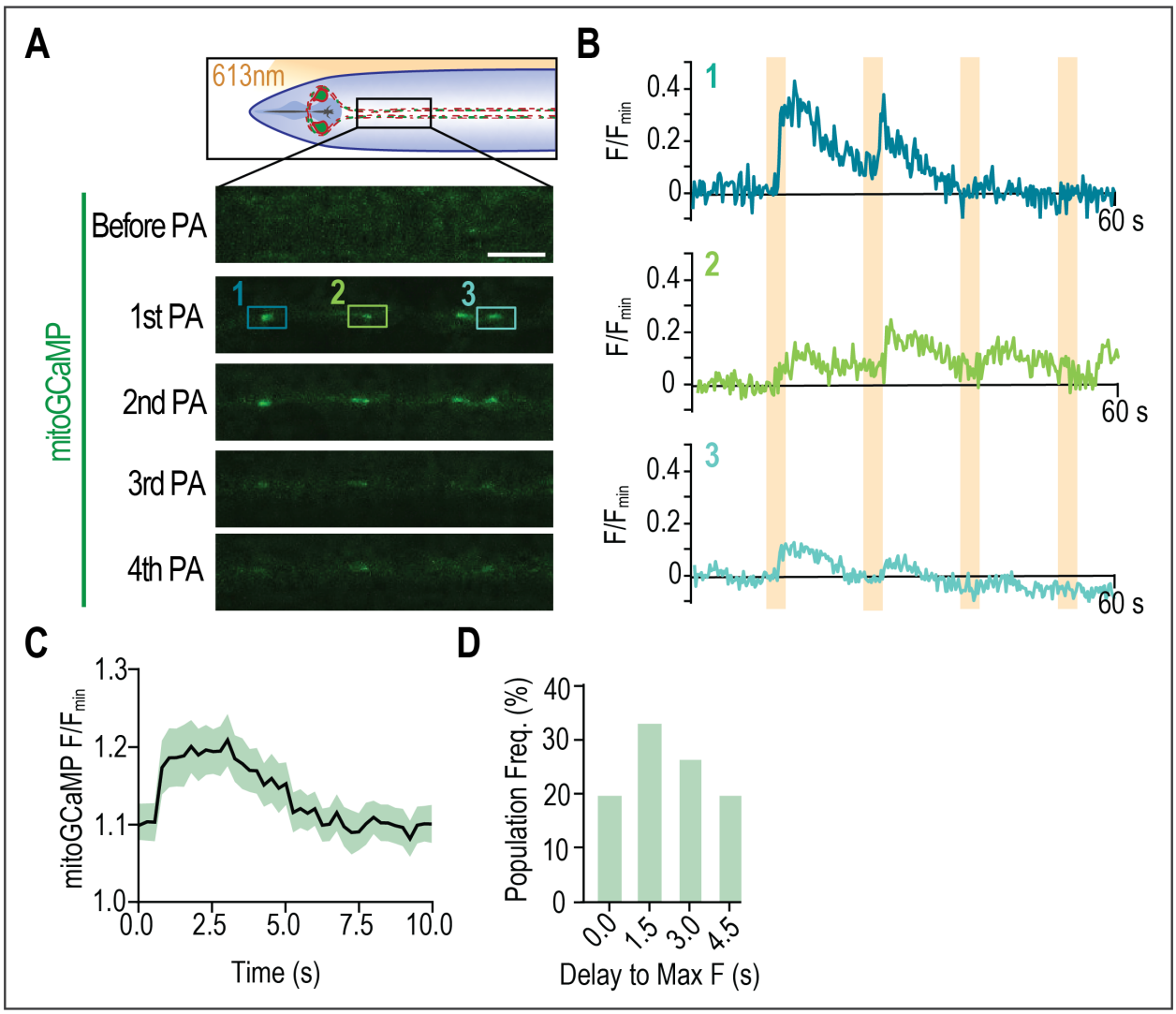

Figure 3.2 - Mitochondrial calcium uptake follows neuronal activation.
A) Top. Illustration of dual ChRimson and mitoGCaMP expression in AVA. Bottom. Representative images of mitoGCaMP fluorescence in the AVA neurite following 4 photoactivations (PA) with 613 nm light. Scale bar = 5 µm. B) Changes in mitoGCaMP fluorescence over time for the individual mitochondria numbered in panel A. Orange bars = 3 sec light pulse (613 nm, 0.04mW/mm^2) C) Average mitoGCaMP response normalized to the minimum fluorescence for individual mitochondria in the 10 s after PA (mean: black line, green shading: SEM; n = 15 mitochondria from 5 worms). D) The time from onset of PA to max. F/F_{min} for individual mitochondria (binned every 1.5 s; n = 15 mitochondria from 5 worms).

repeatedly activated ChRimson prior to fluorescence imaging of the mitochondria-localized ROS indicator, mito-roGFP (Figure 3.3 A). The duration of repeated ChRimson activation (33.3 mHz) positively correlated with 405/488nm roGFP fluorescence ratio (Figure 3.3 B). Since an increased 405/488nm roGFP fluorescence ratio indicates increased oxidation of the tool, this

finding implies that neuronal activity is positively correlated with mitochondrial ROS production. Taken together, these data suggest that neuronal activation leads to mitochondrial calcium uptake which in turn causes ROS production that is proportional the neuron's activity level.

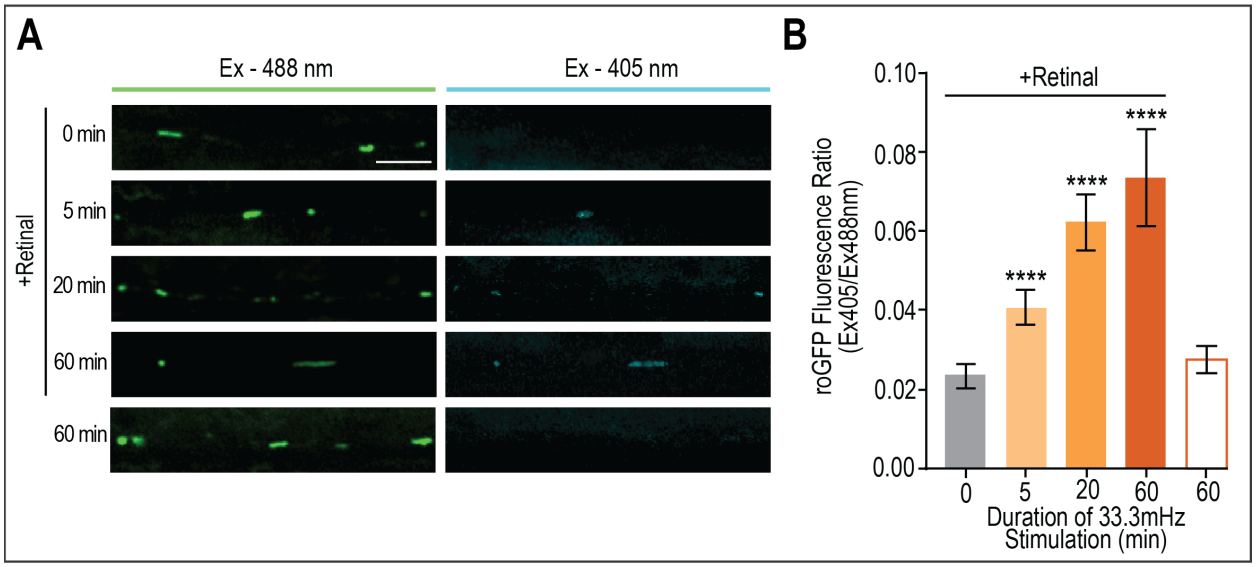

Figure 3.3 - Repeated neuronal activation leads to increased mitochondrial ROS production.
A) Confocal images of mitochondrial-targeted roGFP fluorescence due to 488nm (left column) or 405nm (right column) excitation after 0 – 60 min of repeated neuronal activation. B) Average roGFP fluorescence ratio following 0, 5, 20, or 60 minutes of repeated stimulation of ChRimson (at 33.3 mHz) with or without retinal (n=8 for each). ****: $p<0.0001$. Two-way ANOVA with Dunnett's correction.

3.4 Localized Calcium and ROS Signaling Alter Dynamics of Glutamate Receptor Transport and Delivery in Dendrites.

We have shown that whole-animal changes in calcium and ROS levels are correlated with altered GLR-1 transport dynamics within the neurite (Figure 2.1 and 2.3). We next sought direct evidence for the regulation of GLR-1 transport within the neurite by calcium and ROS. To do this, we optimized simultaneous calcium and GLR-1 transport imaging as well as the use of genetic tools for temporal and spatial control of ROS production *in vivo*.

To begin to clarify calcium's role within the dendrite in synaptic targeting of GLR-1, we quantified relative calcium concentrations within the AVA neurite in relation to the dynamics of

GLR-1 transport events. To do this, we optimized a simultaneous GCaMP and GLR-1 transport imaging protocol. Changes in the dynamics of a GLR-1 transport event (i.e., velocity and stopping) were matched with the relative GCaMP fluorescence at the corresponding timepoint and position within the neurite. This analysis revealed that higher cytoplasmic calcium levels led to slower or stopped GLR-1 transport events (Figure 3.4 A and B).

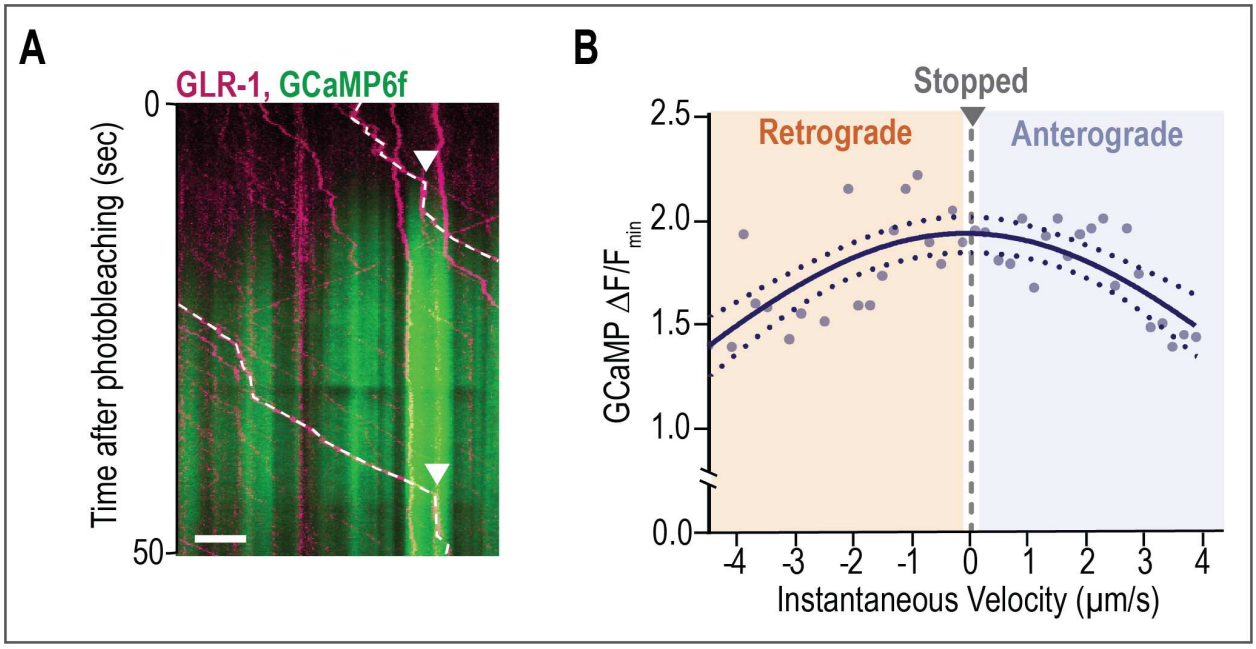

Figure 3.4 - Increased calcium levels correspond to slowed or stopped GLR-1 transport events.
A) Representative dual kymograph of GLR-1::mCherry fluorescence overlayed onto GCaMP fluorescence throughout the neurite (x-axis) over time (y-axis). Dashed lines highlight the movement of two GLR-1 transport events that stopped (vertical line segments; arrow heads) within a region of high GCaMP fluorescence. B) Plot of velocities of GLR-1 transport vs corresponding GCaMP fluorescence. Segment velocities were binned every 0.2 µm/s and their corresponding GCaMP fluorescence values (normalized to the GCaMP baseline, F_{min}) were averaged within each bin.

Since increased cytoplasmic calcium is thought to lead to mitochondrial calcium uptake and ROS production, we next assessed how mitochondrial ROS production within the AVA would impact the amount and dynamics of GLR-1 transport. To get at this, we cell-specifically expressed the genetically encoded photosensitizer, KillerRed which was tethered to the outer membrane of mitochondria (mito-KR) facing the cytoplasm. This enabled us to use green light to increase ROS at mitochondria in the AVA neuron exclusively. We first tested mito-KR and

optimized a stimulation protocol by co-expressing it with the mito-roGFP in the AVA (Figure 3.9). We learned that continuous illumination for at least 5 minutes was required to measure even a slight increase in mito-roGFP oxidation (Figure 3.9). After this optimization, we activated mito-KR cell-wide using the moderate light stimulation protocol (5 min of 567 nm light at 0.025mW/mm^2) prior to GLR-1 transport imaging.

We found that the amount of GLR-1 transport was reduced in a strain expressing mito-KR (*akIs141* + *csfEx188*) in comparison to controls (*akIs141*) without deliberate activation of mito-KR (Figure 3.5 A and B). Cell-wide activation of mito-KR with exposure to 5 min of 576 nm light further diminished the amount of GLR-1 transport in the mito-KR$^+$ strain. These results indicate that mitochondrial ROS production was likely stimulated by light used to mount worms for imaging and locate the AVA neurite. Regardless, further mito-KR activation decreased the amount of GLR-1 transport. A more detailed analysis of transport events also revealed that the presence of mito-KR reduced anterograde velocities and the addition of a 5 min light exposure exacerbated this effect in mito-KR$^+$ animals (Figure 3.5 C).

Interestingly, retrograde velocities were unaffected in any condition suggesting that increased ROS does not alter anterograde transport by damaging microtubules or inhibiting other necessary components of this process (Figure 3.5 C). It is important to note that exposure of *akIs141* controls to 5 min of 567 nm light had an off-target effect on anterograde velocity, but not on retrograde velocity or stop probability. Lastly, light activation of mito-KR led to a large increase in the stop probability of GLR-1 transport events (Figure 3.5 D). These results led us to ask: does local ROS production alter GLR-1 transport dynamics within a region of the neurite?

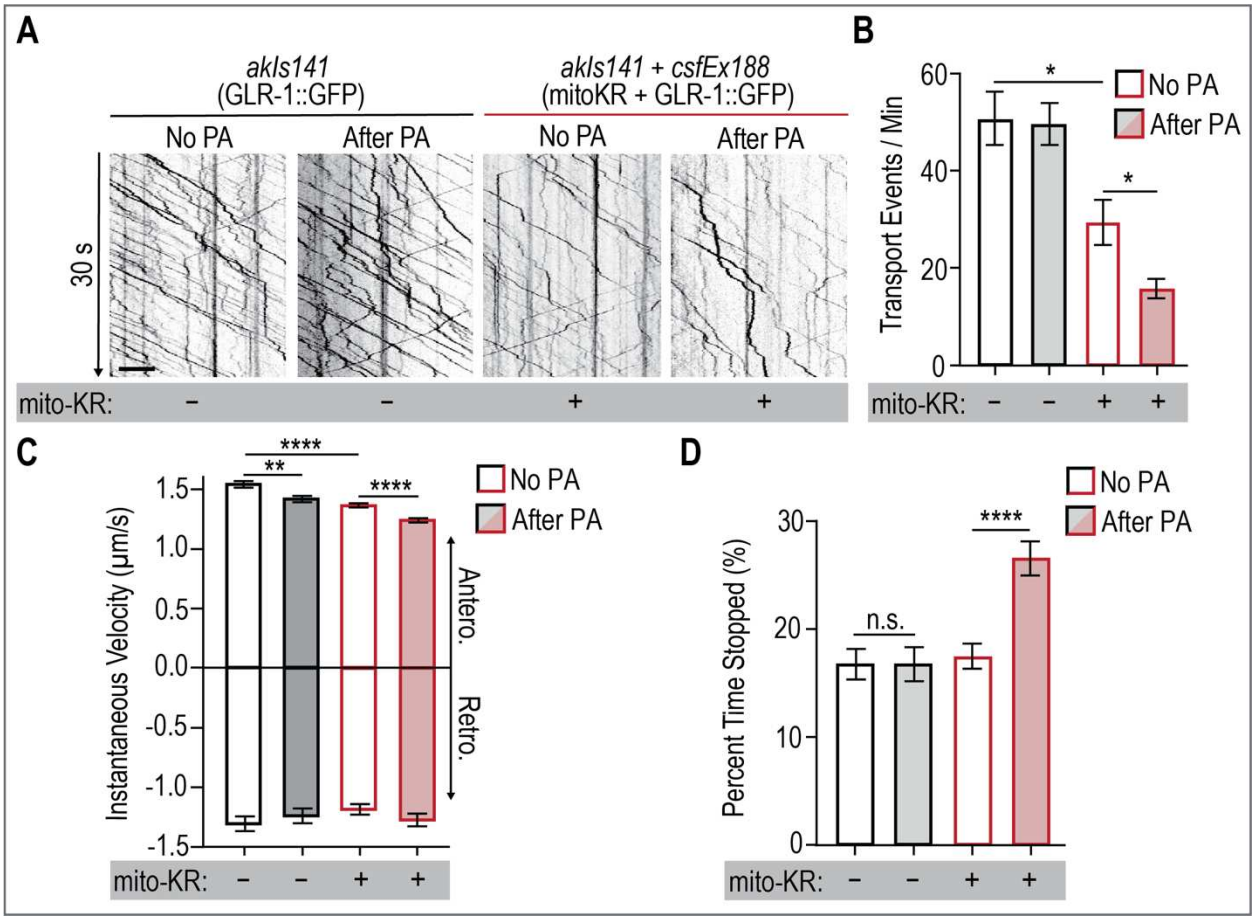

Figure 3.5 - Mitochondrial ROS production decreases GLR-1 transport and alters transport dynamics. A) Representative kymographs of GLR-1::GFP movement in the AVA neurite without or after 5 min of photo-activation (PA). Scale bar = 5 µm. B) Total number of transport events per minute quantified from kymographs representative of a 3 min image stream. n = 8 for each. *: $p<0.05$. C) Velocities of individual segments composing GLR-1 transport events for controls and mito-KR$^+$ animals with or without PA. n > 250 transport events from 8 animals for each. **: $p<0.005$, ****: $p<0.0001$. D) The percentage of time GLR-1 transport events spent stopped. One-way ANOVA with a Tukey multiple comparisons test.

Using a modified mito-KR activation protocol involving an LED system that was incorporated into our microscope, we selectively illuminated individual mitochondria for several seconds which was sufficient in increasing oxidation of mito-roGFP at illuminated mitochondria but not their neighbors (Figure 3.6 A and B). Next, we activated individual mito-KR$^+$ mitochondria with a 15 s pulse of low (2.5 µW) or high (10 µW) intensity 561 nm light immediately before 3 min of GLR-1 transport imaging (Figure 3.6 C). A detailed analysis of transport within

and outside of the targeted region showed that low and high light intensities for mito-KR activation differentially impacted GLR-1 transport velocities.

Anterograde velocities were decreased in the target region following a low but not high intensity light pulse when compared to other regions of the neurite within the same animal (Figure 3.6 D). Alternatively, retrograde velocities were unchanged by a low intensity light pulse but decreased by high intensity light (Figure 3.6 E). Both anterograde and retrograde velocities were slightly decreased outside of the light-targeted region in comparison to unstimulated controls suggesting that light may have diffracted outside of our defined targeting region (Figure 3.6 E). Slowed transport velocities could be an off-target effect of light similar to previously observed since *akIs141* controls that had a portion of their neurite illuminated with a high intensity light pulse also had a slight decrease in anterograde and retrograde transport velocities (Figure 3.10).

The stop probability was increased within the light-targeted regions only if mito-KR was present (Figure 3.6). More specifically, a low intensity light pulse resulted in a slight, but not significant increase in probability of GLR-1 transport stopping within the targeted region in comparison to adjacent, non-illuminated regions. In the case of the higher intensity light pulse, stop probability was significantly increased. A regional analysis of transport following stimulation of local ROS production at mitochondria complements the data trends seen for whole-cell activation of mito-KR+ (Figure 3.5). Together, they support that ROS signaling originating at mitochondria can regulate the amount of GLR-1 transport and alter transport dynamics within the neurite in a spatially specific manner.

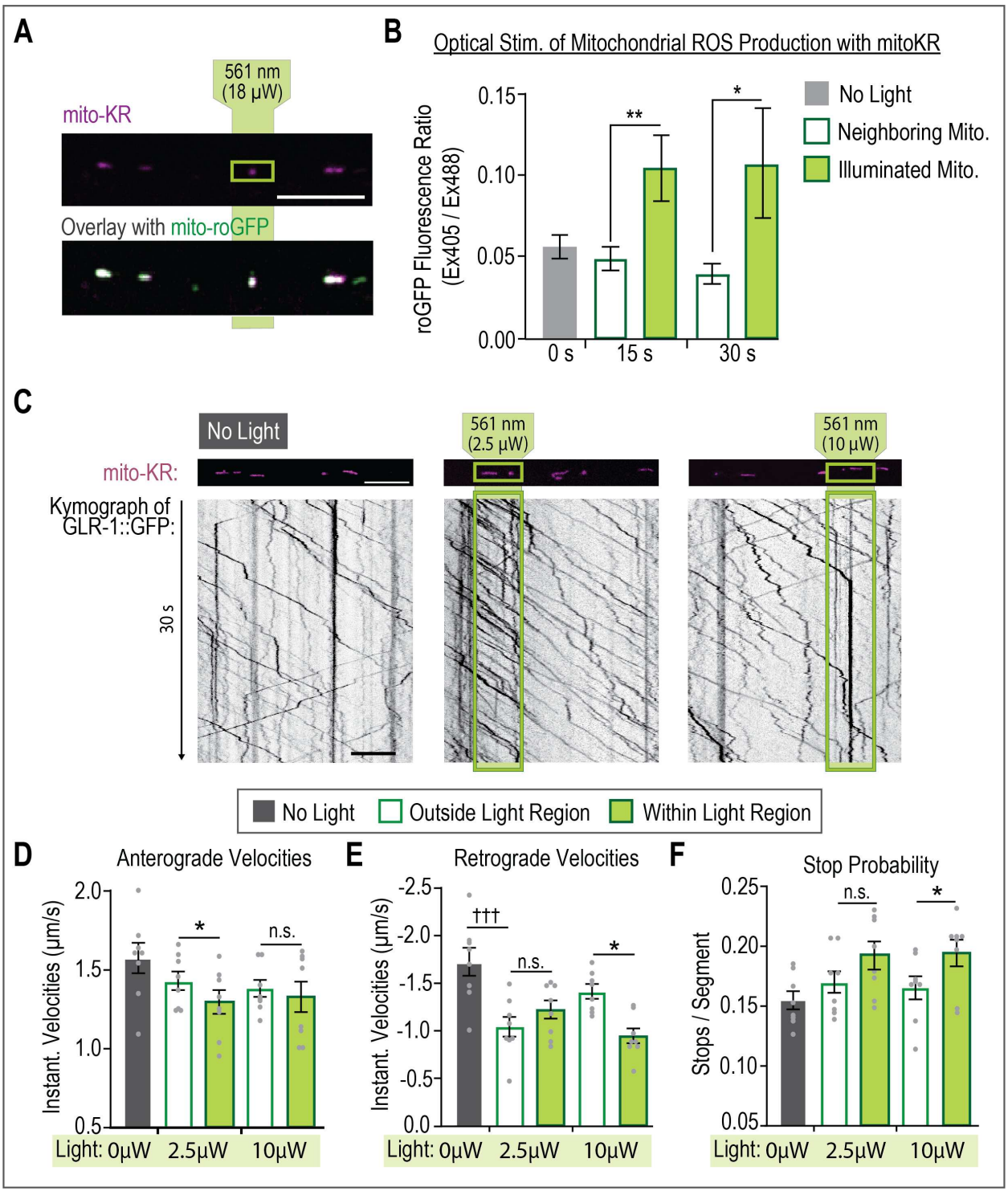

Figure 3.6 - Local ROS signaling originating from mitochondria alter GLR-1 transport dynamics in a spatially specific manner.

A) Representative fluorescent images of mitochondria-localized KillerRed (mito-KR) and its overlay with mitochondria-localized roGFP (mito-roGFP). Scale bar = 5 µm. B) The fluorescence ratio of mito-roGFP when excited by 405 to 488 nm light in mitochondria that were (white bars; n = 8 mitochondria from 8 worms) or were not (green bars; n > 20 mitochondria from 8 worms) targeted for light stimulation as well as in worms without any additional optical activation (gray bars; n > 20 mitochondria from 8 worms). *: $p<0.05$, **: $p < 0.005$…

Figure 3.6 - Two-tailed Student's t-test. No significant difference between the no light controls and the neighboring mitochondria (one-way ANOVA with Dunnett's test). C) Representative images of mito-KR fluorescence in the AVA neurite (top images). Green boxes indicate light targeted regions. Representative kymographs of GLR-1::GFP movement (bottom images). Green boxes on kymographs indicate the corresponding region in which mito-KR^{+} was light activated. Scale bar = 5 µm. D) Average instantaneous velocities for anterograde and E) retrograde transport without light as well as within or outside of regions targeted for a 2.5 µW or 10 µW light pulse. F) The number of stops normalized to total no. of segments within corresponding regions (grey points: average for an individual animal). n>250 transport events from 8 animals each. n.s: not significant; *: $p<0.05$; ***; Paired Student's t-test. †††: $p<0.0005$; One-way ANOVA with Dunnett's test.

Since we had previously shown that elevated ROS signaling regulates GLR-1 transport by modulating calcium influx into the AVA neuron (Figure 2.2 and 2.5), we hypothesized that these effects of ROS production at mitochondria on GLR-1 transport were also due to redox regulation of calcium influx. To address this, we collected an image stream of GCaMP fluorescence before and after light activation of mito-KR with a localized light pulse (15 s, 561 nm, 10 µW; Figure 3.7 A). We observed a slight, but not significant increase in both the amplitude of peaks and total GCaMP activity per minute in regions targeted for mito-KR activation compared to GCaMP activity in those regions before the activation of mito-KR (Figure 3.7 B and C). Importantly, the light pulse itself did not have an effect on controls (*csfEx62*). The high variation in this dataset prompts the need for additional replicates in order to determine if mito-KR activation truly increases calcium influx within localized regions of neurites.

3.5 Conclusion and Discussion

Abnormal mitochondrial function and ROS dyshomeostasis have been recognized to accompany many conditions and diseases that impact cognition, learning and memory (Cuestas Torres and Cardenas, 2020; Müller et al., 2018; Stefanatos and Sanz, 2018). Despite this, the roles ROS play in regulating the function of healthy neurons have been understudied. Here, we provide proof that activity-dependent ROS production from mitochondria (Figures 3.2 and 3.3) play a role in regulating GLR-1 transport at various levels (Figure 3.5 and 3.6). First, cell-wide

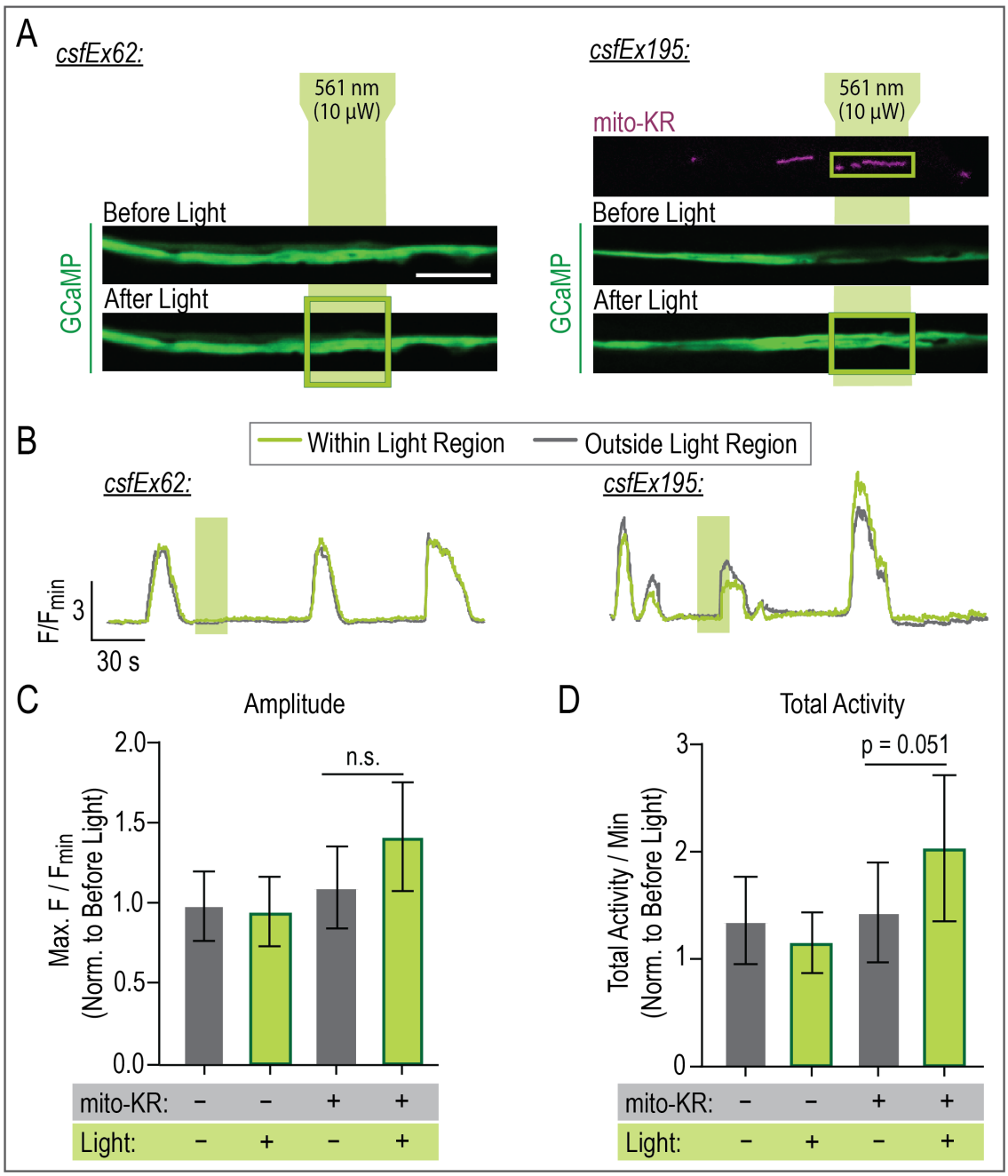

Figure 3.7 – Mitochondrial ROS production slightly increases local calcium influx within neurites.
A) Representative fluorescent images of GCaMP6f at individual timepoints before and after a 15 s light pulse for controls (*csfEx62*) and mito-KR^{+} animals (*csfEx195*). Green boxes represent region to which light was targeted. Scale bar = 5 µm. Top right. A corresponding fluorescent image of mito-KR indicating the mitochondria that were targeted for light stimulation. B) Traces of GCaMP fluorescence normalized to baseline (F/F_{min}) measured within (green traces) and outside (grey traces) of the light-targeted region throughout the entire image stream (4.25 min). Light green bar indicates the 15 s light pulse. C) The peak amplitude (maximum F/F_{min}) after the light pulse within (green bars) or outside (grey bars) the light-targeted region normalized to max. F/F_{min} before light in the corresponding region. n.s. = not significant. D) Total activity per minute calculated as a summation of GCaMP fluorescence above baseline per unit time. Data from each genotype and region (within, Light +, and outside, Light -, of targeted region) was normalized to total activity per minute that was recorded before light pulse for the corresponding regions. Two-tailed Student's t-test.

increases in mitochondria-derived ROS reduce the total amount of GLR-1 transport (Figure 3.5 B). In the neurite, this cell-wide increase in ROS slowed transport of newly synthesized receptors that were traveling from the cell body toward synapses, but not of retrograde transport that is thought to carry out the redistribution or recycling of receptors (Figure 3.5 C). A slowing of GLR-1 transport was also initiated by local increases in mitochondrial ROS production within small sections of the neurite (Figure 3.6 B). Both local and cell-wide increases in ROS originating at mitochondria increased the stopping of GLR-1 transport events which contrasts the effect of moderate, cell-wide increases in cytoplasmic ROS resulting from *ctl-2(lf)* (Figure 2.3, 3.5 D and 3.6 C). Relative calcium levels within a neurite correspond to the speed and stopping of GLR-1 transport events (Figure 3.4). Interestingly, local increases in mitochondria-derived ROS slightly increased calcium influx in a localized manner (Figure 3.7). This may explain how elevated ROS are acting on GLR-1 transport, but it is also possible that direct redox modifications of transport machinery or GLR-1 adaptor proteins cause the observed changes in transport dynamics.

Mitochondrial Calcium Buffering and ROS Production in Neurons

The high variation in calcium buffering observed following neuronal activation suggests that mitochondria throughout the neurite have different calcium handling abilities. This coincides with descriptions of synaptic and non-synaptic mitochondria having different susceptibilities to calcium overloads (Brown et al., 2006). Variation in mitochondrial calcium buffering would allow mitochondria to not only shape calcium signaling at an individual synapse, but also alter the sensitivity of metabolic rate to neuronal activity. Future work on what mitochondrial properties or components regulate the mitochondrial calcium buffering is a necessary first step toward understanding the functional diversity of mitochondria and the significance of this diversity on

synaptic function. Newly developed tools for measuring and controlling mitochondrial calcium uptake have finally made addressing this question possible (Ashrafi et al., 2020; Kanemaru et al., 2020; Kichuk et al., 2021). Lastly, it is clear that upregulation of OXPHOS by calcium would increase ROS production, so variation in mitochondrial calcium buffering would also contribute to diverse, localized ROS signaling.

Local ROS Signaling in the Regulation of Transport and Synaptic Targeting of GLR-1

Localized ROS signaling has been theorized to occur for quite some time (Gerich et al., 2009; Halliwell, 1992; Sies, 2017), but the inability to measure physiological level of ROS with subcellular resolution has prevented direct proof of such. By combining the light-sensitive ROS producer, KillerRed with an innovative integration of an LED system, we were able to address the impact of localized increases in ROS (with ~5 µm resolution) on GLR-1 delivery to synapses. To our knowledge, this study is the first of its kind for assessing the impact of local ROS production. However, other research has shown that ROS are involved in the intracellular transport of other cargo. For example, in vertebrate neurons, mitochondrial mobility was inhibited by global increases in ROS (Debattisti et al., 2017). In axons, ROS inhibited transport of mitochondria and Golgi-derived vesicles whose cargos were unidentified (Fang et al., 2012). This may indicate that ROS regulate transport via molecular motors in a way that is non-specific to the transport cargo. Additional research on the role of ROS in the transport of other types of synaptic receptors (i.e., acetylcholine receptors) and vesicles subtypes (i.e., lysosomes) is required to determine the specificity of this regulation by ROS.

Altogether, these data suggest that ROS produced from mitochondria in the nerite increase local calcium influx which initiates the slowing and stopping of molecular motors carrying GLR-1. These changes in transport dynamics likely precede the delivery of GLR-1 to

synaptic sites. However, additional experiments that directly measure receptor delivery rates is required to support this idea. Identifying this potential role of mitochondria in the regulation of glutamate receptor targeting to synapses has broad implications for our mechanistic models of synaptic plasticity, neurodegeneration and aging.

3.6 New Methods

Cloning and Transgenic Strains

Plasmids were created using In-Fusion Cloning (Takara Bio) or the Gateway recombination (Invitrogen) method. DNA primers for In-Fusion were created using Takara Bio's online In-Fusion Primer Design Tool and with the opensource ApE Plasmid Editor (M. Wayne Davis) for Gateway. Cloning methods specific to plasmids used in this Chapter are detailed in Table 3.1. The microinjection method described in Chapter 2.2F was used create the transgenic strains in Table 3.2 via injection of plasmids in Table 3.1.

Table 3.1 - Plasmids

Plasmid Name	Gene/Insert	Source
pAS1	*Prig-3::GCaMP6f*	Stetak Lab, Univ. of Basel
pJM23	lin-15p::*lin-15*	Maricq Lab, Univ. of Utah
pCT61	*egl-20p*::*nls*::DsRed	Maricq Lab, Univ. of Utah
pDM1556	*Prig-3::GLR-1::mCherry*	Maricq Lab, Univ. of Utah
pDM2251	*Prig-3::EAT-4::mRFP*	Maricq Lab, Univ. of Utah
pRD15	*Pflp-18::TOMM20::roGFP::let-858*	Gateway Cloning
pRD36	*Pflp-18::TOMM20::KillerRed::let-858*	In-Fusion Cloning
pRD22	*Pflp-18::PH::KillerRed::let-858*	Gateway
pRD30	*Pflp-18::ChRimson::TdTomato*	Gateway Cloning
pRD27	*Pflp-18::ChRimson::let-858*	Gateway Cloning
pKK01	*Pflp-18::mito4x-GCaMP6f::let-858*	In-Fusion Cloning

Table 3.2 - Transgenic Strains		
Strain	Genotype	Contents
FJH 18	*akIs141 II; glr-1(ky176) III*	*Prig-3::GLR-1::GFP* (integrated)
FJH 185	*lin-15(n765ts) X; csfEx62*	pAS1 + pJM23 + pCT61
FJH 266	*lin-15(n765ts) X; csfEx115*	pAS1 + pRD22 + pJM23
FJH 276	*glr-1(ky176) III; csfIs1*	pAS1 + pDM1556 + pJM23 (integrated)
FJH 296	*lin-15(n765ts) X; glr-1(ky176) III; csfEx67*	pRD15 + pDM1556 + pJM23
FJH 402	*lin-15(n765t)s, lite-1(ok530) X; csfEx160*	pRD30 + pRD15 + pJM23 + pCT61
FJH 412	*lin-15(n765t)s, lite-1(ok530) X; csfEx167*	pRD30 + pAS1 + pJM23
FJH 416	*lin-15(n765ts), lite-1(ok530) X; csfEx168*	pRD36 + pRD15 + pJM23
FJH 431	*lin-15(n765ts), lite-1(ok530) X; csfEx187*	pKK01 + pRD27 + pDM2251 + pJM23
FJH 553	*lin-15(n765ts) X; csfEx195*	pRD36 + pAS1 + pJM23 + pCT61
FJH 555	*akIs141 II; glr-1(ky176) III; csfEx188*	*akIs141;* pRD36 + pJM23 + pCT61

Whole-cell Activation of AVA ChRimson

L4s from strains expressing the extrachromosomal array *csfEx160*, *csfEx167* or *csfEx187* were picked onto an NGM/OP50 plate that was coated with a 100 μM concentration of all-Trans Retinal (Sigma-Aldrich, cat no: R2500-25; diluted with M9 buffer). Worms were left overnight on Retinal plates before optical neuronal activation via an LED array (613 nm, CoolBase 7 LED module from LuxeonStar). ChRimson expression was verified in these strains behaviorally by testing light-induced reversals. For mitoGCaMP experiments, the LED array was placed above the DIC condenser lens and controlled remotely using a pattern generator that pulsed the LED every 15 s for 3 s. LED intensity adjusted at the beginning of each experiment to 40 μW/mm^2 using a custom potentiometer in combination with a digital optical power console (ThorLabs,

PM100C) and microscope slide photodiode sensor (ThorLabs, S170C). For ChRimson activation before roGFP imaging, freely behaving one-day-old adults were placed onto a fresh NGM/OP50 plate 2 inches beneath the 613 nm LED array (40 μW/mm^2). The pattern generator pulsed the LED for 1 s ever 30 s (33.3 mHz) for 5 to 60 min before being mounted for imaging.

Stream Imaging of and Analysis mitoGCaMP Fluorescence

Worms were mounted for imaging in mixture containing 15 mM Muscimol and polystyrene beads as previously described. Image streams of mitoGCaMP fluorescence were collected on our spinning disk confocal (see Chapter 2.2F) using a 5% output of our 488 nm imaging laser and a 250 ms exposure. One-minute-long streams were collected capturing 4 pulses of 613 nm light. Average fluorescence values of individual mitochondria for each frame were determined using MetaMorph's region measurement tool. Background fluorescence near each mitochondrion was quantified per frame using the same method which was later subtracted from mitoGCaMP fluorescence for each frame in Excel. Then, all fluorescence values were normalized to the minimum value (F/F_{min}). Fluorescence peaks were aligned using the first frame of light stimulation. From this alignment, averaged fluorescence peak and delay from light-on to maximum fluorescence was calculated.

Ratiometric Fluorescence Imaging and Analysis of mito-roGFP

Immediately after ChRimson stimulation, worms were mounted for imaging in a 15 mM Muscimol solution. The AVA neurite containing roGFP$^+$ mitochondria was located, and images were collected with a 500 ms exposure every 0.25 μm to capture a 5.25 μm stack of images around the neurite. The 525 nm emission was imaged with 405 nm then 488 nm illumination at each Z-plane. The average roGFP fluorescence due to 405 or 488 nm excitation was measured at individual mitochondria using MetaMorph's region measurement at a single Z-plane in which

the roGFP fluorescence due to 488 nm excitation was the highest. The average background fluorescence at that Z-plane was also logged. The mitochondria region was copied to the fluorescence image collected with 405 nm excitation at the corresponding Z-plane, then roGFP and background fluorescence values were logged identically.

Localized mito-KR Activation with GCaMP/GLR-1 Imaging

To activate mito-KR (TOMM20::KillerRed) within discrete regions of the AVA, the neurite was located using a 100x objective and the co-expressed fluorescent reagents (GCaMP or GLR-1::GFP) and the 488 nm imaging laser. An image of mito-KR fluorescence in a single Z-plane was briefly acquired using a 100 ms exposure and 561 nm imaging laser. Then, using this image, a mask was created around a region with one or two mito-KR^{+} mitochondria. Using the green LED from a CoolLED system (pE-300^{ultra}) that is directed to illuminate the masked region with a Mosaic II digital mirror device (Andor Mosaic 3) controlled through MetaMorph. LED intensity was adjusted to 2.5 or 10 µW total output using a digital optical power console (ThorLabs, PM100C) and photodiode sensor (ThorLabs, S130C).

The LED was pulsed to illuminate the masked region for 15 s during image streaming via MetaMorph's 'Trigger Components' functions. For GCaMP imaging, a 60 s image stream was collected with 5% power of our 488 nm imaging laser and a 250 ms exposure. Then, the shutter for the CoolLED system was opened for 15 s before imaging GCaMP for another 3 min. When KillerRed was activated before GLR-1 transport imaging, an RFP image was acquired as previously described to create a mask region for targeting of the LED. Then, using an image of GLR-1::GFP, a larger region of the neurite was selected for photobleaching using the parameters described for other transport experiments (see Chapter 2.2F). A 3 min image stream of GFP fluorescence was collected using a 100 ms exposure time (50% 488 nm imaging laser power). For

both GCaMP and GLR-1 transport imaging, a consistent Z-plane was held in focus for the entire imaging session using the continuous focus function of a Z drift compensator (Olympus, IX3-ZDC2).

Analysis of GCaMP Imaging with mito-KR Activation

Using MetaMorph's region measurement tool, the GCaMP fluorescence within the region that was or was not targeted for activation of mito-KR was quantified for each frame. These fluorescence values were exported as individual comma delineated files for each animal which were then imported into an Excel document with custom functions (created in Excel's Visual Basic Editor). These functions calculated the baseline (F_{min}) by determining the lowest maximum fluorescence value and averaging all values within 30% of that minimum. Then, separate calculations for the following were done for the first minute (before light stimulation) and the 3 min post-stimulation. Any values above the baseline range were summed and normalized to the baseline for that animal to calculate total GCaMP activity. The maximum fluorescence value was divided by the baseline to calculate the amplitude (maximum F/F_{min}). Representative traces are raw fluorescence values normalized to F_{min}.

Analysis of GLR-1 Transport with Mito-KR Activation

Image streams were converted into kymographs using MetaMorph's kymograph function which were analyzed using the ImageJ plug-in KymoAnalyzer as previously described (see Chapter 2.2F). The x- and y-coordinates for individual GLR-1 transport events were imported into an Excel document where instantaneous velocities were calculated by multiplying the Δx (in pixels) by the relative pixel size when imaging with our 100x objective (0.104 nm) and the Δy by the frame rate (0.1 s). These velocities were separated by whether the corresponding segment was within or outside of the light-targeted region. The light-targeted region was defined as

+/- 25 pixels surrounding the center of the light-targeted region. Then, velocities were further categorized into anterograde (positive) or retrograde (negative) velocities as well as stops (velocity = 0) by custom Excel functions. This allowed for the calculation of average velocities within vs outside light stimulated regions. Additionally, stop probability was calculated by summing the number of stops within each region and normalizing to number of transport segments that traveled through that region.

Whole Animal Activation of Mito-KR in AVA

Individual one-day-old adults of transgenic strains (*csfEx168, csf195* or *csfEx188*) containing pRD36 [*Pflp-18::TOMM20::KillerRed::let-858*] without multi-vulva phenotype were transferred onto a fresh NGM/OP50 and placed 2 inches below a 567 nm LED array (CoolBase 7 LED module from LuxeonStar). The light intensity was adjusted to 25 μW/mm^2 with our potentiometer, digital optical power console and photodiode sensor (S130C). Worms were illuminated for 5 min before being immediately mounted in Muscimol solution for GLR-1 transport imaging.

Dual Imaging and Analysis of GCaMP and GLR-1 Transport

In one-day-old adults (strain: FJH 276), image streams of GCaMP6f fluorescence and GLR-1::mCherry were simultaneously acquired on our Olympus Confocal (see Chapter 2.2F for details) that is additionally equipped with two Andor iXon Ultra EMCCD cameras and a 565 nm long pass beam splitter integrated into a WaveFx-F1 spinning disk by Applied Spectral. First, camera alignment was adjusted as needed with guidance from a Tetraspeck fluorescent microsphere slide (sphere size = 0.5 µm, Thermo Fisher Scientific T14792). Using the 100x objective, a region of the AVA neurite was located using the 561 nm excitation laser and a 250 ms exposure. The GLR-1::mCherry fluorescence was photobleached in a ~25 µm long section of the

neurites using our Coherent steady-state 3 W laser set to an output of 0.5 W with a 1 s pulse time. A 100 s dual image stream was then collected with a 200 ms exposure.

Analysis of Dual GCaMP and GLR-1 Transport Data

Both GCaMP and GLR-1 kymographs were created using identical line segments and MetaMorph's kymograph function. Then, GCaMP fluorescence values throughout the neurite for each frame was quantitated using MetaMorph's Region Measurement function to gain pixel-by-pixel GCaMP fluorescence values of the kymographs. GLR-1 transport events were identified using kymographs and the ImageJ plug-in KymoAnalyzer as previously described. The pixel-by-pixel GCaMP fluorescence values and track coordinates for a given animal was imported into an Excel document with custom functions created with Excel's Visual Basic Editor. These functions calculated the velocities of each track segment and output the average GCaMP fluorescence from a 17x17 pixel square around the coordinate value corresponding to the start of the track segment. This data was binned by velocities (every 0.2 μm/sec) using custom R code that was created in R Studio (1.1.456) with tools from the following R libraries: rbin (0.2.0), usethis (1.6.1), devtools (2.3.1), fields (10.3).

Data and Statistical Analysis

All datasets were tested for outliers using Thompson's Tau Test. Cleaned data was imported into Graph Pad's Prism for generation of graphs and statistical testing. The effect of a treatment within individual animals was tested using a two-tailed paired Student's t-test. Unpaired data was tested with a one-way ANOVA using a Tukey's or Dunnett's multiple comparison test depending on whether means between all columns were to be compared (Tukey's) or if the mean of a control was to be compared to that of all other groups (Dunnett's). If only two

means from separate groups were compared, a two-tailed Student's t-test was used. The statistical test used is indicated in the figure legends of each figure.

Chapter 4 – Methods for *In Vivo* Optogenetic Control of Cytoplasmic Calcium Levels in *C. elegans*

4.1 Summary

The transparent cuticle, mapped neuronal connectome and ability for cell-specific expression in *C. elegans* allows for *in vivo* optogenetics in combination with calcium imaging in an intact animal. This makes using *C. elegans* valuable over vertebrate models for optimization of optogenetic techniques for a given question. If and how synaptic activation dictates the delivery and exocytosis of new glutamate receptors has not been directly demonstrated. This is due to technical challenges that have prevented reliable activation of individual synapses *in vivo* while also imaging the transport of these receptors. To overcome these challenges and enable this experiment, I characterized the use of different light-sensitive tools for increasing cytoplasmic calcium in the AVA neuron. In Chapter 4.3, I detail how four different light-sensitive tools lead to increased calcium when expressed directly in the AVA. Of the four tools, the calcium releaser PACR, the calcium channel regulator optoSTIM and classic ChR2 were the least reliable for elevating calcium. The red-shifted ChR, ChRimson, was the most reliable and resulted in the largest increase in calcium. Then, Chapter 4.4 describes the caveats of optically stimulating mechanosensory neurons that are presynaptic to AVA. Specifically, optical activation was rarely achievable when *C. elegans* are mounted for imaging making this paradigm unusable for activating AVA while doing any type of imaging. The results shared in this chapter indicate that low expression of ChRimson in AVA is the most promising optogenetic approach for future questions.

4.2 Introduction

The transparent cuticle of *C. elegans* enables *in vivo* activation of optical tools in an intact organism. Furthermore, cell-specific expression of these tools permits single-cell manipulation without the need of high-end, spatially precise laser setups. Because of this, *C. elegans* have been recognized for their ability to help us understand the properties and limitations of optogenetic tools (Fischer et al., 2018). *In vivo* optogenetics using *C. elegans* have been largely used for circuit analysis where the functional output is behavior. However, understanding the dynamics and reliability of optical activation in individual neurons will allow for better selection of optogenetic tools (low or high light sensitivity), guidance on subcellular targeting (plasma or synaptic membrane), and optimization of stimulation protocols for each neurobiological question. In *C. elegans*, there have been detailed functional measurements of optical activation in muscle cells and some neurons (Jensen et al., 2012; Liu et al., 2009; Narayan et al., 2011) which have helped identify ideal tools for certain neurobiological questions. For instance, the light toxicity associated with long-term neuronal activation was overcome after the identification of a Channelrhodopsin (ChR) variant that allowed for prolonged neuronal activation *in vivo* in *C. elegans* (Berndt et al., 2009; Schultheis et al., 2011). Additionally, the low calcium conductance of many light-sensitive channels has led to the development of specific ChR variants as well as other tools for specifically elevating cytoplasmic calcium (Fukuda et al., 2014; Kleinlogel et al., 2011; Kyung et al., 2015).

The next wave of optogenetic innovation involves combining optical manipulation and measurement of neuronal activity which were made possible by a new generation of calcium and voltage indicators with fast kinetics (Beck and Gong, 2019; Inoue, 2021). These advancements not only allow for validation of optical tools, but also characterization of the temporal and spatial

dynamics of neuronal activation due to a specific optical tool or stimulation protocol *in vivo*. Using a combination of light-sensitive tools and calcium indicators, we assessed the light-induced activation of the AVA interneuron *in vivo*. The overarching goal for characterizing different optogenetic approaches for AVA activation was to identify an approach that would allow for optical stimulation of the AVA in combination with GLR-1 transport imaging. The advantages and downfalls of the approaches explored are detailed in this chapter to aid the further optimization of *in vivo* activation of AVA with light.

4.3 Use of Genetically Encoded Reagents for Postsynaptic Increases in Calcium

Two different optogenetic approaches can be used for activating a neuron of interest. First, the optical tool can be expressed directly in the neuron of interest to control activity independent of synaptic function and efficacy. Second, the optical tool could be expressed in the presynaptic neuron where light activation is intended to activate the postsynaptic neuron of interest via synaptic transmission. Each approach has its advantages, so both were explored for light-induced activation of the AVA interneuron. This chapter specifically focuses on characterizing how optical tools expressed in the AVA elicit elevations in cytoplasmic calcium.

It has been shown that ChRimson expression in AVA leads to increases in cytoplasmic calcium (Gordus et al., 2015), however, characterizing other optical tools such as ChR2 or other blue-light sensitive tools would allow for additional combinations of fluorescent reagents. Additionally, since ChRimson and ChR2 have low calcium conductance, it is worthwhile understanding the utility of other optical tools for temporal control of cytoplasmic calcium levels. One such tool is a photoactivatable Ca^{2+} releaser (PACR). PACR is a chimera of Calmodulin and a

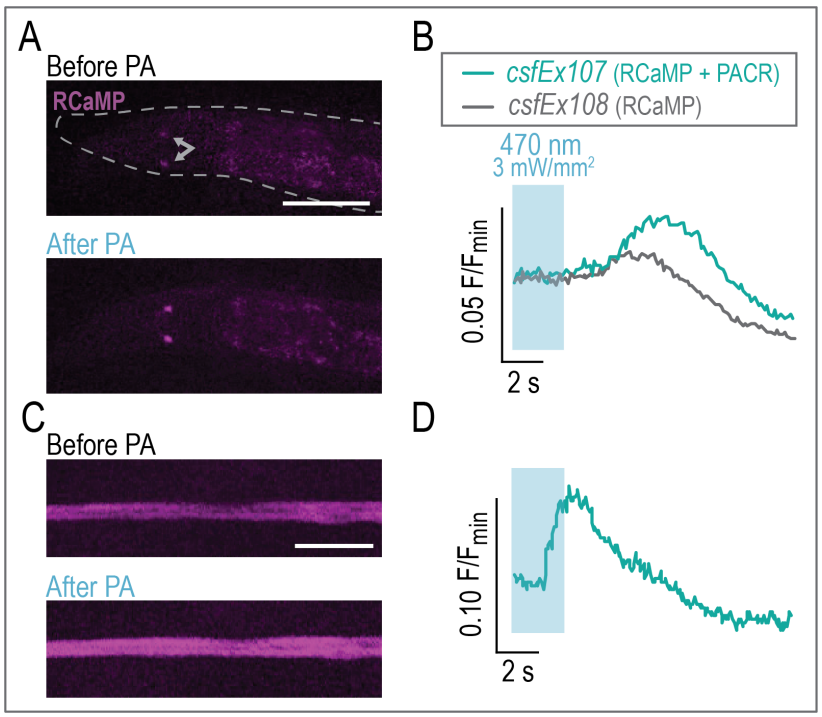

Figure 4.1 – PACR activation in the AVA interneuron.
A) Fluorescent images of RCaMP in the AVA cell bodies at a single z-plane before or after photoactivation (PA) with a 3 s pulse of 470 nm light (3 mW/mm^2). Gray dashed line is outlining the head of the worm and arrows indicate the placement of the AVA cell bodies. Scale bar = 50 µm. B and D) Representative traces of RCaMP fluorescence in AVA cell bodies normalized to minimum fluorescence (F/F_{min}) following PA with (turquoise trace) or without (gray trace) PACR. C) Fluorescent images of RCaMP in the AVA neurite at a single z-plane before or after PA. Scale bar = 5 µm.

photosensitive protein domain called LOV2 (Fukuda et al., 2014). This cytoplasmic tool binds up calcium during basal conditions. Then, upon stimulation with blue light (~450 nm), PACR undergoes a conformational change that causes the release of bound calcium.

When expressed in AVA with the calcium indictor RCaMP, small increases in RCaMP fluorescence were measured following a 3 s pulse of bright blue light (3 mW/mm^2; Figure 4.1). Light-induced increases in RCaMP fluorescence were observed in the AVA cell bodies (Figure 4.1 A and B) as well as in the neurite (Figure 4.1 C and D). At both locations, PACR activation was unreliable in eliciting an increase is RCaMP fluorescence (~60% response rate), and when it did, the increase was only ~5% (Figure 4.1 B and D). In the absence of PACR, blue light often increased RCaMP fluorescence albeit to a lesser extent than when PACR was present (Figure 4.1

B). This suggested that there is a native light-sensitive protein in AVA that can increase cytoplasmic calcium. The only light-sensitive protein identified in *C. elegans* is a gustatory receptor encoded by the *lite-1* gene, so we conducted all subsequent optogenetic experiments in *C. elegans* with a loss-of-function mutation in *lite-1* (Table 4.2).

A different type of optogenetic tool for increasing cytoplasmic calcium is a light-sensitive regulator of endogenous calcium channels called optoSTIM. It was engineered using a light-sensitive domain of a plant-derived photoreceptor and a portion of human STIM-1, a regulator of calcium-release activated calcium (CRAC) channels. When activated with light, the photoreceptor homodimerizes forcing oligomerization of STIM-1. Then, STIM-1 oligomers bind and activate CRAC channels to allow calcium influx. This association and redistribution of eGFP::optoSTIM can be visualized in single cells following light stimulation. However, during initial testing of optoSTIM in the AVA neuron, I did not observe light-dependent congregation or redistribution of eGFP::optoSTIM (Figure 4.2 A). This suggested that despite conservation of STIM-1 and CRAC channels, human STIM-1 was not similar enough to *C. elegans* STIM-1 to activate endogenous CRAC channels.

To create a *C. elegans*-specific version of this tool (optoCSTIM), I exchanged the human STIM-1 fragment for *C. elegans* STIM-1. Light stimulation of eGFP::optoCSTIM with a 488 nm imaging laser (5% power) caused the diffuse eGFP fluorescence to change into punctate eGFP signal in the cell body and neurite within a few seconds (Figure 4.2 B and C). Co-expression with RCaMP confirmed that optoCSTIM binds and activates CRAC channels in the AVA neuron since changes in RCaMP fluorescence (30 – 80% increase) were observed immediately after the start of imaging (Figure 4.2 D). Unfortunately, the response to light was unreliable and variable

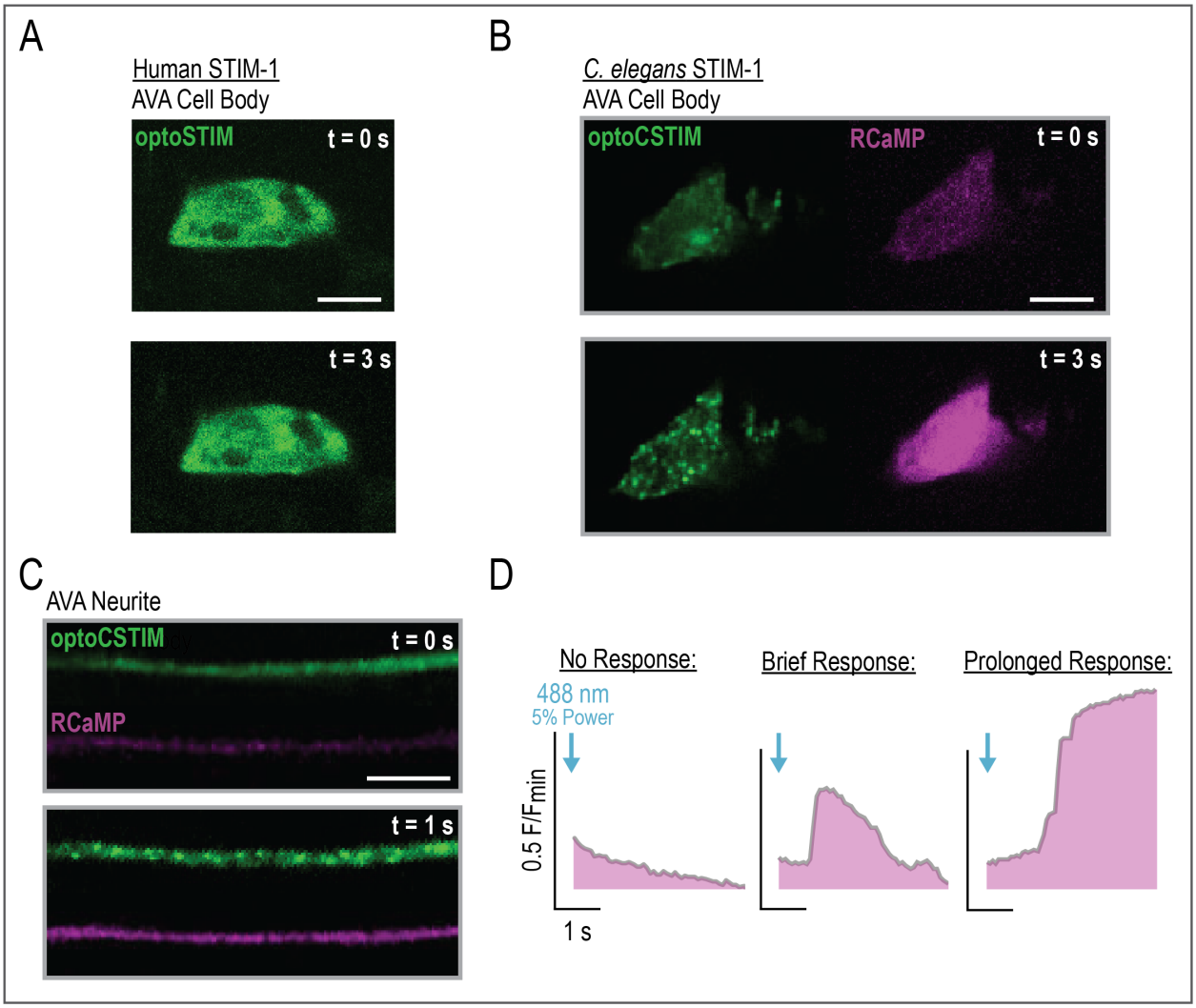

Figure 4.2 – Activation of endogenous calcium channels in the AVA with optoCSTIM.
A) Fluorescent images of eGFP::optoSTIM with the human STIM-1 fragment in the AVA cell body at the beginning and 3 s into acquisition of an image stream using a 488 nm imaging laser (5% power). Scale bar = 5 µm. B and C) Fluorescent images of eGFP::optoCSTIM (with *C. elegans* SITM-1) and RCaMP simultaneously acquired in the AVA cell body (B) or neurite (C) at the beginning and a few seconds into the dual image stream. Scale bar = 5 µm. D) Representative traces of the RCaMP fluorescence in the AVA neurite during the first 5 s of imaging that are representative of the different responses observed.

(Figure 4.2 D). This is hypothesized to be due to irreversibility or slow dissociation (>5 min) of channel-bound optoCSTIM or of the light-sensitive domain. Since neither of these calcium-specific tools resulted in reliable, large increases in cytoplasmic calcium, I turned to optimizing the use of Channelrhodopsins in AVA.

First, ChRimson was used to activate AVA directly. High ChRimson expression prevented calcium imaging with GCaMP due to activation of ChRimson by the 488 nm imaging laser. Lowering ChRimson expression and reducing the power of our 488 nm imaging laser (0.1%) allowed for calcium imaging while activating ChRimson. During a 3 s pulse of 613 nm light (0.1 mW/mm^2), large increases in GCaMP fluorescence were observed only when worms were supplemented with Retinal (Figure 4.3 A and B). Repeated optical activation within the same imaging session reliably initiated similar increases in GCaMP fluorescence (Figure 4.3 B). The GCaMP fluorescence peak occurred consistently within a few seconds of the light stimulus onset and peak amplitudes varied by ±27% from the average peak fluorescence (Figure 4.3 C).

Since ChRimson's high sensitivity to light proved to be problematic initially for calcium imaging, we also created a strain with AVA expression of ChR2 since it is less light-sensitive. The co-expression of ChR2 with RCaMP readily allowed for calcium imaging during light stimulation (Figure 4.3 D). While imaging RCaMP fluorescence, activation of ChR2 with a 3 s light pulse often increased RCaMP fluorescence, but repeated simulation was less reliable than ChRimson in eliciting increases in RCaMP fluorescence (Figure 4.3 B and E). Taken together, low ChRimson expression in AVA appears to be the best suited of these optical tools for reliably inducing large increases in cytoplasmic calcium.

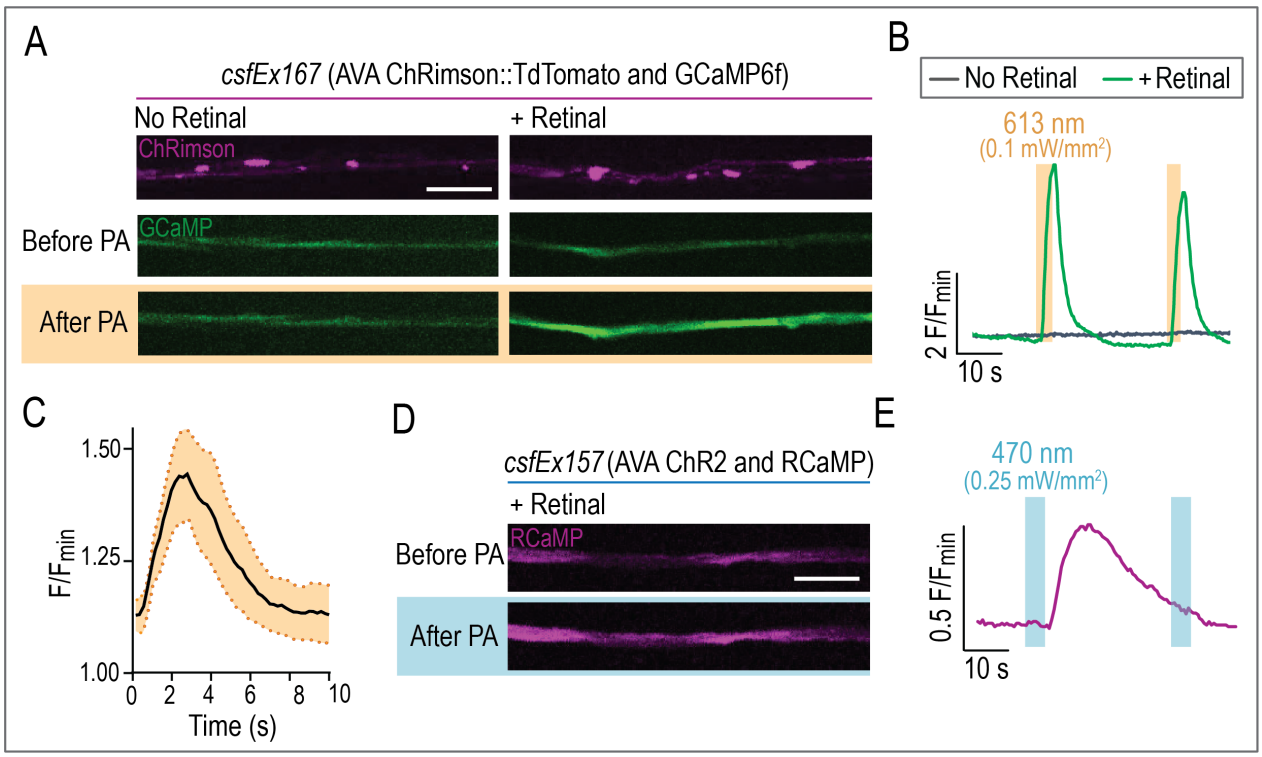

Figure 4.3 – Activation of AVA interneurons with Channelrhodopsins.
A) Representative fluorescent images of ChRimson::TdTomato (top images) as well as GCaMP in a single z-plane of the AVA neurite before and after photoactivation (PA) in *csfEx167*-containing strain with and without Retinal treatment. Scale bar = 5 µm. B) Changes in GCaMP6f fluorescence normalized to minimum baseline fluorescence (F/F_{min}) in individual *csfEx167* worms over a 60 s image session with 2 pulses of 613 nm light (orange bars, duration = 3 s, 0.1 mW/mm^2) in *csfEx167* worms that were (green trace) or were not (gray trace) supplemented with Retinal. C) Averaged GCaMP F/F_{min} in the 10 s following onset of light pulse. Black line indicates average F/F_{min} and orange area represents SEM. n = 15. D) Fluorescent images of RCaMP in AVA neurite in Retinal treated *csfEx157*-containing worm before and after PA of ChR2 with 470 nm light. Scale bar = 5 µm. E) Change in RCaMP F/F_{min} from a Retinal treated *csfEx157* worm over a 60 s imaging session with 2 pulses of 470 nm light (blue bars, duration = 3s, 0.25 mW/mm^2).

4.4 Use of Genetically Encoded Reagents for Optical Activation of Presynaptic Release

One could argue that the dissimilarity between neuronal stimulation with optogenetics and synaptic transmission make optogenetic stimulation physiologically irrelevant. A solution to this argument is to express optical tools presynaptic to the neuron in which the neurobiological question is being assessed. In theory, this approach would allow for optical control of synaptic transmission via presynaptic activation. Application of this approach for the AVA interneurons has been demonstrated: Optical stimulation of neurons presynaptic to AVA led to a postsynaptic

response in AVA that was measured with electrophysiology (Lindsay et al., 2011) or calcium imaging (Guo et al., 2009; Shipley et al., 2014). It is important to note that the presynaptic partners in these studies synapse onto AVA in the head where we are unable to visualize GLR-1 transport. The activation of presynaptic partners with axodendritic synapses onto AVA have not been described. Since most of the results shown thus far indicate that synaptic activation may dictate GLR-1 delivery, we were interested in assessing synaptic activation of AVA due to optical activation of presynaptic mechanosensory neurons that synapse onto the AVA neurite.

To do this, we sought to express ChRimson in a neuron or group of neurons that fulfilled the following requirements: 1) Form synaptic connections with the AVA neurite, 2) release glutamate in an activity-dependent manner, and 3) there is a cell-specific promoter that would allow for expression of optical tools in these neurons. We identified three mechanosensory neurons whose axons span the worm to sense harsh touch and relay this information to the AVA via synapses within the AVA neurite (Figure 4.4 A). These three neurons, FLP, PVD, and PLM, release glutamate and have cell-specific expression of the gene *mec-3* (Lee et al., 1999; Schafer, 2015; Way and Chalfie, 1989). So, expression of ChRimson under the control of the *mec-3* promotor should allow for optical activation of these mechanosensory neurons.

We tested this using a strain expressing ChRimson in presynaptic mechanosensory neurons and GCaMP in the AVA (*csfEx99*, see Table 4.2) but observed little to no increase in GCaMP fluorescence in the AVA cell bodies or neurites following optical activation of presynaptic ChRimson (Figure 4.4 B). Co-expression of RFP-tagged EAT-4, the vesicular glutamate transmitter that is localized to presynaptic terminal (VGluT1 homologue), supported that *mec-3* expressing neurons have presynaptic terminals directly adjacent to a proximal portion of the AVA neurite (Figure 4.4 B). Experimental replicates proved that optical stimulation of

ChRimson in *mec-3* neurons rarely provoked an increase in AVA GCaMP (Figure 4.4 C). Since AVA controls locomotion (Figure 2.9), the expression and proper function of ChRimson in the presynaptic neurons was validated with light-induced reversals in which Retinal treated *csfEx99* worms consistently reversed their locomotion in response to green light (Figure 4.4 D). This suggests that when worms are mounted for imaging, optical activation of *mec-3* neurons is inhibited.

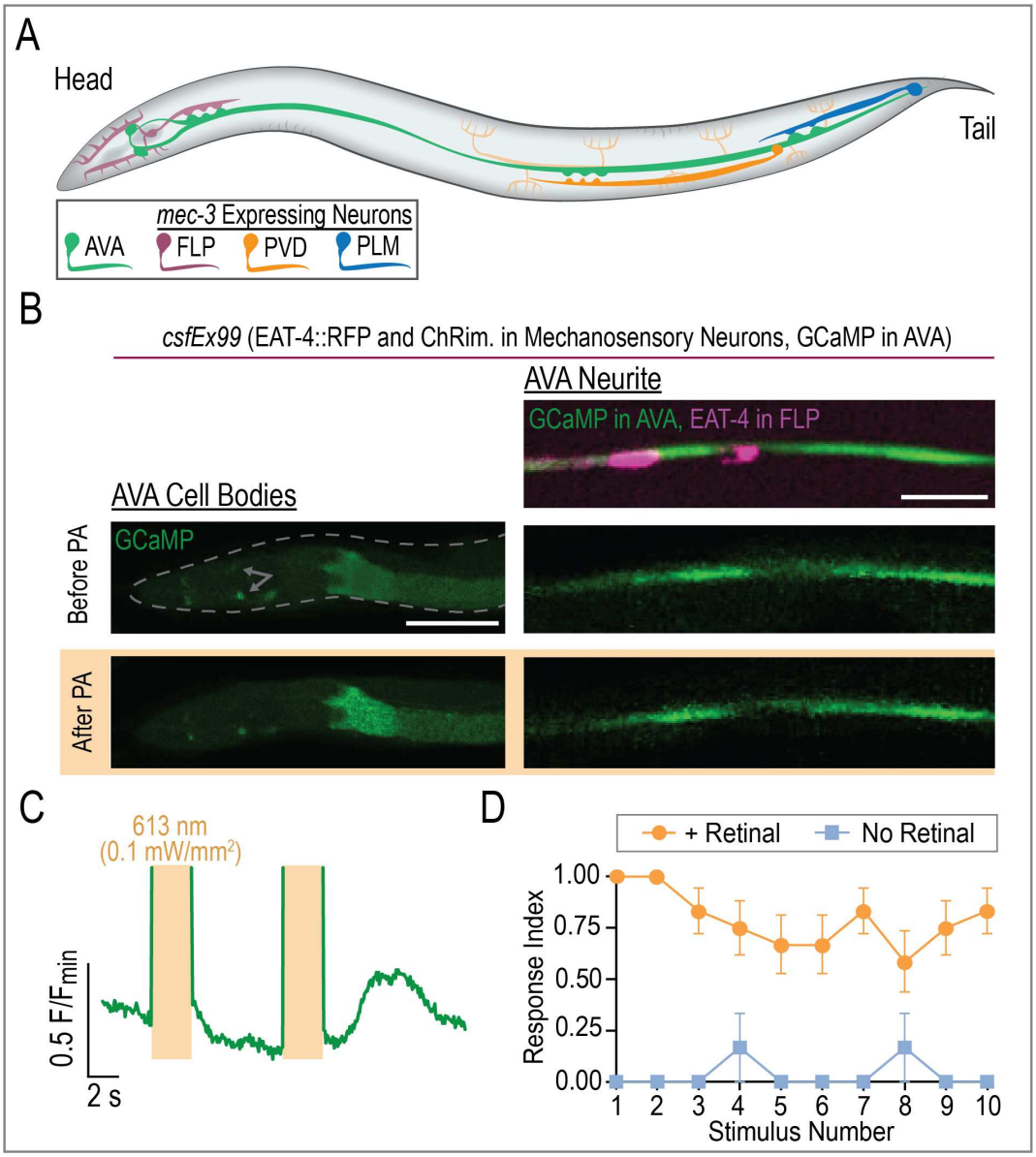

Figure 4.4 – Activation of AVA by optical stimulation of presynaptic mechanosensory neurons is blocked during imaging.
A) Illustration of the relative anatomical position of the AVA (green neuron) and the presynaptic mechanosensory neurons (FLP in magenta, PVD in orange, PLM in blue). Synapses are depicted as protrusions in neuronal processes.

Figure 4.4 B) Left. Fluorescent images of GCaMP in the AVA cell bodies in a *csfEx99*-containing strain before and after photoactivation (PA) with a 3 s pulse of 613 nm light (0.1 mW/mm^2). Gray dashed line outlined the worm's head, and the gray arrows indicate the position of the AVA cell bodies. Scale bar = 50 µm. Right. In a proximal portion of the neurite in the same strain, EAT-4::RFP (EAT-4 = VGluT1 orthologue) in FLP presynaptic terminals is found adjacent to the AVA (top right image). GCaMP fluorescence in neurite before and after PA. Scale bar = 5 µm. C) Change in GCaMP6f fluorescence normalized to minimum fluorescence (F/F_{min}) during 20 s of stream imaging. Orange bars indicate 3 s light pulse (613 nm, 0.1 mW/mm^2). D) Response indices (fraction of light-induced reversals at each stimulus) for *csfEx99* worms that were (n = 12) or were not (n=6) supplemented with Retinal.

From these experiments, we provide direct evident that *mec-3* expressing neurons make functional synaptic connections with AVA as has been suggested by earlier studies (Schafer, 2015). The biological difficulties that were encountered suggest that these harsh touch neurons function as on/off pressure sensors and their activity is clamped during the pressure stimulus. These neurons are likely clamped by the harsh pressure necessary to restrain worms during imaging which may explain the inability to optically activate synaptic transmission to the AVA during calcium imaging.

4.5 Conclusion, Discussion and Future Directions

Overall, the best combination of tools for optical manipulation and measurement of neuronal activity *in vivo* that was tested was postsynaptic ChRimson and GCaMP6f. The caveats and biological hurdles posed by the other tool combinations and approaches make them less reliable for light-induced activation or nonideal for measuring relatively quick changes in neuronal activity. First, activation of the light-sensitive calcium releaser PACR was not consistent in causing increases in calcium. Additionally, when calcium increased following PACR activation, the increase was minimal. This is likely a characteristic of the tool itself and not due to properties of the AVA neuron or caveats of *in vivo* use since others have also seen only a moderate increase in calcium (8-20%) due to PACR activation in various cell types *in vitro* (Fukuda et al., 2014). This

all suggests that PACR cannot be used to reach higher calcium concentrations normally achieved by neuronal activation (Kyung et al., 2015).

Next, the activation of optoCSTIM, our *C. elegans*-specific version of optoSTIM, is seemingly irreversible or has slow dissociation from CRAC channel. This prolonged binding of STIM-1 to CRAC channels may be functionally conserved between the human and *C. elegans* orthologs of STIM-1 since continuous calcium elevations were observed for nearly 10 minutes following optical activation of optoSTIM (Kyung et al., 2015). This characteristic of optoCSTIM prevented repeated stimulation and made assessing light-induced calcium influx difficult since light is used for mounting worms for imaging and localizing the AVA neuron. This exposure to light likely activated optoCSTIM prior to imaging which would explain the lack of light-induced calcium influx during RCaMP imaging. Overall, the slow kinetics of optoCSTIM make it unsuitable for eliciting repeated activation on a timescale that is relevant to normal neuronal activity patterns. However, it would be useful for experiments in which long-term increases in cytoplasmic calcium are desired.

The Channelrhodopsin subtypes (ChRimson and ChR2) that were expressed postsynaptically both elicited the largest increases in cytoplasmic calcium. When expressed at relatively low levels, ChRimson was reliably and repeatedly activated during calcium imaging (Figure 4.3 B). Although ChR2 was also reliably activated during calcium imaging, the fluctuation in calcium was slower which did not allow for repeated activations with an interstimulus interval less than 30 s (Figure 4.3 E). These slow dynamics of the calcium events following ChR2 activation could be explained by slower light-induced activation of ChR2, however, this is not consistent with what has been reported in *C. elegans* neurons or other excitable cell types. Instead, depolarization due to ChR2 has faster on- and off-rates than ChRimson (Akerboom et al., 2013; Klapoetke

et al., 2014). A better supported explanation is that the rise and decay rate of RCaMP fluorescence is much slower than that of GCaMP6f (Akerboom et al., 2013; Chen et al., 2013), so different kinetics of the calcium indicator used likely account for the delayed and prolonged increase in RCaMP fluorescence due to ChR2 stimulation when compared to GCaMP with ChRimson. Newly developed red-shifted calcium indicators with faster kinetics (Hussein and Berlin, 2020; Kerruth et al., 2019) will be useful for better characterization of ChR2 in activating AVA as well as other neurons and cell types.

Our approach to activating presynaptic neurons *in vivo* with ChRimson revealed that the biology of the neuron can inhibit its optical activation. We observed that optical stimulation of presynaptic ChRimson activated the AVA neurons only when worms were freely behaving, and that this stimulation was insufficient in initiating synaptic transmission from *mec-3* neurons to AVA when worms were mounted for imaging. This may be explained by the fact that *mec-3* neurons sense harsh touch with an "on" and an "off" response to a pressure stimulus (Li et al., 2011). This method of encoding touch in these neurons is different than in gentle touch neurons expressing *mec-2* and *mec-4* which have graded and sustained responses to various types of stimuli (Suzuki et al., 2003). Because of this difference, a viable alternative for optical control of synaptic transmission to AVA could be expression of ChRimson in the gentle touch neurons using the *mec-4* promoter. This would allow for control of the glutamatergic posterior touch neurons, AVM and ALM, which are known to provide input to AVA. However, where these neurons synapse onto the AVA is unknown, so locating these synaptic sites would be a necessary first step for this alternative approach.

These experiments increase our understanding of *C. elegans* neurobiology and these tools. This knowledge should guide further optimization of an optogenetic approach for

activating the AVA neurite as it would allow for fundamentally interesting questions to be addressed regarding the activity-dependent regulation of glutamate receptor transport to synapses. The 'holy grail' of this work would be to optically stimulate a precise region of the AVA neurite while simultaneously imaging GLR-1 transport *in vivo*. Although we have seen that spatially precise activation of the AVA is possible using ChRimson (data not shown), the difficulty in repeating this experiment suggests that we do not know enough about how subcellular organization of Channelrhodopsins influence their function. This prompts the need for additional characterization of optogenetic approaches for single cell activation *in vivo*.

4.6 New Methods

Cloning and Transgenic Strains

All cloning of the plasmids in Table 4.1 and microinjection for transgenic strains in Table 4.2 was done as described in Chapter 3.6. Modification of optoSTIM to optoCSTIM was done by replacing the portion of human STIM-1 in optoSTIM with the entire length of the *C. elegans stim-1* gene which was amplified from cDNA with the following primers: 3' GATCTAAGGAGCACACAAAAACAAAAGGCTCAGCAAAAAG 5' and 5'ACTGCAGAATTCCTATTAATTAGAAGTGCCACCCAGACTG 3'. Components for creating pRD plasmids were either gifts from Attila Stetak (ChRimson and ChR2) or were purchased from AddGene (PACR, #55774; optoSTIM, #70159).

Table 4.1 – Plasmids		
Plasmid Name	Contents	Source
pSM1	*Prig-3::RCaMP*	Stetak Lab, Univ. of Basel
pDM2444	*Pmec-3::ChRimson*	Stetak Lab, Univ. of Basel
pDM2251	*Pmec-3::EAT-4::mRFP*	Stetak Lab, Univ. of Basel
pRD24	*Pflp-18::eGFP::optoSTIM*	In-Fusion Cloning
pRD25	*Pflp-18::eGFP::PACR*	In-Fusion Cloning
pRD29	*Pflp-18::eGFP::optoCSTIM*	In-Fusion Cloning
pRD27	*Pflp18::ChRimson::let-858*	Gateway Cloning
pRD30	*Pflp-18::ChRimson:: TdTomato let-858*	Gateway Cloning
pRD31	*Pflp-18::ChR2::let-858*	In-Fusion Cloning

Table 4.2 – Transgenic Strains		
Strain Name	Genotype	Array Contents
FJH 250	*lin-15(n765ts) X; csfEx107*	pRD25 + pAS1 + pJM23
FJH 251	*lin-15(n765ts); csfEx108*	pSM1 + pJM23
FJH 277	*lin-15(n765ts), lite-1(ok530) X; csfEx122*	pRD29 + pSM1 + pJM23
FJH 369	*lin-15(n765ts), lite-1(ok530) X; csfEx99*	pDM2251 + pDM2444 + pAS1 + pJM23
FJH 385	*lin-15(n765ts), lite-1(ok530) X; csfEx147*	pRD29 + pJM23
FJH 399	*lin-15(n765ts), lite-1(ok530) X; csfEx157*	pRD31 + pSM1 +pJM23
FJH 412	*lin-15(n765ts), lite-1(ok530) X; csfEx167*	pRD30 + pAS1 +pJM23

Whole cell activation of Channelrhodopsins with calcium imaging

L4s from strains expressing the extrachromosomal array *csfEx157*, *csfEx167* or *csfEx399* were picked onto NGM/OP50 plates coated with 100 μM all-Trans Retinal (diluted with M9 buffer). After 12 – 16 hrs on Retinal plates, ChRimson-containing worms (*csfEx157* and *csfEx167*) were stimulated during calcium imaging as described in Chapter 3.6. GCaMP imaging involved acquisition of a 30 to 60 s image stream using a 250 ms exposure and 488 nm imaging laser set to 0.1% power. For the ChR2-containing strain (*csfEx157*), the LED setup on the confocal and pulse generator setting were the same as with ChRimson-containing strains but with a blue LED adjusted to 0.25 mW/mm^2 (470 nm, CoolBase 7 LED module from LuxeonStar).

RCaMP imaging in these strains used the same acquisition parameters and a 561 nm imaging laser set to 5% power.

Whole-Cell Activation of Other Optical Tools with Calcium Imaging

One-day-old *csfEx107* animals were mounted for imaging identically to other optogenetic experiments (see Chapter 3.6). PACR and optoCSTIM were activated during imaging of RCaMP fluorescence (250 ms with a 561 nm imaging laser set to 5% power) by our 470 nm LED array set to 3 mW/mm^2. To visualize light-induced clustering of optoCSTIM with calcium imaging, our dual imaging setup (see Chapter 3.6) was used to image eGFP::optoCSTIM with the 488 nm imaging laser (5% power) and RCaMP with the 561 nm imaging laser (20% power) at a frame rate of 100 ms. No additional optical stimulation was used during these experiments since the 488 nm imaging laser irreversibly initiated clustering of optoCSTIM.

Light-induced Reversal Assay

Single one-day-old adults that had been placed onto Retinal plates 12 – 16 hrs prior were transferred onto a fresh NGM/OP50 plate. They were located using dim white light on a fluorescent stereoscope (Nikon, SMZ18) equipped with a bandpass filter cube (Nikon, Texas Red/mCherry) and a solid-state white light excitation source (SOLA SMII). This allowed for illumination with 560 nm (+/- 40 nm) that was turned on manually for 3 s when the worm was stopped or moving forward while continuously observing the worm's locomotion. If the worm was performing a spontaneous reversal, then there was a delay in the light pulse until the worm changed direction or stopped. If a reversal was not initiated within the 3 s light pulse, it was considered as unresponsive to the light pulse. Freezing and hypercontraction were not considered as reversals but were noted to occur for a given strain since these behaviors suggest high levels of ChRimson expression. For testing ChRimson expression in all strains using this method, each

worm was subject to 5 light pulses with 10-20 seconds between each pulse. For a more detailed analysis of light responses (Figure 4.4), each worm was tested using 10 light pulses. Animals of the same genotype that were not supplemented with Retinal were used as negative controls for these assays.

Calcium Imaging Analysis

Fluorescence of calcium indicators for each frame was normalized to the minimum fluorescence. These normalized fluorescence values were compared qualitatively for most datasets since many involved the lack of a light-induced calcium response. For datasets with consistent light-induced calcium responses, an additional analysis was done to assess the variation in calcium responses. To do this, fluorescence peaks were aligned using the onset of the light stimulus from which an average fluorescence and standard error of the mean could be calculated per frame after the light stimulus.

Chapter 5 – Discussion

Many of the experiments shared here are largely explorational since the field of physiological ROS signaling in neurons is still in its early years. Key conclusions from these experiments include that ROS signaling regulates transport of AMPARs to synapses in a way that impacts neuronal activation and learning (Chapter 2). Furthermore, calcium influx and ROS signaling regulate the rate of AMPAR delivery to synapses by influencing transport dynamics within the neurite (Doser et al., 2020). This observation led us to more closely address how AMPAR transport within the neurite is regulated by localized calcium and ROS signaling. We found that local calcium and ROS levels affect the stopping of AMPAR transport events which is thought to precede receptor delivery to postsynaptic sites (Chapter 3.4). In trying to understand local calcium and ROS signaling in neurites, we also observed that there is activity-dependent calcium uptake and ROS production in mitochondria located at or near synapses (Chapter 3.3). Together, these results propose a novel bidirectional relationship between a neuron's metabolic rate and excitability.

However, many more questions are posed by these findings than are answered by them, such as: Is this regulation by ROS specific to AMPARs? How does diminished ROS signaling decrease glutamate receptor transport? Is activity-dependent mitochondrial ROS production dependent on calcium? How does synaptic activation influence receptor delivery? Addressing some of these questions would require optogenetic tools such as those characterized in Chapter 4. These studies are worth pursuing as they would provide a mechanistic understanding of the proposed relationship between neuronal activity and metabolism via a calcium-ROS interplay which

would be insightful for why mitochondrial dysfunction and abnormal neuronal excitation are commonly found together in the aged and diseased nervous system.

5.1 ROS as a Physiological Regulatory Molecule

ROS Regulation of AMPA Receptor Transport to Synapses

Our findings show that ROS levels must be within a specific physiological range (10-100 nM in vertebrates; Sies and Jones, 2020) for normal transport and delivery of AMPARs to synapses (Chapter 2.2 and 2.4). The impact of increased and decreased ROS on this transport occurs via two seemingly different mechanisms. In the case of increased ROS levels, AMPAR transport is decreased due to modulation of calcium influx through VGCCs (Chapter 2.2). Alternatively, diminished ROS also decreased AMPAR transport but through a mechanism that does not seem to alter calcium influx (Chapter 2.4). These results are interesting when compared to studies that assessed synaptic plasticity or memory in instances of low or high ROS. These studies reported similar defects in the induction of LTP and memory during both decreased and increased ROS levels (Klann, 1998; Knapp and Klann, 2002b; Massaad and Klann, 2011). The mechanisms that underly this differential regulation by ROS have remained largely unknown.

There have been reports of concentration-dependent regulation of calcium channels and other kinases by ROS that could in part explain the results presented here and in other studies. For instance, calcium influx through L-type VGCCs has been shown to be inhibited as well as enhanced by increased ROS levels (Hidalgo and Donoso, 2008). This disagreement on the effect of elevated ROS on L-type VGCC function may be explained by the ROS treatment (i.e. high vs. low concentrations) or by cell type (Görlach et al., 2015). However, discrepancies in experimental design and cell types from these studies do not allow for a definitive explanation.

Alternatively, it is well agreed upon that many cation channels within the transient receptor potential (TRP) family are constitutively activated by ROS levels above the physiological range (Nazıroğlu and Lückhoff, 2008) and inhibited by increased scavenging of ROS (Nazıroğlu, 2012). The kinase PKC has a similar sensitivity to ROS levels. High ROS levels activate PKC whereas increased antioxidation inhibits its kinase function (Gopalakrishna and Jaken, 2000). Interestingly, PKC's redox sensitivity has been shown to be necessary for ROS-induced enhancement of excitatory synaptic transmission (Knapp and Klann, 2002b). So, the regulation of AMPAR transport by ROS may be due to concentration-dependent redox modulation of calcium sources or regulatory proteins such as CaM and CaMKII (Erickson et al., 2008; Snijder et al., 2011; Tonks, 2006). Future work specifically addressing if redox regulation of AMPAR transport requires oxidation of CaM or CaMKII may detail a mechanism in which ROS regulates this transport.

It is also likely that ROS homeostasis is subcellularly distinct and that certain cellular compartments are better suited for maintaining ROS at relatively low levels. For instance, we observed that basal ROS levels at the plasma membrane were higher in the cell body compared to the neurite of the AVA neurons (somatic plasma membrane roGFP (PM-roGFP) fluorescence ratio = 0.11 ± 0.007; neurite PM-roGFP fluorescence ratio = 0.09 ± 0.036; mean ± SEM; data not shown). Furthermore, in the neurite, the fluorescence ratio of mito-roGFP was significantly less than PM-roGFP (0.03 ± 0.003 vs. 0.09 ± 0.036 respectively; mean ± SEM; data not shown). This suggests that even within the neurite, ROS levels can vary between compartment sub-domains such as the plasma membrane and in the cytoplasm near mitochondria. The development of new tools with higher ROS sensitivity are required to validate these ideas.

Comparing results in Chapter 2.2 with 3.4 further support that ROS concentration and cellular context influence the effect of ROS signaling. In Chapter 2.2, moderate, cell-wide increases in ROS resulted in reduced velocities and stopping of AMPAR transport in the nerite. Alternatively, in Chapter 3.4, localized increases in ROS due to optical activation of the photosensitizer KillerRed in a portion of the neurite had the opposite effect on stopping. Activation of KillerRed likely increased the relative ROS concentration well above the physiological range. To investigate this, we measured the impact of our KillerRed activation protocol with roGFP and saw a two-fold increase in the roGFP fluorescence ratio. Others have shown that a two-fold increase in roGFP's fluorescence ratio correlates with ROS levels well above the physiological range (Carmona et al., 2019). This concentration-dependent regulation of transport dynamics seems to be due to attenuation of calcium influx by moderate increases in ROS (Figure 2.2) but enhancement by much higher ROS levels (Figure 3.7). To understand how relative ROS concentrations may differentially impact calcium influx, electrophysiological studies would need to be conducted since *in vivo* calcium imaging is likely not sensitive enough for this characterization.

Based on what is known about redox regulation of proteins involved in synaptic activation and AMPAR transport, we proposed a model (Figure 5.1) that would partially explain how physiological ROS levels permit normal levels of receptor transport while lower and higher ROS levels decrease it. When the cytoplasmic ROS concentration is within the physiological range, some regulatory proteins such as CaMKII and PKC have oxidized residues that cause prolonged, calcium-independent and dependent activation respectively (Erickson et al., 2008; Gopalakrishna and Jaken, 2000). Enhanced activation of these kinases would increase channel conductance of AMPARs and L-type VGCCs (Jenkins et al., 2010; Jenkins and Traynelis, 2012). Prolonged activation of CaMKII would also increase loading of AMPAR-contain vesicles onto kinesin for

transport (Hoerndli et al., 2015). Then, if ROS is diminished in a neuron, there would be less oxidation of these kinases meaning less calcium influx and CaMKII activation, and therefore, less AMPAR transport. In the case of abnormally high ROS, excessive oxidation of proteins could explain decreased AMPAR transport. Although direct oxidation of L-type VGCCs is thought to increase their conductance, synaptic activation would be diminished due to oxidation of AMPARs and NMDARs decreasing their activation and synaptic expression (Aizenman et al., 2020; von Ossowski et al., 2017). Oxidation of CaM could also diminish calcium signaling by preventing its activation of CaMKII, which could explain the decrease in AMPAR transport observed during elevated ROS.

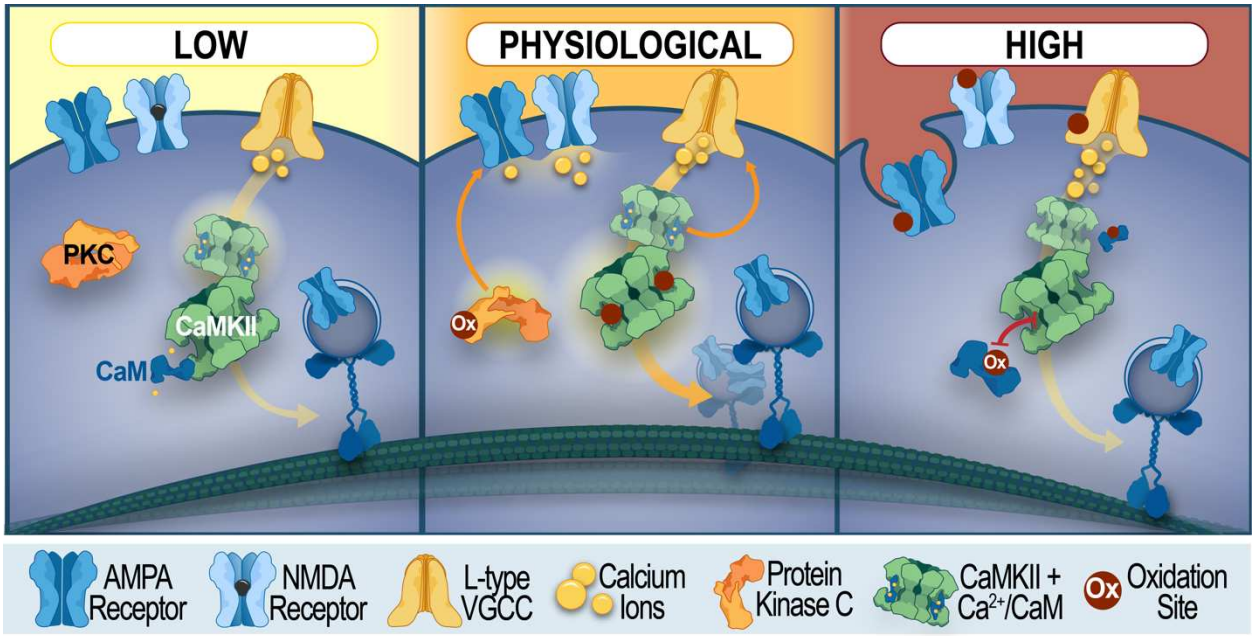

Figure 5.1 – Physiological ROS signaling is required for normal AMPAR transport.
Our model that may explain why ROS level must be within a specific concentration range for a normal amount of AMPAR transport.

Regulation of Other Cellular Mechanism by ROS

As the field of physiological ROS signaling grows, it becomes increasingly obvious that redox regulation is integral to many mechanisms in neurons. It is important for the regulation of

cytoskeleton remodeling, activation of regulatory proteins as well as transport of mitochondria. First, physiological ROS levels are required for normal F-actin assembly and microtubule dynamics *in vivo*. The influence of ROS on cytoskeletal dynamics is especially apparent during neurodevelopment where abnormally low and high ROS levels both cause collapsed or shrunken axonal growth cones (Wilson and González-Billault, 2015). Secondly, ROS are required for the activation of certain kinases such as extracellular signal-regulated kinase (ERK) as well as transcription factors like cAMP response element-binding protein (CREB) which are important for the long-term changes in synapses efficacy (Beckhauser et al., 2016).

Lastly, transport of mitochondria via molecular motors is redox regulated via a calcium-independent mechanism such that oxidation of a mitogen-activated protein kinase causes reversible inhibition of mitochondrial transport (Debattisti et al., 2017). Since transport of mitochondria is carried out by the same kinesin motor as AMPAR transport, these findings suggest that redox regulation of kinesin-based transport is specific to the cargo. Further study of how ROS signaling is involved in the development, maintenance, and plasticity of the nervous system will provide insight for future research on why abnormal neuronal function occurs during ROS dyshomeostasis.

5.2 Initiation of ROS Signaling in Neurons

As previously mentioned, the major sources of ROS in neurons are NADPH oxidase and mitochondrial OXPHOS (see Chapter 1.4; Beckhauser et al., 2016). Although ROS production by mitochondria has been recognized for a long time, it has been regarded as only a byproduct of OXPHOS without a physiological purpose. Results shared in Chapters 2.5 and 3.4 suggest that mitochondria-derived ROS are required for AMPAR transport and abnormally high mitochondrial ROS production is detrimental to this process. This necessitated that we understand the

production of ROS by mitochondria and if it is regulated by neuronal activity in *C. elegans* neurons. There is strong evidence supporting upregulation of OXPHOS by calcium as well as positive correlation between rate of OXPHOS and mitochondrial ROS production. However, it is not clear how calcium uptake into the mitochondria corresponds to ROS production (Görlach et al., 2015). Most of this evidence comes from studies done *in vitro* or in isolated mitochondria, so *in vivo* studies like the one presented here are beginning to allow us to understand the physiological relevance of mitochondrial calcium handling and ROS production (Pozzan and Rudolf, 2009).

In Chapter 3.3, we show that activity-induced increases in cytoplasmic calcium led to increased mitochondrial calcium (Figure 3.2), suggesting that elevations in cytoplasmic calcium triggers uptake into mitochondria. Repetitive neuronal activation also increased mitochondrial ROS production (Figure 3.3). These results indicate that activity-dependent calcium uptake by mitochondria upregulate OXPHOS and therefore ROS production. To demonstrate the link between mitochondrial calcium uptake and ROS production, future studies will be conducted in the absence of the pore-forming subunit of the mitochondrial calcium uniporter (MCU-1). We hypothesize that in MCU-1 loss-of-function mutants, repetitive neuronal activation will not increase mitochondrial ROS production. If MCU-1 mutants still have activity-dependent increases in ROS production, then it is possible that repetitive neuronal activity causes inefficient OXPHOS due to glucose depletion or other metabolites (Isaev et al., 2008; Vergara et al., 2019).

It will be impossible to provide a mechanistic explanation for how mitochondrial dysfunction in aging or neurodegeneration impacts neuronal excitation until we understand how mitochondria function is regulated by neuronal activity and vice versa. The metabolic demand and distant location of synapses make them reliant on their local mitochondrial energy supply. This makes synapse function especially susceptible to the effects of ATP deficits, increased ROS

production and calcium mishandling. So, specifically studying the relationship between synaptic activation and mitochondrial function (calcium buffering and ROS production) will be informative for the synaptic loss and dysfunction that occurs during natural aging or due to neurodegeneration.

5.3 The Future of Studying Synaptic Function and Plasticity *In Vivo*

The goal for the optimization and characterization of the optogenetic approaches described in Chapter 4 was to identify an optical tool that would allow for temporal control of single synapse activation *in vivo*. In an *in vivo* system, there is little proof of subcellular activation of optogenetic tools (Kichuk et al., 2021) and no demonstration of optical activation of single synapses that we are aware of. So, future optimization of *in vivo* optogenetics using what was learned from experiments shared in Chapter 4 would be novel and impactful. Controlling synapse activity patterns *in vivo* would open doors to new questions regarding mechanisms of synaptic scaling and site-specific targeting of synaptic proteins as well as provide a means for testing the physiological relevance of mechanisms underlying synaptic plasticity and maintenance in native, intact circuitry.

5.4 Limitations and Considerations

The conclusions drawn from our results do have their limitations since these experiments were not replicated in other model systems. Studies done in vertebrate neurons (Hangen et al., 2018) support our conclusions that calcium levels dictate the stopping of transport vesicles containing AMPARs in dendrites (Chapter 2.2 and Figure 3.4). Alternatively, relatively little has been done on ROS signaling in vertebrate glutamatergic neurons, so it is difficult to assess the

relevance of our results using *C. elegans*. It is possible that vertebrate neurons have a different sensitivity to regulation by ROS. In *C. elegans*, it is known that ROS is sensed by sensory neurons to regulate avoidance and feeding behaviors (Bhatla and Horvitz, 2015; Quintin et al., 2021). It is also known that ROS signaling is important for cuticle biogenesis, molting, embryogenesis and epidermal wound healing in *C. elegans*. So, it is possible that *C. elegans* neurons are especially sensitive or capable of ROS signaling (Miranda-Vizuete and Veal, 2017). Despite this, many key players involved in redox homeostasis as well as oxidizable sites within important synaptic proteins such as CaM and CaMKII are conserved in *C. elegans*. This suggests that the function of *C. elegans* and vertebrate glutamatergic synapses may be similarly sensitive to ROS signaling.

References

Abraham, W.C., Williams, J.M., 2008. LTP maintenance and its protein synthesis-dependence. Neurobiol. Learn. Mem. 89, 260–268. https://doi.org/10.1016/j.nlm.2007.10.001

Aizenman, E., Loring, R.H., Reynolds, I.J., Rosenberg, P.A., 2020. The Redox Biology of Excitotoxic Processes: The NMDA Receptor, TOPA Quinone, and the Oxidative Liberation of Intracellular Zinc. Front. Neurosci. 14. https://doi.org/10.3389/fnins.2020.00778

Akaishi, T., Nakazawa, K., Sato, K., Saito, H., Ohno, Y., Ito, Y., 2004. Modulation of Voltage-Gated Ca2+ Current by 4-Hydroxynonenal in Dentate Granule Cells. Biol. Pharm. Bull. 27, 174–179. https://doi.org/10.1248/bpb.27.174

Akerboom, J., Carreras Calderon, N., Tian, L., Wabnig, S., Prigge, M., Tolo, J., Gordus, A., Orger, M.B., Severi, K.E., Macklin, J.J., Patel, R., Pulver, S.R., Wardill, T.J., Fischer, E., Schuler, C., Chen, T.W., Sarkisyan, K.S., Marvin, J.S., Bargmann, C.I., Kim, D.S., Kugler, S., Lagnado, L., Hegemann, P., Gottschalk, A., Schreiter, E.R., Looger, L.L., 2013. Genetically encoded calcium indicators for multi-color neural activity imaging and combination with optogenetics. Front Mol Neurosci 6, 2. https://doi.org/10.3389/fnmol.2013.00002

Ali, F., Kwan, A.C., 2019. Interpreting in vivo calcium signals from neuronal cell bodies, axons, and dendrites: a review. Neurophotonics 7, 1. https://doi.org/10.1117/1.nph.7.1.011402

Alvarez, J., Alvarez-Illera, P., García-Casas, P., Fonteriz, R.I., Montero, M., 2020. The Role of Ca2+ Signaling in Aging and Neurodegeneration: Insights from Caenorhabditis elegans Models. Cells 9, 204. https://doi.org/10.3390/cells9010204

Amberg, G.C., Earley, S., Glapa, S.A., 2010. Local regulation of arterial L-type calcium channels by reactive oxygen species. Circ. Res. 107, 1002–1010. https://doi.org/10.1161/CIRCRESAHA.110.217018

Angelova, P.R., Abramov, A.Y., 2018. Role of mitochondrial ROS in the brain: from physiology to neurodegeneration. FEBS Lett. 592, 692–702. https://doi.org/10.1002/1873-3468.12964

Ashby, M., Daw, M., Issac, J., 2008. AMPA Receptors, in: Gereau, R., Swanson, G. (Eds.), The Glutamate Receptors. Humana Press, Totowa, NJ, pp. 1–44.

Ashrafi, G., de Juan-Sanz, J., Farrell, R.J., Ryan, T.A., 2020. Molecular Tuning of the Axonal Mitochondrial Ca2+ Uniporter Ensures Metabolic Flexibility of Neurotransmission. Neuron 105, 678-687.e5. https://doi.org/10.1016/j.neuron.2019.11.020

Back, P., Braeckman, B.P., Matthijssens, F., 2012. ROS in Aging Caenorhabditis elegans : Damage or Signaling? Oxid. Med. Cell. Longev. 2012, 1–14. https://doi.org/10.1155/2012/608478

Baltaci, S.B., Mogulkoc, R., Baltaci, A.K., 2019. Molecular Mechanisms of Early and Late LTP. Neurochem. Res. 44, 281–296. https://doi.org/10.1007/s11064-018-2695-4

Bargmann, C.I., Hartwieg, E., Horvitz, H.R., 1993. Odorant-selective genes and neurons mediate olfaction in C. elegans. Cell 74, 515–527. https://doi.org/10.1016/0092-8674(93)80053-H

Barja, G., 2013. Updating the Mitochondrial Free Radical Theory of Aging: An Integrated View, Key Aspects, and Confounding Concepts. Antioxid. Redox Signal. 19, 1420–1445. https://doi.org/10.1089/ars.2012.5148

Bayer, K.U., Schulman, H., 2019. CaM Kinase: Still Inspiring at 40. Neuron 103, 380–394.

https://doi.org/10.1016/j.neuron.2019.05.033
Beck, C., Gong, Y., 2019. A high-speed, bright, red fluorescent voltage sensor to detect neural activity. Sci. Rep. 9, 15878. https://doi.org/10.1038/s41598-019-52370-8
Beckhauser, T.F., Francis-Oliveira, J., De Pasquale, R., 2016. Reactive Oxygen Species: Physiological and Physiopathological Effects on Synaptic Plasticity. J. Exp. Neurosci. 10, 23–48. https://doi.org/10.4137/JEN.S39887
Ben Arous, J., Tanizawa, Y., Rabinowitch, I., Chatenay, D., Schafer, W.R., 2010. Automated imaging of neuronal activity in freely behaving Caenorhabditis elegans. J. Neurosci. Methods 187, 229–234. https://doi.org/10.1016/j.jneumeth.2010.01.011
Berndt, A., Yizhar, O., Gunaydin, L.A., Hegemann, P., Deisseroth, K., 2009. Bi-stable neural state switches. Nat. Neurosci. 12, 229–234. https://doi.org/10.1038/nn.2247
Bhatla, N., Horvitz, H.R., 2015. Light and Hydrogen Peroxide Inhibit C. elegans Feeding through Gustatory Receptor Orthologs and Pharyngeal Neurons. Neuron 85, 804–818. https://doi.org/10.1016/j.neuron.2014.12.061
Bienert, G.P., Schjoerring, J.K., Jahn, T.P., 2006. Membrane transport of hydrogen peroxide. Biochim. Biophys. Acta - Biomembr. 1758, 994–1003. https://doi.org/10.1016/j.bbamem.2006.02.015
Bindokas, V., Jordan, J., Lee, C., Miller, R., 1996. Superoxide production in rat hippocampal neurons: selective imaging with hydroethidine. J. Neurosci. 16, 1324–1336. https://doi.org/10.1523/JNEUROSCI.16-04-01324.1996
Blanke, M.L., VanDongen, A.M., 2009. Activation Mechanisms of the NMDA Receptor., in: AM, V.D. (Ed.), Biology of the NMDA Receptor. CRC Press/Taylor & Francis, Boca Raton, FL.
Bliss, T.V.P., Collingridge, G.L., 1993. A synaptic model of memory: long-term potentiation in the hippocampus. Nature 361, 31–39. https://doi.org/10.1038/361031a0
Bodhinathan, K., Kumar, A., Foster, T.C., 2010. Intracellular Redox State Alters NMDA Receptor Response during Aging through Ca2+/Calmodulin-Dependent Protein Kinase II. J. Neurosci. 30, 1914–1924. https://doi.org/10.1523/JNEUROSCI.5485-09.2010
Boehm, J., Kang, M.G., Johnson, R.C., Esteban, J., Huganir, R.L., Malinow, R., 2006. Synaptic Incorporation of AMPA Receptors during LTP Is Controlled by a PKC Phosphorylation Site on GluR1. Neuron 51, 213–225. https://doi.org/10.1016/j.neuron.2006.06.013
Bolisetty, S., Jaimes, E., 2013. Mitochondria and Reactive Oxygen Species: Physiology and Pathophysiology. Int. J. Mol. Sci. 14, 6306–6344. https://doi.org/10.3390/ijms14036306
Bommel, B., Konietzny, A., Kobler, O., Bär, J., Mikhaylova, M., 2019. F-actin patches associated with glutamatergic synapses control positioning of dendritic lysosomes. EMBO J. 38. https://doi.org/10.15252/embj.2018101183
Bouayed, J., Bohn, T., 2010. Exogenous Antioxidants—Double-Edged Swords in Cellular Redox State: Health Beneficial Effects at Physiologic Doses versus Deleterious Effects at High Doses. Oxid. Med. Cell. Longev. 3, 228–237. https://doi.org/10.4161/oxim.3.4.12858
Bourke, A.M., Schwartz, S.L., Bowen, A.B., Kleinjan, M.S., Winborn, C.S., Kareemo, D.J., Gutnick, A., Schwarz, T.L., Kennedy, M.J., 2021. zapERtrap: A light-regulated ER release system reveals unexpected neuronal trafficking pathways. J. Cell Biol. 220. https://doi.org/10.1083/jcb.202103186
Braeckman, B.P., Smolders, A., Back, P., De Henau, S., 2016. In Vivo Detection of Reactive Oxygen Species and Redox Status in Caenorhabditis elegans. Antioxid. Redox Signal. 25, 577–592. https://doi.org/10.1089/ars.2016.6751

Brechet, A., Buchert, R., Schwenk, J., Boudkkazi, S., Zolles, G., Siquier-Pernet, K., Schaber, I., Bildl, W., Saadi, A., Bole-Feysot, C., Nitschke, P., Reis, A., Sticht, H., Al-Sanna'a, N., Rolfs, A., Kulik, A., Schulte, U., Colleaux, L., Abou Jamra, R., Fakler, B., 2017. AMPA-receptor specific biogenesis complexes control synaptic transmission and intellectual ability. Nat. Commun. 8, 15910. https://doi.org/10.1038/ncomms15910

Brenner, S., 2003. Nature's gift to science (Nobel lecture). ChemBioChem 4, 683–687. https://doi.org/10.1002/cbic.200300625

Brini, M., Calì, T., Ottolini, D., Carafoli, E., 2014. Neuronal calcium signaling: function and dysfunction. Cell. Mol. Life Sci. 71, 2787–2814. https://doi.org/10.1007/s00018-013-1550-7

Brown, M.R., Sullivan, P.G., Geddes, J.W., 2006. Synaptic Mitochondria Are More Susceptible to Ca2+Overload than Nonsynaptic Mitochondria. J. Biol. Chem. 281, 11658–11668. https://doi.org/10.1074/jbc.M510303200

Burbea, M., Dreier, L., Dittman, J.S., Grunwald, M.E., Kaplan, J.M., 2002. Ubiquitin and AP180 regulate the abundance of GLR-1 glutamate receptors at postsynaptic elements in C. elegans. Neuron 35, 107–120. https://doi.org/10.1016/S0896-6273(02)00749-3

Cai, Q., Lu, L., Tian, J.-H., Zhu, Y.-B., Qiao, H., Sheng, Z.-H., 2010. Snapin-Regulated Late Endosomal Transport Is Critical for Efficient Autophagy-Lysosomal Function in Neurons. Neuron 68, 73–86. https://doi.org/10.1016/j.neuron.2010.09.022

Carmona, M., de Cubas, L., Bautista, E., Moral-Blanch, M., Medraño-Fernández, I., Sitia, R., Boronat, S., Ayté, J., Hidalgo, E., 2019. Monitoring cytosolic H2O2 fluctuations arising from altered plasma membrane gradients or from mitochondrial activity. Nat. Commun. 10, 4526. https://doi.org/10.1038/s41467-019-12475-0

Catterall, W.A., 2011. Voltage-gated calcium channels. Cold Spring Harb. Perspect. Biol. 3, 1–23. https://doi.org/10.1101/cshperspect.a003947

Chaplin, N.L., Amberg, G.C., 2012. Hydrogen peroxide mediates oxidant-dependent stimulation of arterial smooth muscle L-type calcium channels. Am. J. Physiol. Physiol. 302, C1382–C1393. https://doi.org/10.1152/ajpcell.00222.2011

Chávez, V., Mohri-Shiomi, A., Garsin, D.A., 2009. Ce-Duox1/BLI-3 Generates Reactive Oxygen Species as a Protective Innate Immune Mechanism in Caenorhabditis elegans. Infect. Immun. 77, 4983–4989. https://doi.org/10.1128/IAI.00627-09

Chen, T.-W., Wardill, T.J., Sun, Y., Pulver, S.R., Renninger, S.L., Baohan, A., Schreiter, E.R., Kerr, R.A., Orger, M.B., Jayaraman, V., Looger, L.L., Svoboda, K., Kim, D.S., 2013. Ultrasensitive fluorescent proteins for imaging neuronal activity. Nature 499, 295–300. https://doi.org/10.1038/nature12354

Cheng, X.-T., Zhou, B., Lin, M.-Y., Cai, Q., Sheng, Z.-H., 2015. Axonal autophagosomes recruit dynein for retrograde transport through fusion with late endosomes. J. Cell Biol. 209, 377–386. https://doi.org/10.1083/jcb.201412046

Choquet, D., Triller, A., 2013. The Dynamic Synapse. Neuron 80, 691–703. https://doi.org/10.1016/j.neuron.2013.10.013

Chronis, N., Zimmer, M., Bargmann, C.I., 2007. Microfluidics for in vivo imaging of neuronal and behavioral activity in Caenorhabditis elegans. Nat. Methods 4, 727–731. https://doi.org/10.1038/nmeth1075

Citri, A., Malenka, R.C., 2008. Synaptic Plasticity: Multiple Forms, Functions, and Mechanisms. Neuropsychopharmacology 33, 18–41. https://doi.org/10.1038/sj.npp.1301559

Cook, S.G., Buonarati, O.R., Coultrap, S.J., Bayer, K.U., 2021. CaMKII holoenzyme

mechanisms that govern the LTP versus LTD decision. Sci. Adv. 7. https://doi.org/10.1126/sciadv.abe2300
Coultrap, S.J., Freund, R.K., O'Leary, H., Sanderson, J.L., Roche, K.W., Dell'Acqua, M.L., Bayer, K.U., 2014. Autonomous CaMKII Mediates Both LTP and LTD Using a Mechanism for Differential Substrate Site Selection. Cell Rep. 6, 431–437. https://doi.org/10.1016/j.celrep.2014.01.005
Cserne Szappanos, H., Viola, H., Hool, L.C., 2017. L-type calcium channel: Clarifying the "oxygen sensing hypothesis." Int. J. Biochem. Cell Biol. 86, 32–36. https://doi.org/10.1016/j.biocel.2017.03.010
Cuestas Torres, D.M., Cardenas, F.P., 2020. Synaptic plasticity in Alzheimer's disease and healthy aging. Rev. Neurosci. 31, 245–268. https://doi.org/10.1515/revneuro-2019-0058
Dang, A.K., Chaplin, N.L., Murtazina, D.A., Boehm, U., Clay, C.M., Amberg, G.C., 2018. Subplasmalemmal hydrogen peroxide triggers calcium influx in gonadotropes. J. Biol. Chem. 293, 16028–16042. https://doi.org/10.1074/jbc.RA118.001830
De Stefani, D., Patron, M., Rizzuto, R., 2015. Structure and function of the mitochondrial calcium uniporter complex. Biochim. Biophys. Acta - Mol. Cell Res. 1853, 2006–2011. https://doi.org/10.1016/j.bbamcr.2015.04.008
Debattisti, V., Gerencser, A.A., Saotome, M., Das, S., Hajnóczky, G., 2017. ROS Control Mitochondrial Motility through p38 and the Motor Adaptor Miro/Trak. Cell Rep. 21, 1667–1680. https://doi.org/10.1016/j.celrep.2017.10.060
Donato, A., Kagias, K., Zhang, Y., Hilliard, M.A., 2019. Neuronal sub-compartmentalization: a strategy to optimize neuronal function. Biol. Rev. 94, 1023–1037. https://doi.org/10.1111/brv.12487
Dong, Z., Shanmughapriya, S., Tomar, D., Siddiqui, N., Lynch, S., Nemani, N., Breves, S.L., Zhang, X., Tripathi, A., Palaniappan, P., Riitano, M.F., Worth, A.M., Seelam, A., Carvalho, E., Subbiah, R., Jaña, F., Soboloff, J., Peng, Y., Cheung, J.Y., Joseph, S.K., Caplan, J., Rajan, S., Stathopulos, P.B., Madesh, M., 2017. Mitochondrial Ca 2+ Uniporter Is a Mitochondrial Luminal Redox Sensor that Augments MCU Channel Activity. Mol. Cell 65, 1014-1028.e7. https://doi.org/10.1016/j.molcel.2017.01.032
Doser, R.L., Amberg, G.C., Hoerndli, F.J., 2020. Reactive Oxygen Species Modulate Activity-Dependent AMPA Receptor Transport in C. elegans. J. Neurosci. 40, 7405–7420. https://doi.org/10.1523/JNEUROSCI.0902-20.2020
Doser, R.L., Hoerndli, F.J., 2022. Decreased Reactive Oxygen Species Signaling Alters Glutamate Receptor Transport to Synapses in *C. elegans* AVA Neurons. microPublication Biology. 10.17912/micropub.biology.000528.
Eales, K.L., Palygin, O., O'Loughlin, T., Rasooli-Nejad, S., Gaestel, M., Müller, J., Collins, D.R., Pankratov, Y., Corrêa, S.A.L., 2014. The MK2/3 cascade regulates AMPAR trafficking and cognitive flexibility. Nat. Commun. 5, 4701. https://doi.org/10.1038/ncomms5701
Ehlers, M.D., 2000. Reinsertion or Degradation of AMPA Receptors Determined by Activity-Dependent Endocytic Sorting. Neuron 28, 511–525. https://doi.org/10.1016/S0896-6273(00)00129-X
Ehlers, M.D., 1999. Synapse structure: Glutamate receptors connected by the shanks. Curr. Biol. 9, R848–R850. https://doi.org/10.1016/S0960-9822(00)80043-3
Eltokhi, A., Santuy, A., Merchan-Perez, A., Sprengel, R., 2020. Glutamatergic Dysfunction and Synaptic Ultrastructural Alterations in Schizophrenia and Autism Spectrum Disorder:

Evidence from Human and Rodent Studies. Int. J. Mol. Sci. 22, 59. https://doi.org/10.3390/ijms22010059
Erickson, J.R., Joiner, M. ling A., Guan, X., Kutschke, W., Yang, J., Oddis, C. V., Bartlett, R.K., Lowe, J.S., O'Donnell, S.E., Aykin-Burns, N., Zimmerman, M.C., Zimmerman, K., Ham, A.J.L., Weiss, R.M., Spitz, D.R., Shea, M.A., Colbran, R.J., Mohler, P.J., Anderson, M.E., 2008. A Dynamic Pathway for Calcium-Independent Activation of CaMKII by Methionine Oxidation. Cell 133, 462–474. https://doi.org/10.1016/j.cell.2008.02.048
Esteves da Silva, M., Adrian, M., Schätzle, P., Lipka, J., Watanabe, T., Cho, S., Futai, K., Wierenga, C.J., Kapitein, L.C., Hoogenraad, C.C., 2015. Positioning of AMPA Receptor-Containing Endosomes Regulates Synapse Architecture. Cell Rep. 13, 933–943. https://doi.org/10.1016/j.celrep.2015.09.062
Fang, C., Bourdette, D., Banker, G., 2012. Oxidative stress inhibits axonal transport: implications for neurodegenerative diseases. Mol. Neurodegener. 7, 29. https://doi.org/10.1186/1750-1326-7-29
Fink, B.D., Bai, F., Yu, L., Sivitz, W.I., 2017. Regulation of ATP production: dependence on calcium concentration and respiratory state. Am. J. Physiol. Physiol. 313, C146–C153. https://doi.org/10.1152/ajpcell.00086.2017
Fischer, K.E., Vladis, N.A., Busch, K.E., 2018. Optogenetic Applications in the Nematode Caenorhabditis elegans, in: Stroh, A. (Ed.), Optogenetics: A Roadmap. Springer Science, pp. 89–116. https://doi.org/10.1007/978-1-4939-7417-7_6
Foster, T.., Kyritsopoulos, C., Kumar, A., 2017. Central role for NMDA receptors in redox mediated impairment of synaptic function during aging and Alzheimer's disease. Behav. Brain Res. 322, 223–232. https://doi.org/10.1016/j.bbr.2016.05.012
Fujii, S., Sasaki, H., Mikoshiba, K., Kuroda, Y., Yamazaki, Y., Mostafa Taufiq, A., Kato, H., 2004. A chemical LTP induced by co-activation of metabotropic and N-methyl-d-aspartate glutamate receptors in hippocampal CA1 neurons. Brain Res. 999, 20–28. https://doi.org/10.1016/j.brainres.2003.11.058
Fukuda, N., Matsuda, T., Nagai, T., 2014. Optical Control of the Ca 2+ Concentration in a Live Specimen with a Genetically Encoded Ca 2+ -Releasing Molecular Tool. ACS Chem. Biol. 9, 1197–1203. https://doi.org/10.1021/cb400849n
Gahtan, E., Auerbach, J.M., Groner, Y., Segal, M., 1998. Reversible impairment of long-term potentiation in transgenic Cu/Zn-SOD mice. Eur. J. Neurosci. 10, 538–544. https://doi.org/10.1046/j.1460-9568.1998.00058.x
Gerich, F.J., Funke, F., Hildebrandt, B., Faßhauer, M., Müller, M., 2009. H2O2-mediated modulation of cytosolic signaling and organelle function in rat hippocampus. Pflügers Arch. - Eur. J. Physiol. 458, 937–952. https://doi.org/10.1007/s00424-009-0672-0
Gopalakrishna, R., Jaken, S., 2000. Protein kinase C signaling and oxidative stress. Free Radic. Biol. Med. 28, 1349–1361. https://doi.org/10.1016/S0891-5849(00)00221-5
Gordus, A., Pokala, N., Levy, S., Flavell, S.W., Bargmann, C.I., 2015. Feedback from Network States Generates Variability in a Probabilistic Olfactory Circuit. Cell 161, 215–227. https://doi.org/10.1016/j.cell.2015.02.018
Görlach, A., Bertram, K., Hudecova, S., Krizanova, O., 2015. Calcium and ROS: A mutual interplay. Redox Biol. 6, 260–271. https://doi.org/10.1016/j.redox.2015.08.010
Gray, J.M., Hill, J.J., Bargmann, C.I., 2005. A circuit for navigation in Caenorhabditis elegans. Proc. Natl. Acad. Sci. U. S. A. 102, 3184–3191. https://doi.org/10.1073/pnas.0409009101
Griffin, E.F., Scopel, S.E., Stephen, C.A., Holzhauer, A.C., Vaji, M.A., Tuckey, R.A.,

Berkowitz, L.A., Caldwell, K.A., Caldwell, G.A., 2019. ApoE-associated modulation of neuroprotection from Aβ-mediated neurodegeneration in transgenic Caenorhabditis elegans. Dis. Model. Mech. https://doi.org/10.1242/dmm.037218
Grimm, A., Eckert, A., 2017. Brain aging and neurodegeneration: from a mitochondrial point of view. J. Neurochem. 143, 418–431. https://doi.org/10.1111/jnc.14037
Groc, L., Bard, L., Choquet, D., 2009. Surface trafficking of N-methyl-d-aspartate receptors: Physiological and pathological perspectives. Neuroscience 158, 4–18. https://doi.org/10.1016/j.neuroscience.2008.05.029
Groc, L., Choquet, D., 2020. Linking glutamate receptor movements and synapse function. Science (80-.). 368. https://doi.org/10.1126/science.aay4631
Guan, J.-S., Su, S.C., Gao, J., Joseph, N., Xie, Z., Zhou, Y., Durak, O., Zhang, L., Zhu, J.J., Clauser, K.R., Carr, S.A., Tsai, L.-H., 2011. Cdk5 Is Required for Memory Function and Hippocampal Plasticity via the cAMP Signaling Pathway. PLoS One 6, e25735. https://doi.org/10.1371/journal.pone.0025735
Guillaud, L., Wong, R., Hirokawa, N., 2008. Disruption of KIF17–Mint1 interaction by CaMKII-dependent phosphorylation: a molecular model of kinesin–cargo release. Nat. Cell Biol. 10, 19–29. https://doi.org/10.1038/ncb1665
Guo, Z. V, Hart, A.C., Ramanathan, S., 2009. Optical interrogation of neural circuits in Caenorhabditis elegans. Nat. Methods 6, 891–896. https://doi.org/10.1038/nmeth.1397
Gutiérrez, Y., López-García, S., Lario, A., Gutiérrez-Eisman, S., Delevoye, C., Esteban, J.A., 2021. KIF13A drives AMPA receptor synaptic delivery for long-term potentiation via endosomal remodeling. J. Cell Biol. 220. https://doi.org/10.1083/jcb.202003183
Hadziselimovic, N., Vukojevic, V., Peter, F., Milnik, A., Fastenrath, M., Fenyves, B.G., Hieber, P., Demougin, P., Vogler, C., de Quervain, D.J.-F., Papassotiropoulos, A., Stetak, A., 2014. Forgetting Is Regulated via Musashi-Mediated Translational Control of the Arp2/3 Complex. Cell 156, 1153–1166. https://doi.org/10.1016/j.cell.2014.01.054
Hall, C.N., Klein-Flugge, M.C., Howarth, C., Attwell, D., 2012. Oxidative Phosphorylation, Not Glycolysis, Powers Presynaptic and Postsynaptic Mechanisms Underlying Brain Information Processing. J. Neurosci. 32, 8940–8951. https://doi.org/10.1523/JNEUROSCI.0026-12.2012
Halliwell, B., 1992. Reactive Oxygen Species and the Central Nervous System. J. Neurochem. 59, 1609–1623. https://doi.org/10.1111/j.1471-4159.1992.tb10990.x
Hangen, E., Cordelières, F.P., Petersen, J.D., Choquet, D., Coussen, F., 2018. Neuronal Activity and Intracellular Calcium Levels Regulate Intracellular Transport of Newly Synthesized AMPAR. Cell Rep. 24, 1001-1012.e3. https://doi.org/10.1016/j.celrep.2018.06.095
Hanus, C., Geptin, H., Tushev, G., Garg, S., Alvarez-Castelao, B., Sambandan, S., Kochen, L., Hafner, A.-S., Langer, J.D., Schuman, E.M., 2016. Unconventional secretory processing diversifies neuronal ion channel properties. Elife 5. https://doi.org/10.7554/eLife.20609
Hart, A.C., Sims, S., Kaplan, J.M., 1995. Synaptic code for sensory modalities revealed by C. elegans GLR-1 glutamate receptor. Nature 378, 82–85. https://doi.org/10.1038/378082a0
Hayashi, Y., Shi, S.H., Esteban, J.A., Piccini, A., Poncer, J.C., Malinow, R., 2000. Driving AMPA receptors into synapses by LTP and CaMKII: Requirement for GluR1 and PDZ domain interaction. Science (80-.). 287, 2262–2267. https://doi.org/10.1126/science.287.5461.2262
Heisler, F.F., Lee, H.K., Gromova, K. V., Pechmann, Y., Schurek, B., Ruschkies, L., Schroeder, M., Schweizer, M., Kneussel, M., 2014. GRIP1 interlinks N-cadherin and AMPA receptors

at vesicles to promote combined cargo transport into dendrites. Proc. Natl. Acad. Sci. 111, 5030–5035. https://doi.org/10.1073/pnas.1304301111
Hendricks, M., Ha, H., Maffey, N., Zhang, Y., 2012. Compartmentalized calcium dynamics in a C. elegans interneuron encode head movement. Nature 487, 99–103. https://doi.org/10.1038/nature11081
Henley, J.M., Wilkinson, K.A., 2016. Synaptic AMPA receptor composition in development, plasticity and disease. Nat. Rev. Neurosci. 17, 337–350. https://doi.org/10.1038/nrn.2016.37
Henley, J.M., Wilkinson, K.A., 2013. AMPA receptor trafficking and the mechanisms underlying synaptic plasticity and cognitive aging. Dialogues Clin Neurosci 15, 11–27.
Hidalgo, C., Arias-Cavieres, A., 2016. Calcium, Reactive Oxygen Species, and Synaptic Plasticity. Physiology 31, 201–215. https://doi.org/10.1152/physiol.00038.2015
Hidalgo, C., Donoso, P., 2008. Crosstalk Between Calcium and Redox Signaling: From Molecular Mechanisms to Health Implications. Antioxid. Redox Signal. 10, 1275–1312. https://doi.org/10.1089/ars.2007.1886
Higley, M.J., Sabatini, B.L., 2012. Calcium signaling in dendritic spines. Cold Spring Harb. Perspect. Biol. 4, a005686. https://doi.org/10.1101/cshperspect.a005686
Hoerndli, F.J., Maxfield, D.A., Brockie, P.J., Mellem, J.E., Jensen, E., Wang, R., Madsen, D.M., Maricq, A. V., 2013. Kinesin-1 Regulates Synaptic Strength by Mediating the Delivery, Removal, and Redistribution of AMPA Receptors. Neuron 80, 1421–1437. https://doi.org/10.1016/j.neuron.2013.10.050
Hoerndli, F.J., Wang, R., Mellem, J.E., Kallarackal, A., Brockie, P.J., Thacker, C., Madsen, D.M., Maricq, A. V., 2015. Neuronal Activity and CaMKII Regulate Kinesin-Mediated Transport of Synaptic AMPARs. Neuron 86, 457–474. https://doi.org/10.1016/j.neuron.2015.03.011
Hollenbeck, P.J., 2005. Mitochondria and Neurotransmission: Evacuating the Synapse. Neuron 47, 331–333. https://doi.org/10.1016/j.neuron.2005.07.017
Hongpaisan, J., Winters, C.A., Brian Andrews, S., 2003. Calcium-dependent mitochondrial superoxide modulates nuclear CREB phosphorylation in hippocampal neurons. Mol. Cell. Neurosci. 24, 1103–1115. https://doi.org/10.1016/j.mcn.2003.09.003
Hool, L.C., Corry, B., 2007. Redox Control of Calcium Channels: From Mechanisms to Therapeutic Opportunities. Antioxid. Redox Signal. 9, 409–435. https://doi.org/10.1089/ars.2006.1446
Horak, M., Petralia, R.S., Kaniakova, M., Sans, N., 2014. ER to synapse trafficking of NMDA receptors. Front. Cell. Neurosci. 8. https://doi.org/10.3389/fncel.2014.00394
Huganir, R.L., Nicoll, R.A., 2013. AMPARs and Synaptic Plasticity: The Last 25 Years. Neuron 80, 704–717. https://doi.org/10.1016/j.neuron.2013.10.025
Hussein, W., Berlin, S., 2020. Red Photoactivatable Genetic Optical-Indicators. Front. Cell. Neurosci. 14. https://doi.org/10.3389/fncel.2020.00113
Ichinose, S., Ogawa, T., Hirokawa, N., 2015. Mechanism of Activity-Dependent Cargo Loading via the Phosphorylation of KIF3A by PKA and CaMKIIa. Neuron 87, 1022–1035. https://doi.org/10.1016/j.neuron.2015.08.008
Inoue, M., 2021. Genetically encoded calcium indicators to probe complex brain circuit dynamics in vivo. Neurosci. Res. 169, 2–8. https://doi.org/10.1016/j.neures.2020.05.013
Isaev, N.K., Stelmashook, E. V., Dirnagl, U., Plotnikov, E.Y., Kuvshinova, E.A., Zorov, D.B., 2008. Mitochondrial free radical production induced by glucose deprivation in cerebellar granule neurons. Biochem. 73, 149–155. https://doi.org/10.1134/S0006297908020053

Jenkins, M.A., Christel, C.J., Jiao, Y., Abiria, S., Kim, K.Y., Usachev, Y.M., Obermair, G.J., Colbran, R.J., Lee, A., 2010. Ca2+-Dependent Facilitation of Cav1.3 Ca2+ Channels by Densin and Ca2+/Calmodulin-Dependent Protein Kinase II. J. Neurosci. 30, 5125–5135. https://doi.org/10.1523/JNEUROSCI.4367-09.2010

Jenkins, M.A., Traynelis, S.F., 2012. PKC phosphorylates GluA1-Ser831 to enhance AMPA receptor conductance. Channels 6, 60–64. https://doi.org/10.4161/chan.18648

Jensen, M., Hoerndli, F.J., Brockie, P.J., Wang, R., Johnson, E., Maxfield, D., Francis, M.M., Madsen, D.M., Maricq, A. V., 2012. Wnt Signaling Regulates Acetylcholine Receptor Translocation and Synaptic Plasticity in the Adult Nervous System. Cell 149, 173–187. https://doi.org/10.1016/j.cell.2011.12.038

Jeyifous, O., Waites, C.L., Specht, C.G., Fujisawa, S., Schubert, M., Lin, E.I., Marshall, J., Aoki, C., de Silva, T., Montgomery, J.M., Garner, C.C., Green, W.N., 2009. SAP97 and CASK mediate sorting of NMDA receptors through a previously unknown secretory pathway. Nat. Neurosci. 12, 1011–1019. https://doi.org/10.1038/nn.2362

Jin, E.J., Kiral, F.R., Hiesinger, P.R., 2018. The where, what, and when of membrane protein degradation in neurons. Dev. Neurobiol. 78, 283–297. https://doi.org/10.1002/dneu.22534

Jospin, M., Jacquemond, V., Mariol, M.-C., Ségalat, L., Allard, B., 2002. The L-type voltage-dependent Ca2+ channel EGL-19 controls body wall muscle function in Caenorhabditis elegans. J. Cell Biol. 159, 337–348. https://doi.org/10.1083/jcb.200203055

Ju, W., Morishita, W., Tsui, J., Gaietta, G., Deerinck, T.J., Adams, S.R., Garner, C.C., Tsien, R.Y., Ellisman, M.H., Malenka, R.C., 2004. Activity-dependent regulation of dendritic synthesis and trafficking of AMPA receptors. Nat. Neurosci. 7, 244–253. https://doi.org/10.1038/nn1189

Kamsler, A., Segal, M., 2003. Hydrogen Peroxide Modulation of Synaptic Plasticity. J. Neurosci. 23, 269–276. https://doi.org/10.1523/JNEUROSCI.23-01-00269.2003

Kanemaru, K., Suzuki, J., Taiko, I., Iino, M., 2020. Red fluorescent CEPIA indicators for visualization of Ca2+ dynamics in mitochondria. Sci. Rep. 10, 2835. https://doi.org/10.1038/s41598-020-59707-8

Kapur, A., Yeckel, M.F., Gray, R., Johnston, D., 1998. L-Type Calcium Channels Are Required for One Form of Hippocampal Mossy Fiber LTP. J. Neurophysiol. 79, 2181–2190. https://doi.org/10.1152/jn.1998.79.4.2181

Kayadjanian, N., Lee, H.S., Piña-Crespo, J., Heinemann, S.F., 2007. Localization of glutamate receptors to distal dendrites depends on subunit composition and the kinesin motor protein KIF17. Mol. Cell. Neurosci. 34, 219–230. https://doi.org/10.1016/j.mcn.2006.11.001

Kennedy, M.J., Davison, I.G., Robinson, C.G., Ehlers, M.D., 2010. Syntaxin-4 defines a domain for activity-dependent exocytosis in dendritic spines. Cell 141, 524–535. https://doi.org/10.1016/j.cell.2010.02.042

Kerruth, S., Coates, C., Dürst, C.D., Oertner, T.G., Török, K., 2019. The kinetic mechanisms of fast-decay red-fluorescent genetically encoded calcium indicators. J. Biol. Chem. 294, 3934–3946. https://doi.org/10.1074/jbc.RA118.004543

Kichuk, T.C., Carrasco-López, C., Avalos, J.L., 2021. Lights up on organelles: Optogenetic tools to control subcellular structure and organization. WIREs Mech. Dis. 13. https://doi.org/10.1002/wsbm.1500

Kim, C.-H., Lisman, J.E., 2001. A Labile Component of AMPA Receptor-Mediated Synaptic Transmission Is Dependent on Microtubule Motors, Actin, and N -Ethylmaleimide-Sensitive Factor. J. Neurosci. 21, 4188–4194. https://doi.org/10.1523/JNEUROSCI.21-12-

04188.2001
Kim, C.H., Lisman, J.E., 2001. A labile Component of AMPA Receptor-Mediated Synaptic Transmission Is Dependent on Microtbule Motors, Actin and N-Ethylmaleimide-Sensitive Factor. J. Neurosci. 21, 4188–4194. https://doi.org/10.1523/jneurosci.21-12-04188.2001
Kim, K.W., Jin, Y., 2015. Neuronal responses to stress and injury in C. elegans. FEBS Lett. https://doi.org/10.1016/j.febslet.2015.05.005
Kim, S.-U., Jin, M.-H., Kim, Y.S., Lee, S.-H., Cho, Y.S., Cho, K.-J., Lee, K.-S., Kim, Y.I., Kim, G.W., Kim, J.-M., Lee, T.-H., Lee, Y.-H., Shong, M., Kim, H.-C., Chang, K.-T., Yu, D.-Y., Lee, D.-S., 2011. Peroxiredoxin II preserves cognitive function against age-linked hippocampal oxidative damage. Neurobiol. Aging 32, 1054–1068. https://doi.org/10.1016/j.neurobiolaging.2009.05.017
Kim, S.K., Horvitz, H.R., 1990. The Caenorhabditis elegans gene lin-10 is broadly expressed while required specifically for the determination of vulval cell fates. Genes Dev. 4, 357–371. https://doi.org/10.1101/gad.4.3.357
Kishida, K.T., Hoeffer, C.A., Hu, D., Pao, M., Holland, S.M., Klann, E., 2006. Synaptic Plasticity Deficits and Mild Memory Impairments in Mouse Models of Chronic Granulomatous Disease. Mol. Cell. Biol. 26, 5908–5920. https://doi.org/10.1128/MCB.00269-06
Kishida, K.T., Klann, E., 2006. Sources and Targets of Reactive Oxygen Species in Synaptic Plasticity and Memory. Antioxid. Redox Signal. 061121054212009. https://doi.org/10.1089/ars.2007.9.ft-8
Klann, E., 1998. Cell-Permeable Scavengers of Superoxide Prevent Long-Term Potentiation in Hippocampal Area CA1. J. Neurophysiol. 80, 452–457. https://doi.org/10.1152/jn.1998.80.1.452
Klapoetke, N.C., Murata, Y., Kim, S.S., Pulver, S.R., Birdsey-Benson, A., Cho, Y.K., Morimoto, T.K., Chuong, A.S., Carpenter, E.J., Tian, Z., Wang, J., Xie, Y., Yan, Z., Zhang, Y., Chow, B.Y., Surek, B., Melkonian, M., Jayaraman, V., Constantine-Paton, M., Wong, G.K.-S., Boyden, E.S., 2014. Independent optical excitation of distinct neural populations. Nat. Methods 11, 338–346. https://doi.org/10.1038/nmeth.2836
Kleinlogel, S., Feldbauer, K., Dempski, R.E., Fotis, H., Wood, P.G., Bamann, C., Bamberg, E., 2011. Ultra light-sensitive and fast neuronal activation with the Ca2+-permeable channelrhodopsin CatCh. Nat. Neurosci. 14, 513–518. https://doi.org/10.1038/nn.2776
Knapp, L.T., Klann, E., 2002a. Role of reactive oxygen species in hippocampal long-term potentiation: Contributory or inhibitory? J. Neurosci. Res. 70, 1–7. https://doi.org/10.1002/jnr.10371
Knapp, L.T., Klann, E., 2002b. Potentiation of Hippocampal Synaptic Transmission by Superoxide Requires the Oxidative Activation of Protein Kinase C. J. Neurosci. 22, 674–683. https://doi.org/10.1523/JNEUROSCI.22-03-00674.2002
Kumar, A., Yegla, B., Foster, T.C., 2018. Redox Signaling in Neurotransmission and Cognition During Aging. Antioxid. Redox Signal. 28, 1724–1745. https://doi.org/10.1089/ars.2017.7111
Kwok, T.C.Y., Ricker, N., Fraser, R., Chan, A.W., Burns, A., Stanley, E.F., McCourt, P., Cutler, S.R., Roy, P.J., 2006. A small-molecule screen in C. elegans yields a new calcium channel antagonist. Nature 441, 91–95. https://doi.org/10.1038/nature04657
Kyung, T., Lee, S., Kim, J.E., Cho, T., Park, H., Jeong, Y.-M., Kim, Dongkyu, Shin, A., Kim, S., Baek, J., Kim, J., Kim, N.Y., Woo, D., Chae, S., Kim, C.-H., Shin, H.-S., Han, Y.-M., Kim,

Daesoo, Heo, W. Do, 2015. Optogenetic control of endogenous Ca2+ channels in vivo. Nat. Biotechnol. 33, 1092–1096. https://doi.org/10.1038/nbt.3350
Laine, V., Segor, J.R., Zhan, H., Bessereau, J.-L., Jospin, M., 2014. Hyperactivation of L-type voltage-gated Ca2+ channels in Caenorhabditis elegans striated muscle can result from point mutations in the IS6 or the IIIS4 segment of the 1 subunit. J. Exp. Biol. 217, 3805–3814. https://doi.org/10.1242/jeb.106732
Larsch, J., Ventimiglia, D., Bargmann, C.I., Albrecht, D.R., 2013. High-throughput imaging of neuronal activity in Caenorhabditis elegans. Proc. Natl. Acad. Sci. 110, E4266–E4273. https://doi.org/10.1073/pnas.1318325110
Lee, R.Y.N., 1997. Mutations in the alpha 1 subunit of an L-type voltage-activated Ca2+ channel cause myotonia in Caenorhabditis elegans. EMBO J. 16, 6066–6076. https://doi.org/10.1093/emboj/16.20.6066
Lee, R.Y.N., Sawin, E.R., Chalfie, M., Horvitz, H.R., Avery, L., 1999. EAT-4, a Homolog of a Mammalian Sodium-Dependent Inorganic Phosphate Cotransporter, Is Necessary for Glutamatergic Neurotransmission in Caenorhabditis elegans. J. Neurosci. 19, 159–167. https://doi.org/10.1523/JNEUROSCI.19-01-00159.1999
Li, G., Gong, J., Lei, H., Liu, J., Xu, X.Z.S., 2016. Promotion of behavior and neuronal function by reactive oxygen species in C. elegans. Nat. Commun. 7, 13234. https://doi.org/10.1038/ncomms13234
Li, W., Kang, L., Piggott, B.J., Feng, Z., Xu, X.Z.S., 2011. The neural circuits and sensory channels mediating harsh touch sensation in Caenorhabditis elegans. Nat. Commun. 2, 315. https://doi.org/10.1038/ncomms1308
Lindsay, T.H., Thiele, T.R., Lockery, S.R., 2011. Optogenetic analysis of synaptic transmission in the central nervous system of the nematode Caenorhabditis elegans. Nat. Commun. 2, 306. https://doi.org/10.1038/ncomms1304
Liu, Q., Hollopeter, G., Jorgensen, E.M., 2009. Graded synaptic transmission at the Caenorhabditis elegans neuromuscular junction. Proc. Natl. Acad. Sci. 106, 10823–10828. https://doi.org/10.1073/pnas.0903570106
Liu, Q., Kidd, P.B., Dobosiewicz, M., Bargmann, C.I., 2018. C. elegans AWA Olfactory Neurons Fire Calcium-Mediated All-or-None Action Potentials. Cell 175, 57-70.e17. https://doi.org/10.1016/j.cell.2018.08.018
Loubéry, S., Wilhelm, C., Hurbain, I., Neveu, S., Louvard, D., Coudrier, E., 2008. Different Microtubule Motors Move Early and Late Endocytic Compartments. Traffic 9, 492–509. https://doi.org/10.1111/j.1600-0854.2008.00704.x
Luebke, J.I., Dunlap, K., Turner, T.J., 1993. Multiple calcium channel types control glutamatergic synaptic transmission in the hippocampus. Neuron 11, 895–902. https://doi.org/10.1016/0896-6273(93)90119-C
Luo, L., Wen, Q., Ren, J., Hendricks, M., Gershow, M., Qin, Y., Greenwood, J., Soucy, E.R., Klein, M., Smith-Parker, H.K., Calvo, A.C., Colón-Ramos, D.A., Samuel, A.D.T., Zhang, Y., 2014. Dynamic Encoding of Perception, Memory, and Movement in a C. elegans Chemotaxis Circuit. Neuron 82, 1115–1128. https://doi.org/10.1016/j.neuron.2014.05.010
Maeder, C.I., Shen, K., Hoogenraad, C.C., 2014. Axon and dendritic trafficking. Curr. Opin. Neurobiol. 27, 165–170. https://doi.org/10.1016/j.conb.2014.03.015
Malenka, R.C., Bear, M.F., 2004. LTP and LTD. Neuron 44, 5–21. https://doi.org/10.1016/j.neuron.2004.09.012
Maricq, A. V., Peckol, E., Driscoll, M., Bargmann, C.I., 1995. Mechanosensory signalling in C.

elegans mediated by the GLR-1 glutamate receptor. Nature 378, 78–81. https://doi.org/10.1038/378078a0
Massaad, C.A., Klann, E., 2011. Reactive oxygen species in the regulation of synaptic plasticity and memory. Antioxid. Redox Signal. 14, 2013–54. https://doi.org/10.1089/ars.2010.3208
Miranda-Vizuete, A., Veal, E.A., 2017. Caenorhabditis elegans as a model for understanding ROS function in physiology and disease. Redox Biol. 11, 708–714. https://doi.org/10.1016/j.redox.2016.12.020
Monteiro, Michael I., Ahlawat, S., Kowalski, J.R., Malkin, E., Koushika, S.P., Juo, P., 2012. The kinesin-3 family motor KLP-4 regulates anterograde trafficking of GLR-1 glutamate receptors in the ventral nerve cord of Caenorhabditis elegans. Mol. Biol. Cell 23, 3647–3662. https://doi.org/10.1091/mbc.e12-04-0334
Monteiro, M I, Ahlawat, S., Kowalski, J.R., Malkin, E., Koushika, S.P., Juo, P., 2012. The kinesin-3 family motor KLP-4 regulates anterograde trafficking of GLR-1 glutamate receptors in the ventral nerve cord of Caenorhabditis elegans. Mol Biol Cell 23, 3647–3662. https://doi.org/10.1091/mbc.E12-04-0334
Morrison, G.E., Kooy, D. van der, 2001. A mutation in the AMPA-type glutamate receptor, glr-1, blocks olfactory associative and nonassociative learning in Caenorhabditis elegans. Behav. Neurosci. 115, 640–649. https://doi.org/10.1037/0735-7044.115.3.640
Müller, M., Ahumada-Castro, U., Sanhueza, M., Gonzalez-Billault, C., Court, F.A., Cárdenas, C., 2018. Mitochondria and Calcium Regulation as Basis of Neurodegeneration Associated With Aging. Front. Neurosci. 12, 1–8. https://doi.org/10.3389/fnins.2018.00470
Murphy, M.P., 2009. How mitochondria produce reactive oxygen species. Biochem. J. 417, 1–13. https://doi.org/10.1042/BJ20081386
Murphy, M.P., Smith, R.A.J., 2007. Targeting Antioxidants to Mitochondria by Conjugation to Lipophilic Cations. Annu. Rev. Pharmacol. Toxicol. 47, 629–656. https://doi.org/10.1146/annurev.pharmtox.47.120505.105110
Nair, J.D., Wilkinson, K.A., Henley, J.M., Mellor, J.R., 2021. Kainate receptors and synaptic plasticity. Neuropharmacology 196, 108540. https://doi.org/10.1016/j.neuropharm.2021.108540
Narayan, A., Laurent, G., Sternberg, P.W., 2011. Transfer characteristics of a thermosensory synapse in Caenorhabditis elegans. Proc. Natl. Acad. Sci. 108, 9667–9672. https://doi.org/10.1073/pnas.1106617108
Nazıroğlu, M., 2012. Molecular role of catalase on oxidative stress-induced Ca 2+ signaling and TRP cation channel activation in nervous system. J. Recept. Signal Transduct. 32, 134–141. https://doi.org/10.3109/10799893.2012.672994
Nazıroğlu, M., Lückhoff, A., 2008. Effects of antioxidants on calcium influx through TRPM2 channels in transfected cells activated by hydrogen peroxide. J. Neurol. Sci. 270, 152–158. https://doi.org/10.1016/j.jns.2008.03.003
Neumann, S., Chassefeyre, R., Campbell, G.E., Encalada, S.E., 2017. KymoAnalyzer: a software tool for the quantitative analysis of intracellular transport in neurons. Traffic 18, 71–88. https://doi.org/doi:10.1111/tra.12456
Nicholls, D.G., 2009. Mitochondrial calcium function and dysfunction in the central nervous system. Biochim. Biophys. Acta - Bioenerg. 1787, 1416–1424. https://doi.org/10.1016/j.bbabio.2009.03.010
Niciu, M.J., Kelmendi, B., Sanacora, G., 2012. Overview of glutamatergic neurotransmission in the nervous system. Pharmacol. Biochem. Behav. 100, 656–664.

https://doi.org/10.1016/j.pbb.2011.08.008
Nikoletopoulou, V., Tavernarakis, N., 2012. Calcium homeostasis in aging neurons. Front. Genet. 3, 1–17. https://doi.org/10.3389/fgene.2012.00200
Nimchinsky, E.A., Sabatini, B.L., Svoboda, K., 2002. Structure and Function of Dendritic Spines. Annu. Rev. Physiol. 64, 313–353. https://doi.org/10.1146/annurev.physiol.64.081501.160008
Niwa, S., Tanaka, Y., Hirokawa, N., 2008. KIF1Bβ- and KIF1A-mediated axonal transport of presynaptic regulator Rab3 occurs in a GTP-dependent manner through DENN/MADD. Nat. Cell Biol. 10, 1269–1279. https://doi.org/10.1038/ncb1785
Opazo, P., Choquet, D., 2011. A three-step model for the synaptic recruitment of AMPA receptors. Mol. Cell. Neurosci. 46, 1–8. https://doi.org/10.1016/j.mcn.2010.08.014
Ordyan, M., Bartol, T., Kennedy, M., Rangamani, P., Sejnowski, T., 2020. Interactions between calmodulin and neurogranin govern the dynamics of CaMKII as a leaky integrator. PLOS Comput. Biol. 16, e1008015. https://doi.org/10.1371/journal.pcbi.1008015
Oswald, Matthew C.W., Brooks, P.S., Zwart, M.F., Mukherjee, A., West, R.J.H., Giachello, C.N.G., Morarach, K., Baines, R.A., Sweeney, S.T., Landgraf, M., 2018. Reactive oxygen species regulate activity-dependent neuronal plasticity in Drosophila. Elife 7. https://doi.org/10.7554/eLife.39393
Oswald, Matthew C. W., Garnham, N., Sweeney, S.T., Landgraf, M., 2018. Regulation of neuronal development and function by ROS. FEBS Lett. 592, 679–691. https://doi.org/10.1002/1873-3468.12972
Park, E.C., Glodowski, D.R., Rongo, C., 2009. The Ubiquitin Ligase RPM-1 and the p38 MAPK PMK-3 Regulate AMPA Receptor Trafficking. PLoS One 4, e4284. https://doi.org/10.1371/journal.pone.0004284
Park, E.C., Horvitz, H.R., 1986. Mutations with dominant effects on the behavior and morphology of the nematode Caenorhabditis elegans. Genetics 113, 821–852.
Park, E.C., Rongo, C., 2016. The p38 MAP kinase pathway modulates the hypoxia response and glutamate receptor trafficking in aging neurons. Elife 5, e12010. https://doi.org/10.7554/eLife.12010
Park, M., 2018. AMPA Receptor Trafficking for Postsynaptic Potentiation. Front. Cell. Neurosci. 12. https://doi.org/10.3389/fncel.2018.00361
Penn, A.C., Zhang, C.L., Georges, F., Royer, L., Breillat, C., Hosy, E., Petersen, J.D., Humeau, Y., Choquet, D., 2017. Hippocampal LTP and contextual learning require surface diffusion of AMPA receptors. Nature 549, 384–388. https://doi.org/10.1038/nature23658
Petriv, O.I., Rachubinski, R.A., 2004. Lack of Peroxisomal Catalase Causes a Progeric Phenotype in Caenorhabditis elegans. J. Biol. Chem. 279, 19996–20001. https://doi.org/10.1074/jbc.M400207200
Pires, P.W., Earley, S., 2017. Redox regulation of transient receptor potential channels in the endothelium. Microcirculation 24, e12329. https://doi.org/10.1111/micc.12329
Pozzan, T., Rudolf, R., 2009. Measurements of mitochondrial calcium in vivo. Biochim. Biophys. Acta - Bioenerg. 1787, 1317–1323. https://doi.org/10.1016/j.bbabio.2008.11.012
Puthanveettil, S. V., Monje, F.J., Miniaci, M.C., Choi, Y.-B., Karl, K.A., Khandros, E., Gawinowicz, M.A., Sheetz, M.P., Kandel, E.R., 2008. A New Component in Synaptic Plasticity: Upregulation of Kinesin in the Neurons of the Gill-Withdrawal Reflex. Cell 135, 960–973. https://doi.org/10.1016/j.cell.2008.11.003
Quintin, S., Aspert, T., Ye, T., Charvin, G., 2021. Distinct mechanisms underlie H2O2 sensing in

C. elegans head and tail. bioRxiv 2021.07.26.451501. https://doi.org/10.1101/2021.07.26.451501
Rao, V.R., Finkbeiner, S., 2007. NMDA and AMPA receptors: old channels, new tricks. Trends Neurosci. 30, 284–291. https://doi.org/10.1016/j.tins.2007.03.012
Reiner, D.J., Newton, E.M., Tian, H., Thomas, J.H., 1999. Diverse behavioural defects caused by mutations in Caenorhabditis elegans unc-43 CaM kinase II. Nature 402, 199–203. https://doi.org/10.1038/46072
Ren, S.Q., Yan, J.Z., Zhang, X.Y., Bu, Y.F., Pan, W.W., Yao, W., Tian, T., Lu, W., 2013. PKCλ is critical in AMPA receptor phosphorylation and synaptic incorporation during LTP. EMBO J. 32, 1365–1380. https://doi.org/10.1038/emboj.2013.60
Reyes-García, S.E., Escobar, M.L., 2021. Calcineurin Participation in Hebbian and Homeostatic Plasticity Associated With Extinction. Front. Cell. Neurosci. 15. https://doi.org/10.3389/fncel.2021.685838
Robison, A.J., Winder, D.G., Colbran, R.J., Bartlett, R.K., 2007. Oxidation of calmodulin alters activation and regulation of CaMKII. Biochem. Biophys. Res. Commun. 356, 97–101. https://doi.org/10.1016/j.bbrc.2007.02.087
Rongo, C., Kaplan, J.M., 1999. CaMKII regulates the density of central glutamatergic synapses in vivo. Nature 402, 195–199. https://doi.org/10.1038/46065
Rongo C and Kaplan J, M., 1999. CamKII regulates density of glutamatergic synapses in vivo. Nature 402, 195–199.
Rose, J.K., Kaun, K.R., Chen, S.H., Rankin, C.H., 2003. GLR-1, a Non-NMDA Glutamate Receptor Homolog, Is Critical for Long-Term Memory in Caenorhabditis elegans. J. Neurosci. 23, 9595–9599. https://doi.org/10.1523/JNEUROSCI.23-29-09595.2003
Rosenberg, T., Gal-Ben-Ari, S., Dieterich, D.C., Kreutz, M.R., Ziv, N.E., Gundelfinger, E.D., Rosenblum, K., 2014. The roles of protein expression in synaptic plasticity and memory consolidation. Front. Mol. Neurosci. 7. https://doi.org/10.3389/fnmol.2014.00086
Rosendale, M., Jullié, D., Choquet, D., Perrais, D., 2017. Spatial and Temporal Regulation of Receptor Endocytosis in Neuronal Dendrites Revealed by Imaging of Single Vesicle Formation. Cell Rep. 18, 1840–1847. https://doi.org/10.1016/j.celrep.2017.01.081
Sabatini, B.L., Maravall, M., Svoboda, K., 2001. Ca2+ signaling in dendritic spines. Curr. Opin. Neurobiol. 11, 349–356. https://doi.org/10.1016/S0959-4388(00)00218-X
Sander, P., Gudermann, T., Schredelseker, J., 2021. A Calcium Guard in the Outer Membrane: Is VDAC a Regulated Gatekeeper of Mitochondrial Calcium Uptake? Int. J. Mol. Sci. 22, 946. https://doi.org/10.3390/ijms22020946
Sarasija, S., Laboy, J.T., Ashkavand, Z., Bonner, J., Tang, Y., Norman, K.R., 2018. Presenilin mutations deregulate mitochondrial Ca2+ homeostasis and metabolic activity causing neurodegeneration in Caenorhabditis elegans. Elife 7. https://doi.org/10.7554/elife.33052
Sarasija, S., Norman, K.R., 2015. A γ-secretase independent role for presenilin in calcium homeostasis impacts mitochondrial function and morphology in caenorhabditis elegans. Genetics 201, 1453–1466. https://doi.org/10.1534/genetics.115.182808
Schafer, W.R., 2015. Mechanosensory molecules and circuits in C. elegans. Pflügers Arch. - Eur. J. Physiol. 467, 39–48. https://doi.org/10.1007/s00424-014-1574-3
Schild, L.C., Glauser, D.A., 2015. Dual Color Neural Activation and Behavior Control with Chrimson and CoChR in Caenorhabditis elegans. Genetics 200, 1029–1034. https://doi.org/10.1534/genetics.115.177956
Schultheis, C., Liewald, J.F., Bamberg, E., Nagel, G., Gottschalk, A., 2011. Optogenetic Long-

Term Manipulation of Behavior and Animal Development. PLoS One 6, e18766. https://doi.org/10.1371/journal.pone.0018766
Scragg, J.L., Dallas, M.L., Wilkinson, J.A., Varadi, G., Peers, C., 2008. Carbon monoxide inhibits L-type Ca2+ channels via redox modulation of key cysteine residues by mitochondrial reactive oxygen species. J. Biol. Chem. 283, 24412–24419. https://doi.org/10.1074/jbc.M803037200
Sengupta, P., Samuel, A.D., 2009. Caenorhabditis elegans: a model system for systems neuroscience. Curr. Opin. Neurobiol. 19, 637–643. https://doi.org/10.1016/j.conb.2009.09.009
Serrano-Saiz, E., Poole, R.J., Felton, T., Zhang, F., De La Cruz, E.D., Hobert, O., 2013. XModular control of glutamatergic neuronal identity in C. elegans by distinct homeodomain proteins. Cell 155, 659. https://doi.org/10.1016/j.cell.2013.09.052
Setou, M., Nakagawa, T., Seog, D.-H., Hirokawa, N., 2000. Kinesin Superfamily Motor Protein KIF17 and mLin-10 in NMDA Receptor-Containing Vesicle Transport. Science (80-.). 288, 1796–1802. https://doi.org/10.1126/science.288.5472.1796
Setou, M., Seog, D.-H., Tanaka, Y., Kanai, Y., Takei, Y., Kawagishi, M., Hirokawa, N., 2002. Glutamate-receptor-interacting protein GRIP1 directly steers kinesin to dendrites. Nature 417, 83–87. https://doi.org/10.1038/nature743
Shipley, F.B., Clark, C.M., Alkema, M.J., Leifer, A.M., 2014. Simultaneous optogenetic manipulation and calcium imaging in freely moving C. elegans. Front. Neural Circuits 8. https://doi.org/10.3389/fncir.2014.00028
Shirotani, K., Katsura, M., Higo, A., Takesue, M., Mohri, Y., Shuto, K., Tarumi, C., Ohkuma, S., 2001. Suppression of Ca2+ influx through L-type voltage-dependent calcium channels by hydroxyl radical in mouse cerebral cortical neurons. Mol. Brain Res. 92, 12–18. https://doi.org/10.1016/S0169-328X(01)00128-0
Sies, H., 2017. Hydrogen peroxide as a central redox signaling molecule in physiological oxidative stress: Oxidative eustress. Redox Biol. https://doi.org/10.1016/j.redox.2016.12.035
Sies, H., Jones, D.P., 2020. Reactive oxygen species (ROS) as pleiotropic physiological signalling agents. Nat. Rev. Mol. Cell Biol. 21, 363–383. https://doi.org/10.1038/s41580-020-0230-3
Snijder, J., Rose, R.J., Raijmakers, R., Heck, A.J.R., 2011. Site-specific methionine oxidation in calmodulin affects structural integrity and interaction with Ca2+/calmodulin-dependent protein kinase II. J. Struct. Biol. 174, 187–195. https://doi.org/10.1016/j.jsb.2010.12.002
Spiró, Z., Arslan, M.A., Somogyvári, M., Nguyen, M.T., Smolders, A., Dancsó, B., Németh, N., Elek, Z., Braeckman, B.P., Csermely, P., Sőti, C., 2012. RNA Interference Links Oxidative Stress to the Inhibition of Heat Stress Adaptation. Antioxid. Redox Signal. 17, 890–901. https://doi.org/10.1089/ars.2011.4161
Stefanatos, R., Sanz, A., 2018. The role of mitochondrial ROS in the aging brain. FEBS Lett. 592, 743–758. https://doi.org/10.1002/1873-3468.12902
Stetak, A., Hörndli, F., Maricq, A. V., van den Heuvel, S., Hajnal, A., 2009. Neuron-Specific Regulation of Associative Learning and Memory by MAGI-1 in C. elegans. PLoS One 4, e6019. https://doi.org/10.1371/journal.pone.0006019
Stucchi, R., Plucińska, G., Hummel, J.J.A., Zahavi, E.E., Guerra San Juan, I., Klykov, O., Scheltema, R.A., Altelaar, A.F.M., Hoogenraad, C.C., 2018. Regulation of KIF1A-Driven Dense Core Vesicle Transport: Ca2+/CaM Controls DCV Binding and Liprin-α/TANC2

Recruits DCVs to Postsynaptic Sites. Cell Rep. 24, 685–700. https://doi.org/10.1016/j.celrep.2018.06.071
Sumi, T., Harada, K., 2020. Mechanism underlying hippocampal long-term potentiation and depression based on competition between endocytosis and exocytosis of AMPA receptors. Sci. Rep. 10, 14711. https://doi.org/10.1038/s41598-020-71528-3
Suzuki, H., Kerr, R., Bianchi, L., Frøkjær-Jensen, C., Slone, D., Xue, J., Gerstbrein, B., Driscoll, M., Schafer, W.R., 2003. In Vivo Imaging of C. elegans Mechanosensory Neurons Demonstrates a Specific Role for the MEC-4 Channel in the Process of Gentle Touch Sensation. Neuron 39, 1005–1017. https://doi.org/10.1016/j.neuron.2003.08.015
Suzuki, N., Inokuma, K., Yasuda, K., Ishii, N., 1996. Cloning, Sequencing and Mapping of a Manganese Superoxide Dismutase Gene of the Nematode Caenorhabditis elegans. DNA Res. 3, 171–174. https://doi.org/10.1093/dnares/3.3.171
Szibor, M., Gizatullina, Z., Gainutdinov, T., Endres, T., Debska-Vielhaber, G., Kunz, M., Karavasili, N., Hallmann, K., Schreiber, F., Bamberger, A., Schwarzer, M., Doenst, T., Heinze, H.-J., Lessmann, V., Vielhaber, S., Kunz, W.S., Gellerich, F.N., 2020. Cytosolic, but not matrix, calcium is essential for adjustment of mitochondrial pyruvate supply. J. Biol. Chem. 295, 4383–4397. https://doi.org/10.1074/jbc.RA119.011902
Tammineni, P., Ye, X., Feng, T., Aikal, D., Cai, Q., 2017. Impaired retrograde transport of axonal autophagosomes contributes to autophagic stress in Alzheimer's disease neurons. Elife 6. https://doi.org/10.7554/eLife.21776
Tang, S., Yasuda, R., 2017. Imaging ERK and PKA Activation in Single Dendritic Spines during Structural Plasticity. Neuron 93, 1315-1324.e3. https://doi.org/10.1016/j.neuron.2017.02.032
Tardiff, D.F., Jui, N.T., Khurana, V., Tambe, M.A., Thompson, M.L., Chung, C.Y., Kamadurai, H.B., Kim, H.T., Lancaster, A.K., Caldwell, K.A., Caldwell, G.A., Rochet, J.-C., Buchwald, S.L., Lindquist, S., 2013. Yeast Reveal a "Druggable" Rsp5/Nedd4 Network that Ameliorates α-Synuclein Toxicity in Neurons. Science (80-.). 342, 979–983. https://doi.org/10.1126/science.1245321
Tauffenberger, A., Magistretti, P.J., 2021. Reactive Oxygen Species: Beyond Their Reactive Behavior. Neurochem. Res. 46, 77–87. https://doi.org/10.1007/s11064-020-03208-7
Territo, P.R., Mootha, V.K., French, S.A., Balaban, R.S., 2000. Ca 2+ activation of heart mitochondrial oxidative phosphorylation: role of the F 0 /F 1 -ATPase. Am. J. Physiol. Physiol. 278, C423–C435. https://doi.org/10.1152/ajpcell.2000.278.2.C423
Thiels, E., Urban, N.N., Gonzalez-Burgos, G.R., Kanterewicz, B.I., Barrionuevo, G., Chu, C.T., Oury, T.D., Klann, E., 2000. Impairment of long-term potentiation and associative memory in mice that overexpress extracellular superoxide dismutase. J Neurosci 20, 7631–7639. https://doi.org/20/20/7631 [pii]
Todorovic, S.M., Jevtovic-Todorovic, V., 2014. Redox Regulation of Neuronal Voltage-Gated Calcium Channels. Antioxid. Redox Signal. 21, 880–891. https://doi.org/10.1089/ars.2013.5610
Tonks, N.K., 2006. Protein tyrosine phosphatases: from genes, to function, to disease. Nat. Rev. Mol. Cell Biol. 7, 833–846. https://doi.org/10.1038/nrm2039
Trent, C., Tsuing, N., Horvitz, H.R., 1983. Egg-laying defective mutants of the nematode Caenorhabditis elegans. Genetics 104, 619–647.
Treusch, S., Hamamichi, S., Goodman, J.L., Matlack, K.E.S., Chung, C.Y., Baru, V., Shulman, J.M., Parrado, A., Bevis, B.J., Valastyan, J.S., Han, H., Lindhagen-Persson, M., Reiman,

E.M., Evans, D.A., Bennett, D.A., Olofsson, A., DeJager, P.L., Tanzi, R.E., Caldwell, K.A., Caldwell, G.A., Lindquist, S., 2011. Functional Links Between Aβ Toxicity, Endocytic Trafficking, and Alzheimer's Disease Risk Factors in Yeast. Science (80-.). 334, 1241–1245. https://doi.org/10.1126/science.1213210

Umemura, T., 2005. The role of regulatory domain interactions in UNC-43 CaMKII localization and trafficking. J. Cell Sci. 118, 3327–3338. https://doi.org/10.1242/jcs.02457

Umemura, T., Rapp, P., Rongo, C., 2005. The role of regulatory domain interactions in UNC-43 CaMKII localization and trafficking. J. Cell Sci. 118, 3327–3338. https://doi.org/10.1242/jcs.02457

Vandael, D., Borges-Merjane, C., Zhang, X., Jonas, P., 2020. Short-Term Plasticity at Hippocampal Mossy Fiber Synapses Is Induced by Natural Activity Patterns and Associated with Vesicle Pool Engram Formation. Neuron 107, 509-521.e7. https://doi.org/10.1016/j.neuron.2020.05.013

Vergara, R.C., Jaramillo-Riveri, S., Luarte, A., Moënne-Loccoz, C., Fuentes, R., Couve, A., Maldonado, P.E., 2019. The Energy Homeostasis Principle: Neuronal Energy Regulation Drives Local Network Dynamics Generating Behavior. Front. Comput. Neurosci. 13. https://doi.org/10.3389/fncom.2019.00049

von Ossowski, L., Li, L.-L., Möykkynen, T., Coleman, S.K., Courtney, M.J., Keinänen, K., 2017. Cysteine 893 is a target of regulatory thiol modifications of GluA1 AMPA receptors. PLoS One 12, e0171489. https://doi.org/10.1371/journal.pone.0171489

Wacquier, B., Combettes, L., Dupont, G., 2019. Cytoplasmic and Mitochondrial Calcium Signaling: A Two-Way Relationship. Cold Spring Harb. Perspect. Biol. 11, a035139. https://doi.org/10.1101/cshperspect.a035139

Wang, H., Zhuo, M., 2012. Group I Metabotropic Glutamate Receptor-Mediated Gene Transcription and Implications for Synaptic Plasticity and Diseases. Front. Pharmacol. 3. https://doi.org/10.3389/fphar.2012.00189

Wang, N., Xu, J., 2015. Functions of Kinesin Superfamily Proteins in Neuroreceptor Trafficking. Biomed Res. Int. 2015, 1–8. https://doi.org/10.1155/2015/639301

Washbourne, P., Bennett, J.E., McAllister, A.K., 2002. Rapid recruitment of NMDA receptor transport packets to nascent synapses. Nat. Neurosci. 5, 751–759. https://doi.org/10.1038/nn883

Way, J.C., Chalfie, M., 1989. The mec-3 gene of Caenorhabditis elegans requires its own product for maintained expression and is expressed in three neuronal cell types. Genes Dev. 3, 1823–1833. https://doi.org/10.1101/gad.3.12a.1823

Wenthold, R., Petralia, R., Blahos J, I., Niedzielski, A., 1996. Evidence for multiple AMPA receptor complexes in hippocampal CA1/CA2 neurons. J. Neurosci. 16, 1982–1989. https://doi.org/10.1523/JNEUROSCI.16-06-01982.1996

Wilson, C., González-Billault, C., 2015. Regulation of cytoskeletal dynamics by redox signaling and oxidative stress: implications for neuronal development and trafficking. Front. Cell. Neurosci. 9, 1–10. https://doi.org/10.3389/fncel.2015.00381

Wilson, C., Muñoz-Palma, E., González-Billault, C., 2018. From birth to death: A role for reactive oxygen species in neuronal development. Semin. Cell Dev. Biol. 80, 43–49. https://doi.org/10.1016/j.semcdb.2017.09.012

Wong, Y.C., Holzbaur, E.L.F., 2014. The Regulation of Autophagosome Dynamics by Huntingtin and HAP1 Is Disrupted by Expression of Mutant Huntingtin, Leading to Defective Cargo Degradation. J. Neurosci. 34, 1293–1305.

https://doi.org/10.1523/JNEUROSCI.1870-13.2014
Wu, Y., Whiteus, C., Xu, C.S., Hayworth, K.J., Weinberg, R.J., Hess, H.F., De Camilli, P., 2017. Contacts between the endoplasmic reticulum and other membranes in neurons. Proc. Natl. Acad. Sci. 114, E4859–E4867. https://doi.org/10.1073/pnas.1701078114
Wyszynski, M., Kim, E., Dunah, A.W., Passafaro, M., Valtschanoff, J.G., Serra-Pagès, C., Streuli, M., Weinberg, R.J., Sheng, M., 2002. Interaction between GRIP and Liprin-α/SYD2 Is Required for AMPA Receptor Targeting. Neuron 34, 39–52. https://doi.org/10.1016/S0896-6273(02)00640-2
Xu, S., Chisholm, A.D., 2014. C.elegans epidermal wounding induces a mitochondrial ROS burst that promotes wound repair. Dev. Cell 31, 48–60. https://doi.org/10.1016/j.devcel.2014.08.002
Yermolaieva, O., Brot, N., Weissbach, H., Heinemann, S.H., Hoshi, T., 2000. Reactive oxygen species and nitric oxide mediate plasticity of neuronal calcium signaling. Proc. Natl. Acad. Sci. 97, 448–453. https://doi.org/10.1073/pnas.97.1.448
Yin, X., Feng, X., Takei, Y., Hirokawa, N., 2012. Regulation of NMDA Receptor Transport: A KIF17-Cargo Binding/Releasing Underlies Synaptic Plasticity and Memory In Vivo. J. Neurosci. 32, 5486–5499. https://doi.org/10.1523/JNEUROSCI.0718-12.2012
Yudowski, G.A., Puthenveedu, M.A., Leonoudakis, D., Panicker, S., Thorn, K.S., Beattie, E.C., von Zastrow, M., 2007. Real-Time Imaging of Discrete Exocytic Events Mediating Surface Delivery of AMPA Receptors. J. Neurosci. 27, 11112–11121. https://doi.org/10.1523/JNEUROSCI.2465-07.2007
Zhang, X., Connelly, J., Levitan, E.S., Sun, D., Wang, J.Q., 2021. Calcium/Calmodulin–Dependent Protein Kinase II in Cerebrovascular Diseases. Transl. Stroke Res. 12, 513–529. https://doi.org/10.1007/s12975-021-00901-9
Zhao, J., Fok, A.H.K., Fan, R., Kwan, P.-Y., Chan, H.-L., Lo, L.H.-Y., Chan, Y.-S., Yung, W.-H., Huang, J., Lai, C.S.W., Lai, K.-O., 2020. Specific depletion of the motor protein KIF5B leads to deficits in dendritic transport, synaptic plasticity and memory. Elife 9. https://doi.org/10.7554/eLife.53456
Zheng, Y., Brockie, P.J., Mellem, J.E., Madsen, D.M., Maricq, A. V, 1999. Neuronal control of locomotion in C. elegans is modified by a dominant mutation in the GLR-1 ionotropic glutamate receptor. Neuron 24, 347–361. https://doi.org/10.1016/S0896-6273(00)80849-1
Zheng, Z., Keifer, J., 2008. Protein kinase C-dependent and independent signaling pathways regulate synaptic GluR1 and GluR4 AMPAR subunits during in vitro classical conditioning. Neuroscience 156, 872–884. https://doi.org/10.1016/j.neuroscience.2008.08.042
Zorov, D.B., Juhaszova, M., Sollott, S.J., 2014. Mitochondrial Reactive Oxygen Species (ROS) and ROS-Induced ROS Release. Physiol. Rev. 94, 909–950. https://doi.org/10.1152/physrev.00026.2013
Zullo, J.M., Drake, D., Aron, L., O'Hern, P., Dhamne, S.C., Davidsohn, N., Mao, C.-A., Klein, W.H., Rotenberg, A., Bennett, D.A., Church, G.M., Colaiácovo, M.P., Yankner, B.A., 2019. Regulation of lifespan by neural excitation and REST. Nature 574, 359–364. https://doi.org/10.1038/s41586-019-1647-8

Appendix

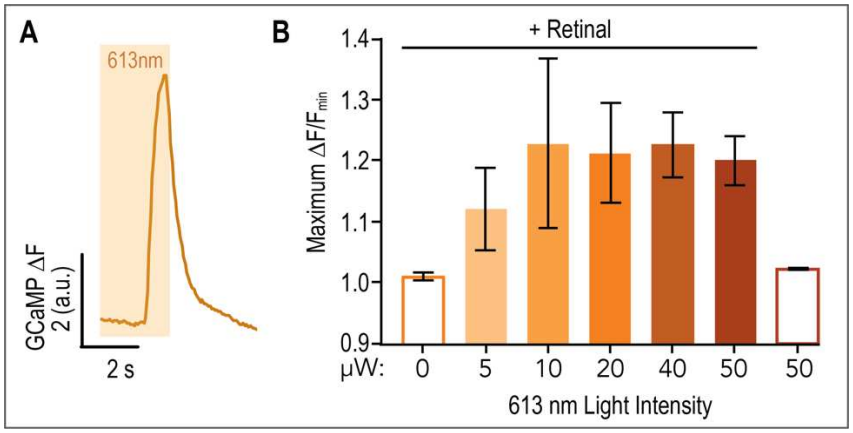

Figure 3.8 - Fluorescence of cytoplasmic GCaMP6f following whole-cell activation of ChRimson. A) A line graph of GCaMP fluorescence subtracted by minimum fluorescence (ΔF) over time. a.u.: arbitrary fluorescence units. B) Maximum ΔF normalized to minimum fluorescence for GCaMP peaks resulting from increasing intensity of 613 nm light (in μW/mm^2) with or without Retinal. n = 5 for each.

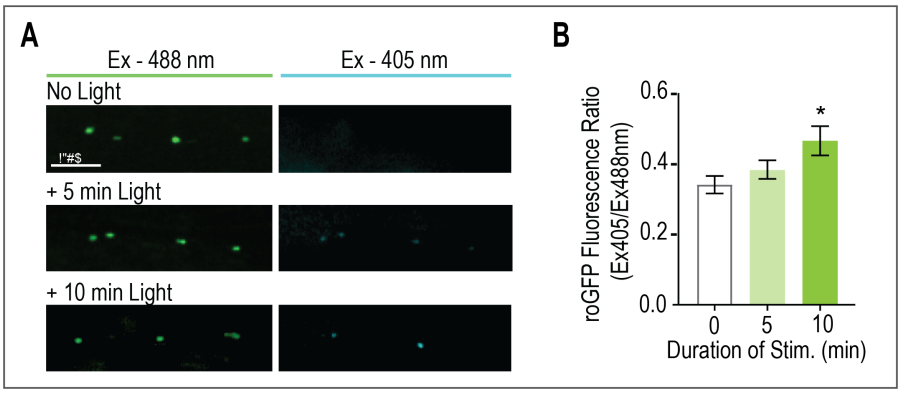

Figure 3.9 - Whole-animal optical stimulation of mitochondrial ROS production. A) Representative fluorescent images of mitochondrial localized roGFP due to 488 or 405 nm excitation with 0, 5, or 10 min of consistent light (567 nm; 0.025mW/mm^2) for activation of mitoKR. Strain: FJH 416. B) Quantification of roGFP fluorescence ratio (Ex405/Ex488 nm) for each group. (n > 30 mitochondria from 8 animals for each; One-way ANOVA with Dunnett's test).

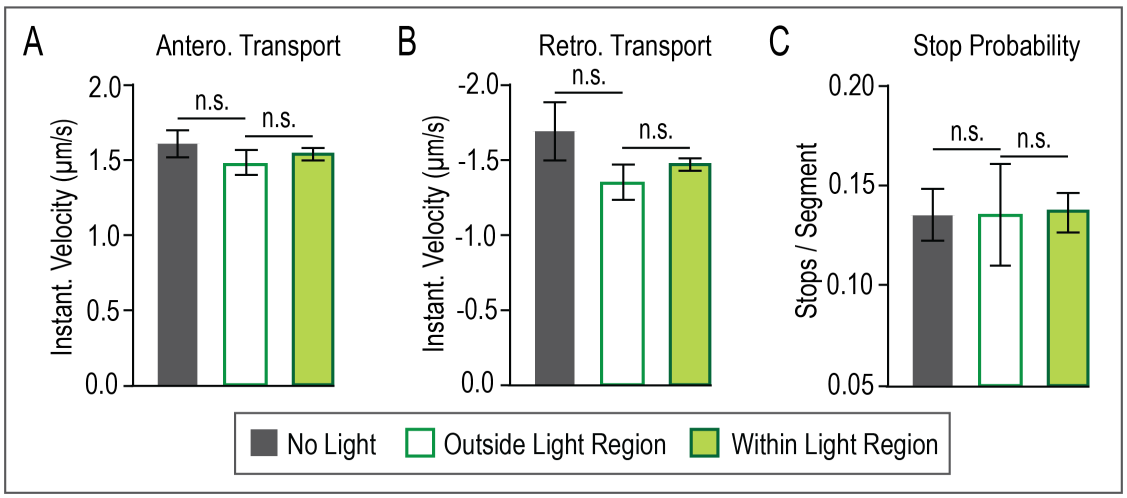

Figure 3.10 - Light stimulation used for mitoKR activation has slight effect on GLR-1 transport velocity. A and B) Segmental velocities of anterograde (A) or retrograde (B) transport in *akIs141* controls without light stimulation as well as within or outside of the light-targeted region (10 µW intensity). n.s. = not significant, One-way ANOVA with Tukey's test. C) The number of stops normalized to the total no. of segments for corresponding regions of the neurite.